Department of Geology

Geomorphological study of the rock-slope failure at Adjet, Storfjord, Troms.

—

Hannah A. Nopper
Master's thesis in Geology June 2015

Abstract

Norway is known for its steep mountains and many fjords. This landscape provides the potential for large rock-slope failures (RSFs) which, in turn, can cause other catastrophic hazards, e.g. tsunamis. In Troms County, northern Norway, many RSFs are found east and west of the Lyngen peninsula, within an area of discontinuous permafrost. The RSF at Adjet is located southeast of the Lyngen peninsula. It is not a hazard for people as such, but it is of interest for better understanding RSFs in general, due to its complexity.

The aim of the present study is to gain an understanding of the rock-slope failure at Adjet, its geomorphological features, and the origin and movement of these features. The features were identified and analyzed using different methods such as field mapping, evaluation of aerial and orthophotographs, as well as InSAR data.

The investigated RSF area is situated on a west facing mountainside, 500 – 1340 m a.s.l., with a ca. 5 km long ridge delimiting the RSF area to the east. The downslope length of the RSF is ca. 2 km. The failure site is of great size and complexity and contains several different geomorphological and structural features.

The predominant lithology is mica schist with various amounts of garnet and/ or quartz. The mountain ridge character above the RSF changes from north to south, from a peak-like ridge and cliffs to a relatively gradual sloping ridge. The study area can therefore be divided into two provinces: province A in the north and province B in the south. These provinces are separated by an ENE-WSW trending fault.

Geomorphological features within the RSF area are rock glaciers, debris fields, talus fan deposits, and slide blocks. They originate through different failure processes, such as rockfall, toppling and rock slide. In province A, mainly rock glaciers and debris fields are prominent. In province B, slide blocks and talus fan deposits are dominant features.

The source of the rock-slope failure is the mountain wall. Folds, faults and fractures are identified, and include abundant steeply (NE-SW, NW-SE) and moderately (NW-SE) dipping fracture sets. These form conjugate fracture sets. Folds are mainly found in the far north of the study area. It is postulated that disintegrated rocks slide on moderately dipping fault/ fractures and that their extent is determined by steeply dipping fracture sets. In the north, a sliding surface is also provided by fold limbs. Rockfall, toppling and rock slide were identified as failure processes.

Movement is indicated by geomorphological features such as transverse ridges and furrows, lobes, and steep barren slopes at rock glaciers. Rockfall at the front of rock glaciers was observed during field work. InSAR data was additionally used to document movement and support movement hypotheses.

The study site displays a broad range of velocity values. ranging from no movement to velocities of ca. 15 cm per day. Most prominent are the rock glaciers, which also display the fastest velocities.

Several rock-slope failure processes are supposed to have occurred at Adjet. They are alternating with periods of no failure... This is indicated by overlapping of geomorphological features of the same or other category. Thus an evolution of the rock-slope failure at Adjet, of 6 relative ages is suggested at the end.

Acknowledgements

Inhalt

1 Introduction

1.1 Objective of the work

Norway is known and loved by tourists for its beautiful mountains adjacent to steep fjords. The steep mountains and many fjords, however, provide an environment for potential rock-slope failures (RSFs). These can lead to dangerous hazards such as tsunamis endangering local villages. The analysis of historical documents concerning rock-slope failures in Norway, led to the conclusion that we have to expect two to four big failure events per century (ngu.no 2015).

Even though the rock-slope failure at Adjet is not a hazard for locals, it is of interest to better understand rock-slope failures in general. The great size and different structural and geomorphological features of the failure site provide considerable scope for scientific investigation.

In this study, geomorphological aspects of the rock-slope failure at Adjet are the focus of attention. Geomorphological features are identified and analyzed using different methods such as field mapping, evaluation of aerial photographs and InSAR data. Although not an immediate hazard, the complex structures and geomorphological features at Adjet can provide fundamental information about RSFs and their geomorphological and structural features, in general.

The aim of the present study is to gain an understanding of the rock-slope failure at Adjet, its geomorphological features, and the origin and movement of these features.

1.2 Setting of the study area

Adjet is situated in the Stofjord municipality, in the northern part of Troms County, Northern Norway (Fig. 1). The area shows alpine topography characterized by a landscape formed by multiple glaciations (Corner, 2005a, 2005b). The study area is at the mountain Adjet in Skibotndalen, Storfjord. . Skibotndalen is a NW-SW striking valley terminating at its northwestern end into the Storfjord (NNE-SSW to N-S striking). Adjet is located southwest of the town Skibotn and at the eastern side of the Skibotndalen valley (Fig. 1). The mountain ridge is about NE-SW trending and the study side faces W-SW towards the Skibotndalen valley (Fig. 2). The maximum height of the mountain is 1400 m a.s.l. The ridge is about 5 km long and the RSF extends about 2 km downslope. The Skibotn field observatory is at the foot of the mountain.

Figure 1: Location of the study area (black rectangle). Map from kartverket.no (2015).

Figure 2: Adjet, east of Skibotndalen valley. Orthophoto from kartverket.no (2014). Yellow dot represents Skibotn field observatory.
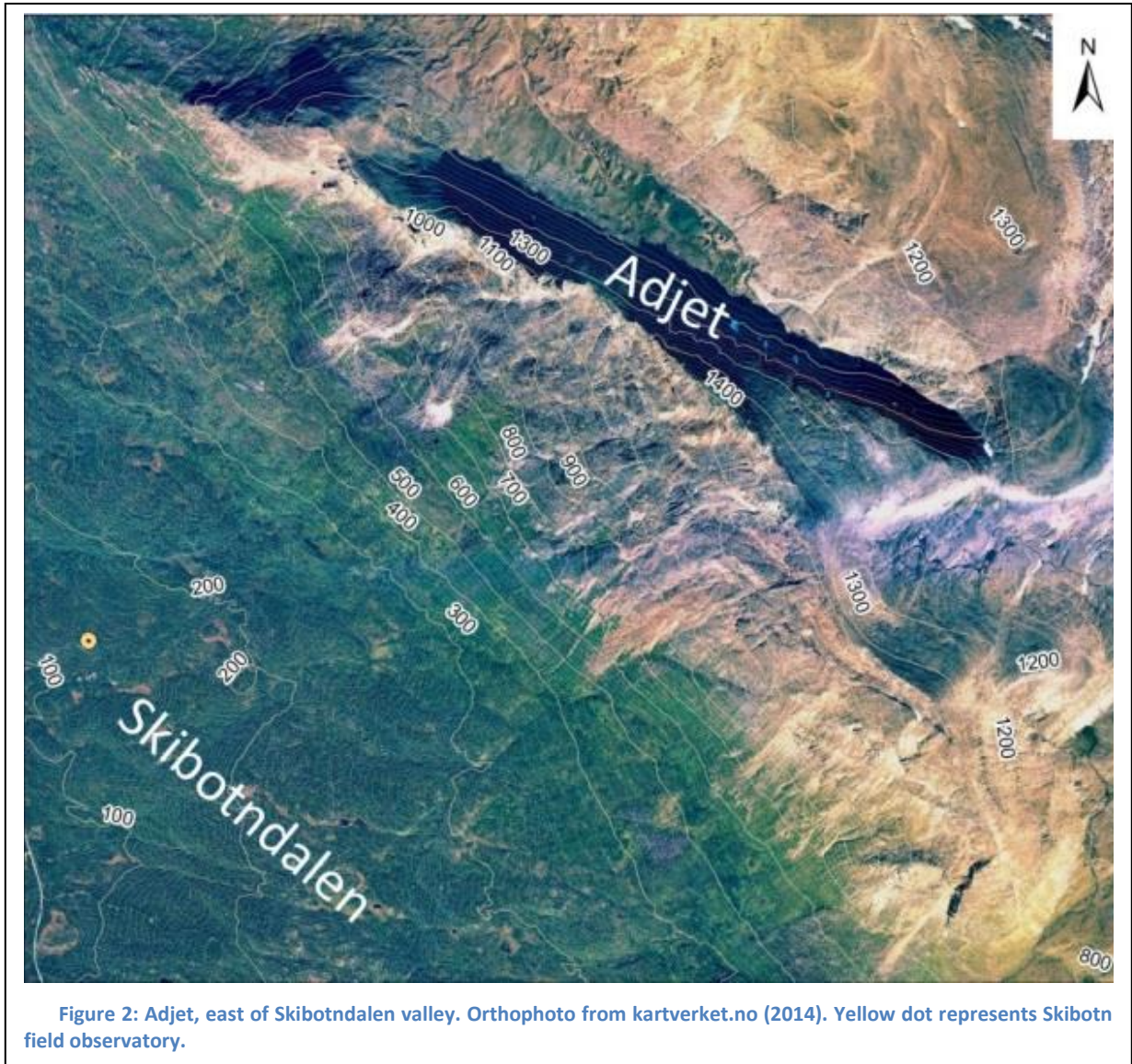
1.3   Regional Geology

1.3.1   Bedrock geology

The study area lies within the Caledonian nappes (Fig. 3). The rocks were metamorphosed during the closure of the Iapetus ocean, as the continents Baltica and Laurentia collided ca. 400 – 500 Ma ago (Fossen, Pedersen, Bergh, & Andresen, 2008). This is referred to as the Caledonian orogeny. Geological units caught between the two continents were eventually thrust over Precambrian basement rocks as nappes. The greater part of Norway was transformed into gneiss and schist. The grade of metamorphism varies between the nappes. The Middle Allochthon has a higher metamorphic degree than the Lower Allochthon, whereas the Upper Allochthon shows a great variation in metamorphic grade.

The study area is situated within the Upper Allochthon. The rocks of this nappe unit show a variety of compostions and style of deformation (Fossen et al., 2008). Typical for this unit are meta-sediments. The Kåfjord nappe is represented in the study area. We find garnet-quartz-mica-schists as characteristic rocks in the study side (Fig. 4).
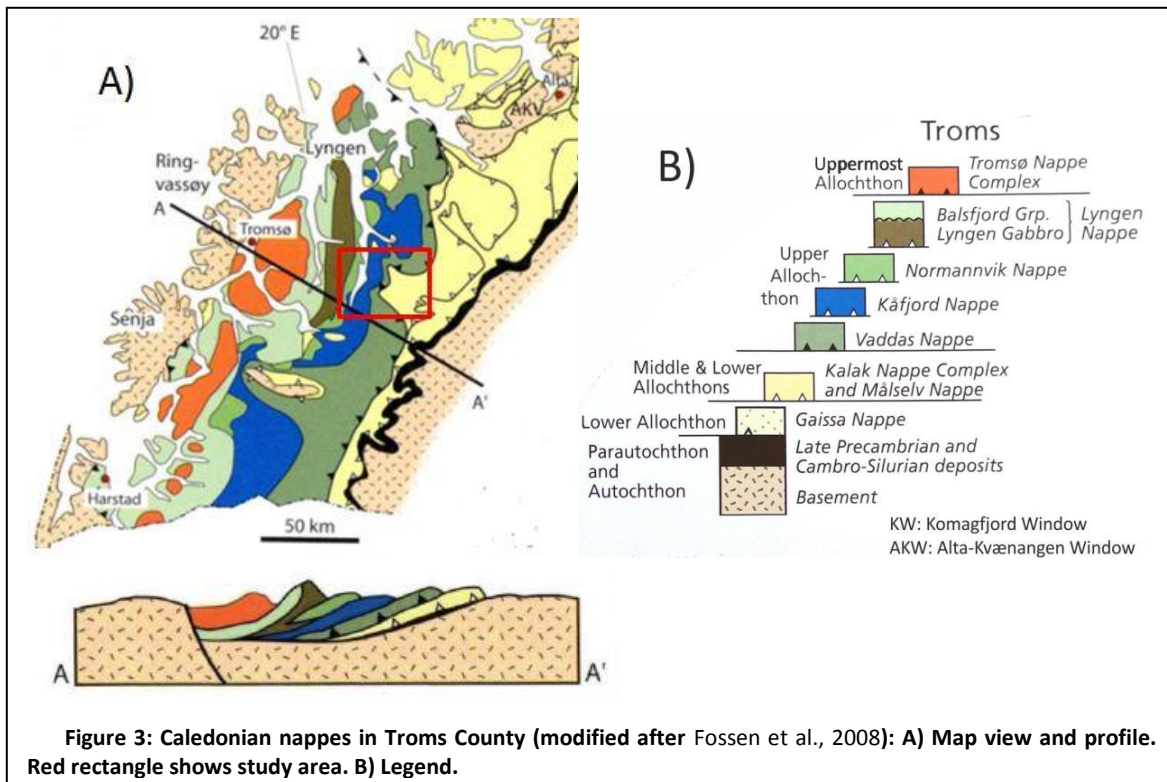
Figure 3: Caledonian nappes in Troms County (modified after Fossen et al., 2008**): A) Map view and profile. Red rectangle shows study area. B) Legend.**

Legend: garnet-quartz-mica-schist, kyanite- and staulite bearing, with layers of amphibolite and conglomerat. Polimictic conglomerate, pegmatite dikes
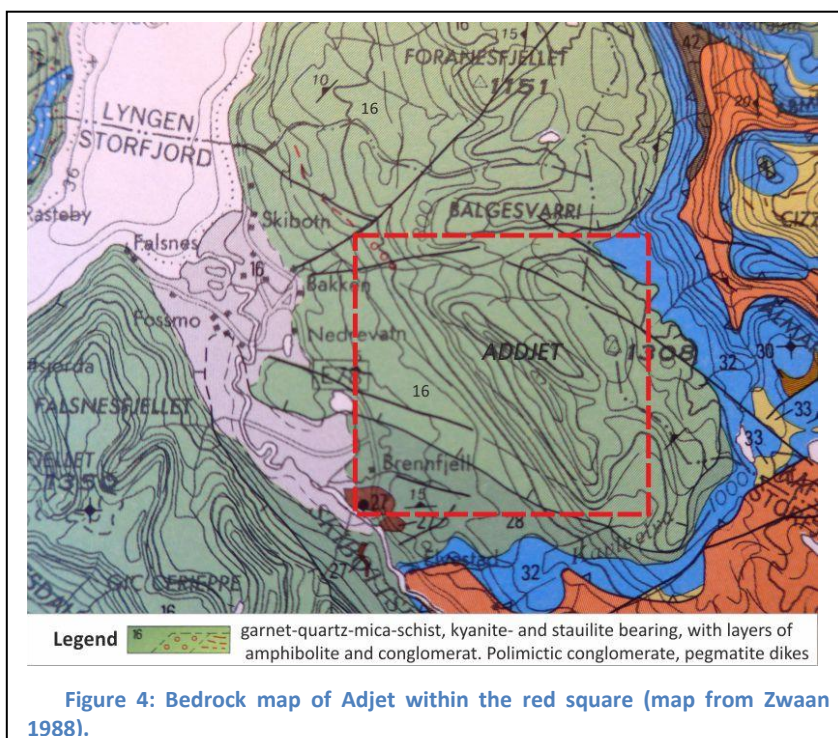
Figure 4: Bedrock map of Adjet within the red square (map from Zwaan 1988).

Regional lineaments

The mountainous topography of Norway is largely fault-controlled (Osmundsen et al., 2010). A Late Cretaceous-Cenozoic and recent rejuvenation of faults has been documented by Osmundsen et al. (2010). Typical strike of lineaments is: (1) NNE-SSW, (2) NE-SW, (3) E-W, and (4) NW-SE to WNW-ESE (Fig. 5 and 6).

(1) NNE-SSW striking faults are detected both onshore and offshore the Lofoten-Vesterålen Margin, as right stepping en echelon faults (Hansen, Bergh, & Henningsen, 2012). They result from the Triassic to Early Cretaceous WNW-ESE extension. In northern Norway are NNE-SSW trending faults brittle, steeply to moderately dipping, normal fault zones (Indrevær et al., 2013). They are suggested to form at least two major NE-SW trending fault complexes, the Troms-Finnmark and Vestfjorden-Vanna complexes, which again bound a major horst, the West Troms Basement Complex. This is concluded by onshore and offshore correlation of fault systems in SW Barents Sea margin in western Troms. The NNE–SSW and also ENE–WSW trending steeply to moderately dipping, brittle normal faults bound major horsts (onshore) and basins (offshore) (Indrevær et al., 2013). The uplift of the West Troms Basement Complex is dated to the Late Cenozoic as a result of unloading and crustal flexure . It belongs to the Mesozoic passive margin, in the SW Barents Sea.

(2) NE-SW striking lineaments are prominent within the Caledonian nappes (Gabrielsen, Braathen, Dehis, & Roberts, 2002). Typical in northern Norway are e.g. the Vestfjorden-Vanna Fault and the Kvaløysletta-Straumshella Fault. They are ascribed to post-Caledonian activity. Precambrian NW-SE fault complexes are suggested to have affected NE-SW trending brittle fault complexes (Indrevær et al., 2013). The brittle faults are suggested to result from reactivation of ductile Precambrian or Caledonian structures forming close to or along these structures.

(3) E-W striking transfer zones link the NNE-SSW striking lineaments (Hansen et al., 2012). They correlate to the late Cretaceous to Paleogene NNW-SSE extension. E-W to ENE-WSW oriented lineaments are more common at the southern tip of Norway than in the north (Gabrielsen et al., 2002).

(4) NW-SE to WNW-ESE striking lineaments are found all over Norway (Gabrielsen et al., 2002). They correspond to Permian, Jurassic-Cretaceous, and possibly Cenozoic activity. In the Lofoten-Vesterålen Margin are NW-SE striking features subdivide into two transfer zones (Tasrianto &

Escalona, 2015). The North Lofoten transfer zone occurring in the Late Jurassic and the Vesterålen transfer zone, dated in the Early-Late Cretaceuos. NW-SE to WNW-ESE striking lineaments transect the Caledonian nappes of Finnmark and partly can be followed offshore into the Troms-Finnmark Platform (Gabrielsen et al., 2002). The structures were reactivated in the Late Paleozoic to mid-Mesozoic. Offshore the Lyngen peninsula cut NE-SW and N-S-trending fault systems Paleozoic and Mesozoic sedimentary rocks (Osmundsen et al., 2010).

Figure 5: Regional onshore and offshore tectonic map and setting of the SW Barents Sea margin, the West Troms Basement Complex, and the mid-Norwegian shelf (Indrevær et al., 2013)**. BKFC, Bothnian-Kvænangen Fault Complex; BSFC, Bothnnian-Senja Fault Complex; TFFC, Troms-Finnmark Fault Complex; VVFC, Vestfjorden-Vanna Fault Complex.**
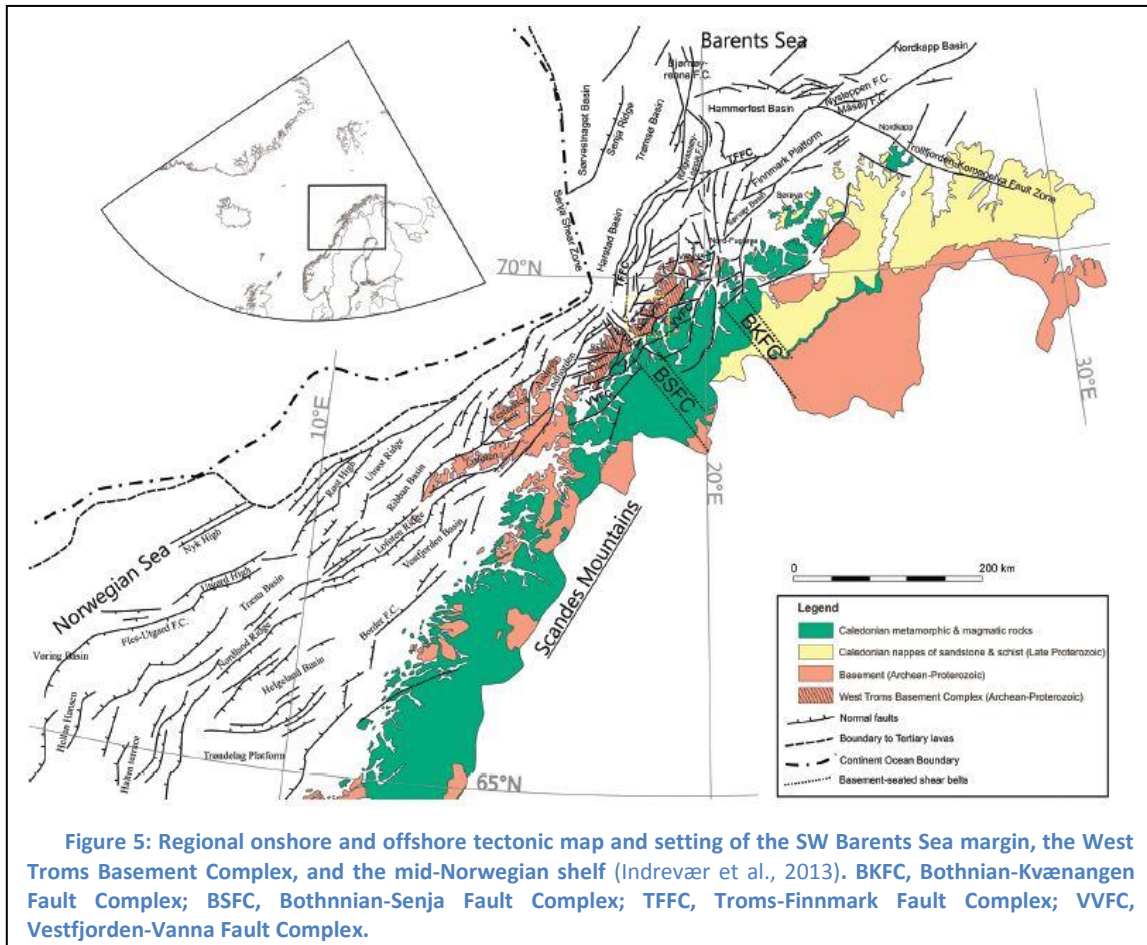
In the study area NW-SE oriented lineaments are most prominent (Fig. 6). NE-SW trending lineaments are second in abundance.

Figure 6: Lineaments in the study area (black square); figure from Gabrielsen et al. (2002)**.**
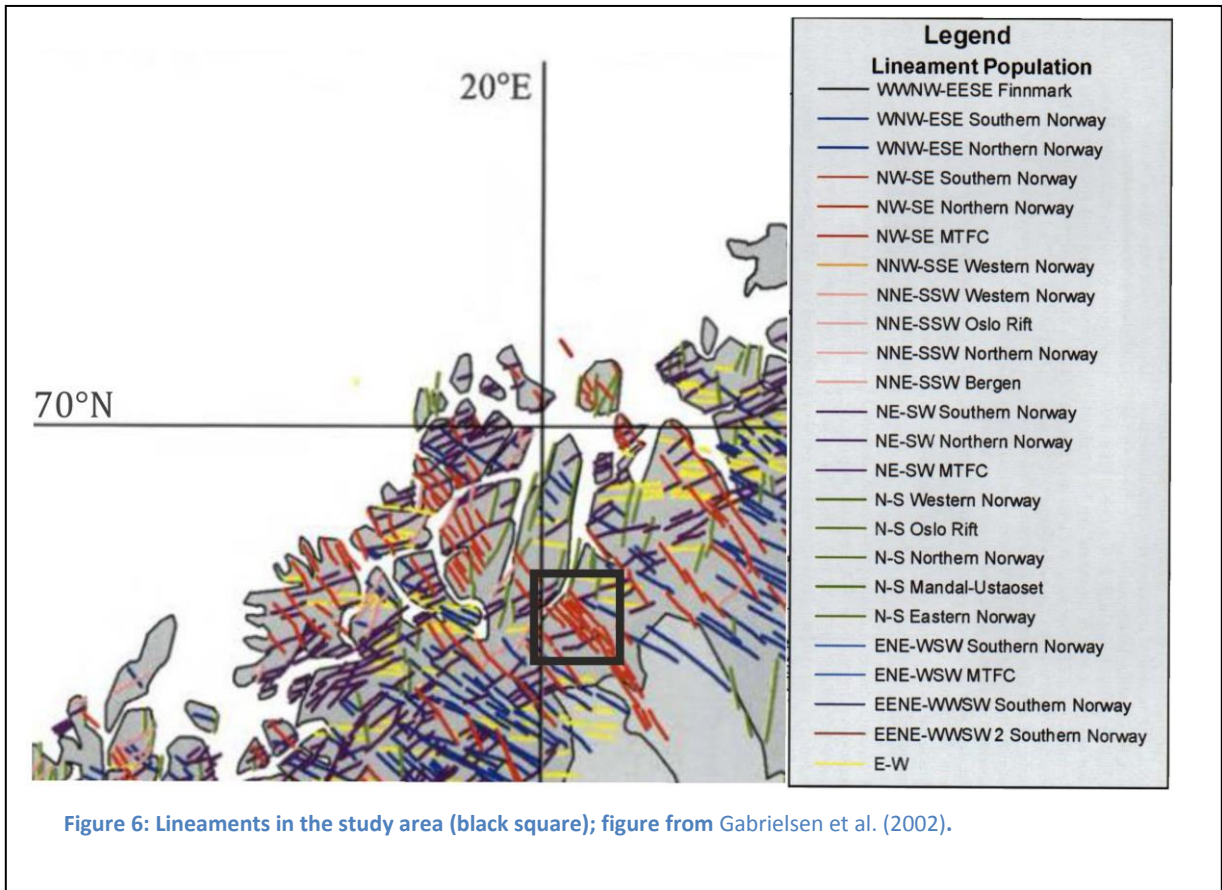
1.3.2 Quaternary Geology

Glaciation

The typical picture of Norwegian topography includes steep mountains, U-valleys, and deep fjords. The landscape is largely influenced by several Quaternary glaciations (Corner 2005 a,b). Surficial sediments are mostly deposits from the Weichselian glaciation (ca. 117 ka – 11.5 ka BP) , especially the final stage (Younger Dryas, ca. 12.8 – 11-5 ka BP; Fig. 7), and the Holocene (e.g. Corner, 1980). The last glaciation in northern Fennoscandia is dated to the Late Weichselian (Dehls, Olesen, Olsen, & Harald Blikra, 2000). The Weichselian ice sheets removed most of the deposits from earlier glaciation (Vorren & Mangerud, 2008). Eight glacial advances or stillstands of the margin of the continental ice sheet are recognized between 25 ka and ca. 10 ka BP. The final retreat of glaciers is associated with milder summers, and a rising sea level resulting from the melting of the North American Ice Sheet. Also during the Younger Dryas (12.8 – 11.5 ka BP) are periods of stillstand observed. In the Lyngen Alps was the ice sheet 20 ka BP at its thickest (Sveian & Corner, 2004). The ice reached limits of 1000 – 1200 m a.s.l., in the fjords, maybe even higher in inner Lyngen. Several mountain tops that lie higher than the ice surface, protruded as nunataks. The large ice sheet withdrew 10 000 years ago, and some local glaciers retained. A new impulse of growth, for the latter, is dated ca. 3000 years ago, reaching a maximum under the little ice age (1750 – 1920). Glaciers retreated again during the last century and continue to retreat.
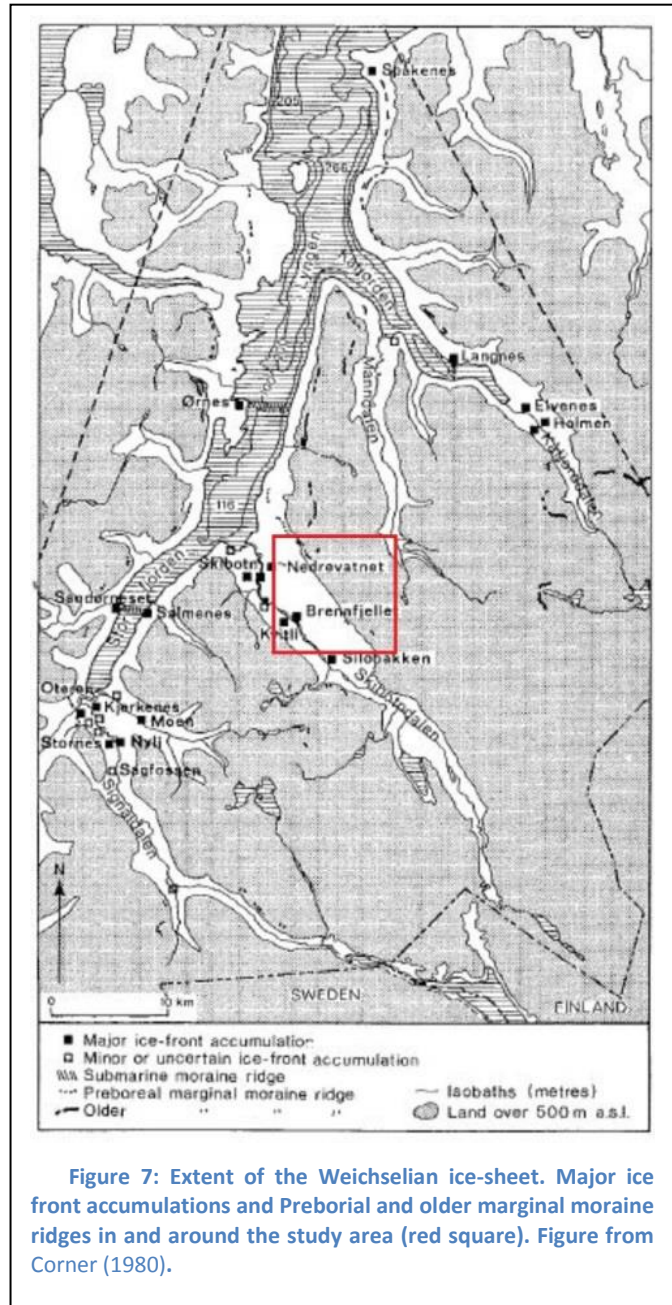
Figure 7: Extent of the Weichselian ice-sheet. Major ice front accumulations and Preborial and older marginal moraine ridges in and around the study area (red square). Figure from Corner (1980).

Glaciers retreated with rates of several hundred meters per year, ca. 10 000 14C yrs BP (e.g. Corner, 1980; Dehls et al., 2000). Figure 8 shows the extent of glaciers of two different events within the Younger Dryas, in the Skibotndalen area. The large decrease in ice volume, within ca. 300 years, is prominent. It is suggested that Signaldalen and lower Skibotndalen were deglaciated by approximately 9100 14C yrs BP (Corner, 1980). Younger Dryas moraines, mapped at the Lyngen peninsula, are found at elevations of 520 m a.s.l., for the Ørnes Event at 570 m a.s.l. and the Skibotn Event at 620 m a.s.l. (Greig, 2011).

Figure 8: Ice-sheet extent of A: the Ørnes event (ca. 9800 - 9900 ±150 14C yrs BP), and B: the Skibotn event (9500 – 9600 ±150 14C yrs BP), based on correlated marginal moraines and marine limits (Corner, 1980).BPBP
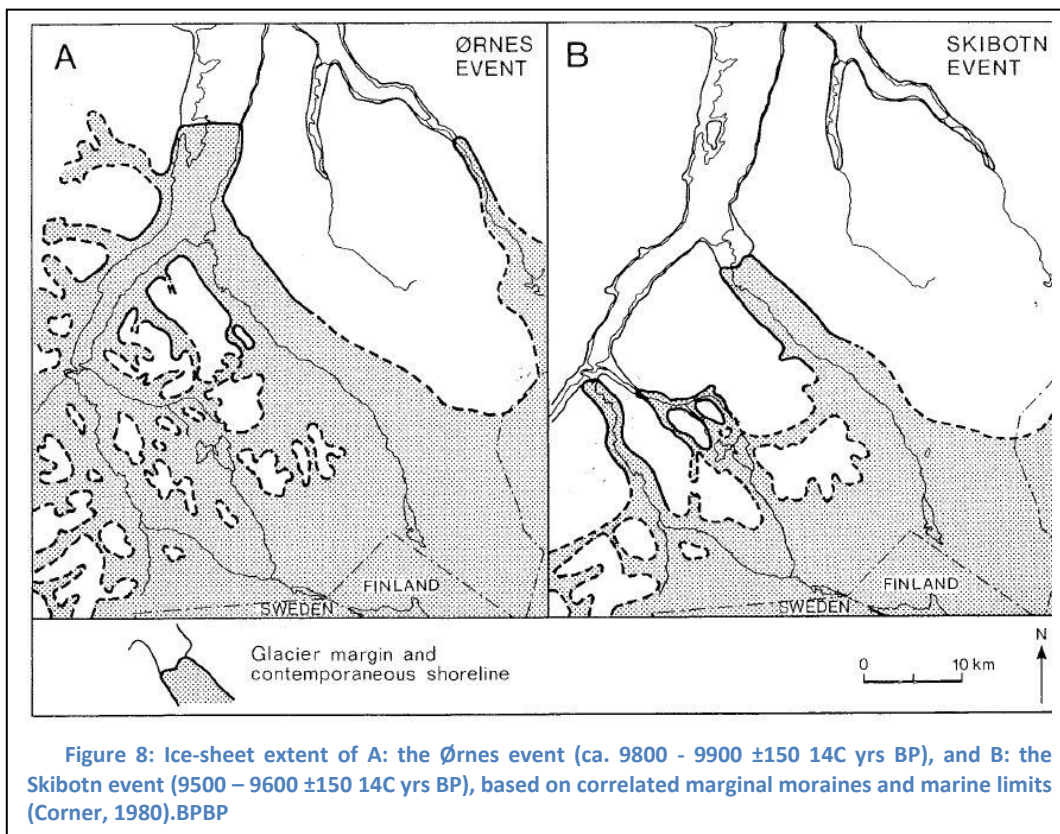
Glacier advance and retreat in the Younger Dryas is suggested to be linked to climate and precipitation (Sveian & Corner, 2004). Landscapes formed by glacial retreat are in an unstable or metastable state, thus slope stability is infliuenced, and consequently liable to modification and erosion (Ballantyne, 2001; McColl, 2012). Three modifications of rock slopes due to landscape relaxation under glacial retreat are postulated by Ballantyne (2001): (1) large-scale catastrophic rock-slope failure, (2) large-scale rock mass deformation, and (3) accumulation of talus, induced by the adjustment of rock faces by frequent rock fall events. The failure processes diminish in time consistent with the decline in stress-redistribution. Figure 9 shows a possible evolution of a rock-slope failure side in the transitions from a glacial to non-glacial condition.
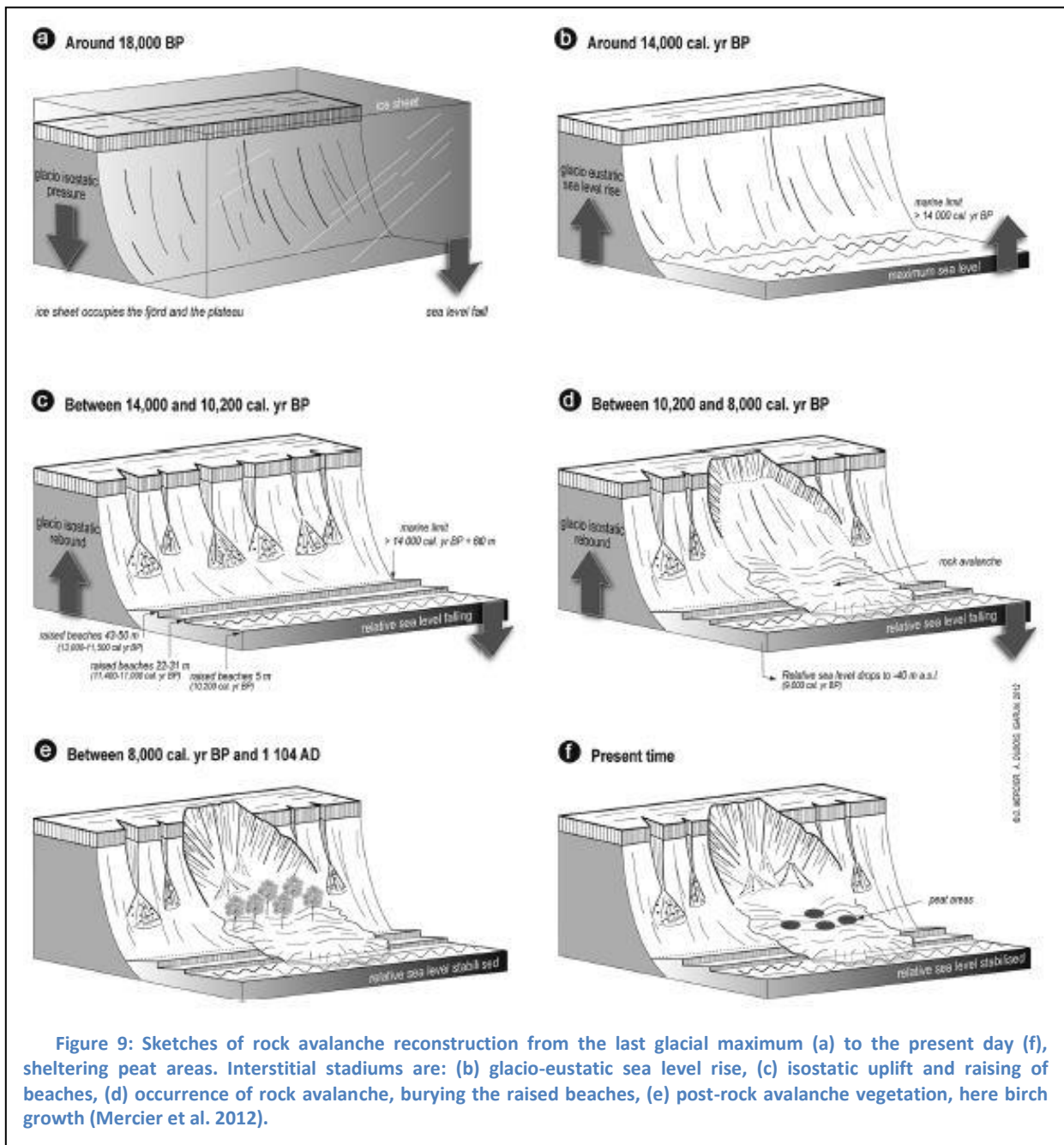
Figure 9: Sketches of rock avalanche reconstruction from the last glacial maximum (a) to the present day (f), sheltering peat areas. Interstitial stadiums are: (b) glacio-eustatic sea level rise, (c) isostatic uplift and raising of beaches, (d) occurrence of rock avalanche, burying the raised beaches, (e) post-rock avalanche vegetation, here birch growth (Mercier et al. 2012).

Glacio-isostatic uplift

The outermost layer of the Earth, the crust, is an elastic element. Great additional weight forces depression of the crust, which then rebounded when the additional weight has vanished, until the land surface is back to its original position. During glaciation weight is added in form of large ice sheets. After deglaciation the isostatic rebound begins.

Deglaciation and herewith the unloading of the crust resulted in differential isostatic rebound. The glacio-isostatic uplift was greatest where ice sheets were thickest (Ballantyne, 2003). It caused, also, the reactivation of ancient faults and triggered earthquakes. In Fennoscandia began the glacio-isostatic uplift after the last glaciation (e.g. Dehls et al., 2000). Dehls et al. (2000) postulate an isostatic-uplift rate of about $1 - 1.5$ mm yr^{-1} along the coast of Troms County (Fig. 10). Stresses in western Scandinavia are supposed to be related to postglacial uplift and ridge push (Fjeldskaar, Lindholm, Dehls, & Fjeldskaar, 2000).
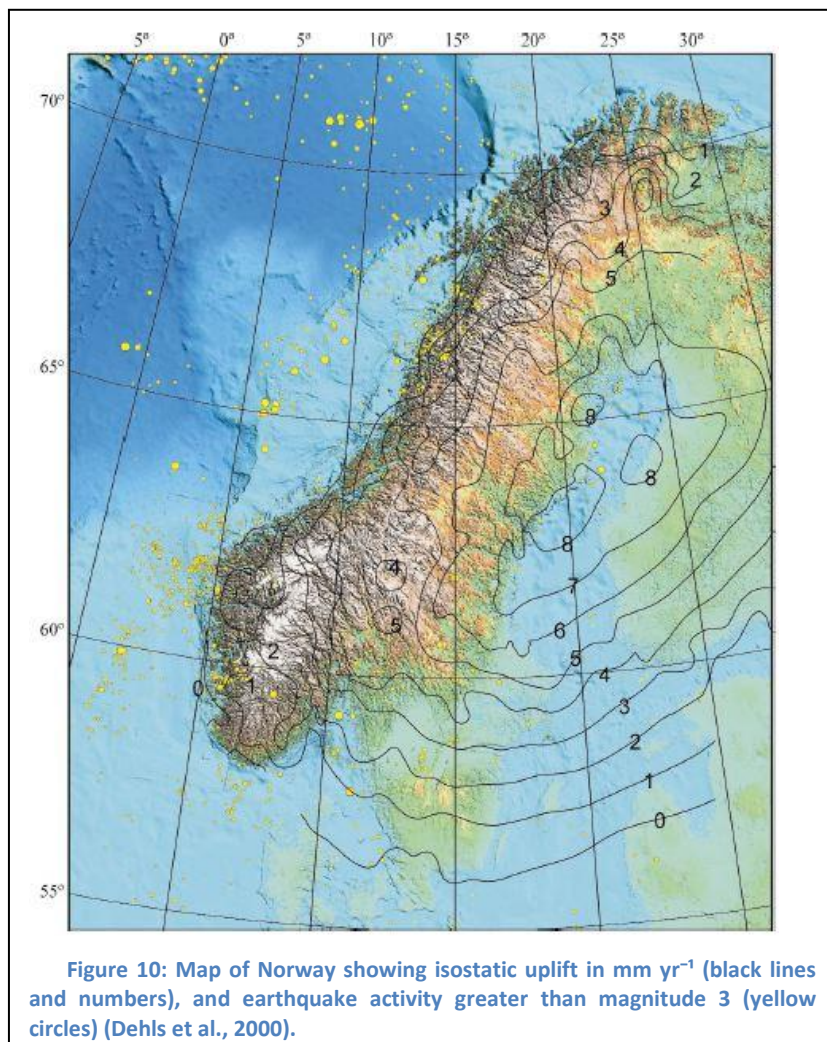
Figure 10: Map of Norway showing isostatic uplift in mm yr^{-1} (black lines and numbers), and earthquake activity greater than magnitude 3 (yellow circles) (Dehls et al., 2000).

Marine Limit

Marine Limit (ML) is the uppermost post-glacial sea-level recorded (Vorren, Mangerud, Blikra, Nesje, & Sveian, 2008). The global sea-level rose by 120 m after the last glaciation. The local MLs, however, vary, due to local isostatic uplift. In Skibotndalen reaches the ML a maximum of 86 m above present sea level (Fig.11). Corner (1980) suggests MLs of ca. 82 – 85.5 m above present sea level, in Skibotndalen.

Figure 11: Marine limit in Skibitndalen. The study area lied within the red rectangle. Numbers in in blue rectangles give m a.s.l. (map from ngu.no 2015)
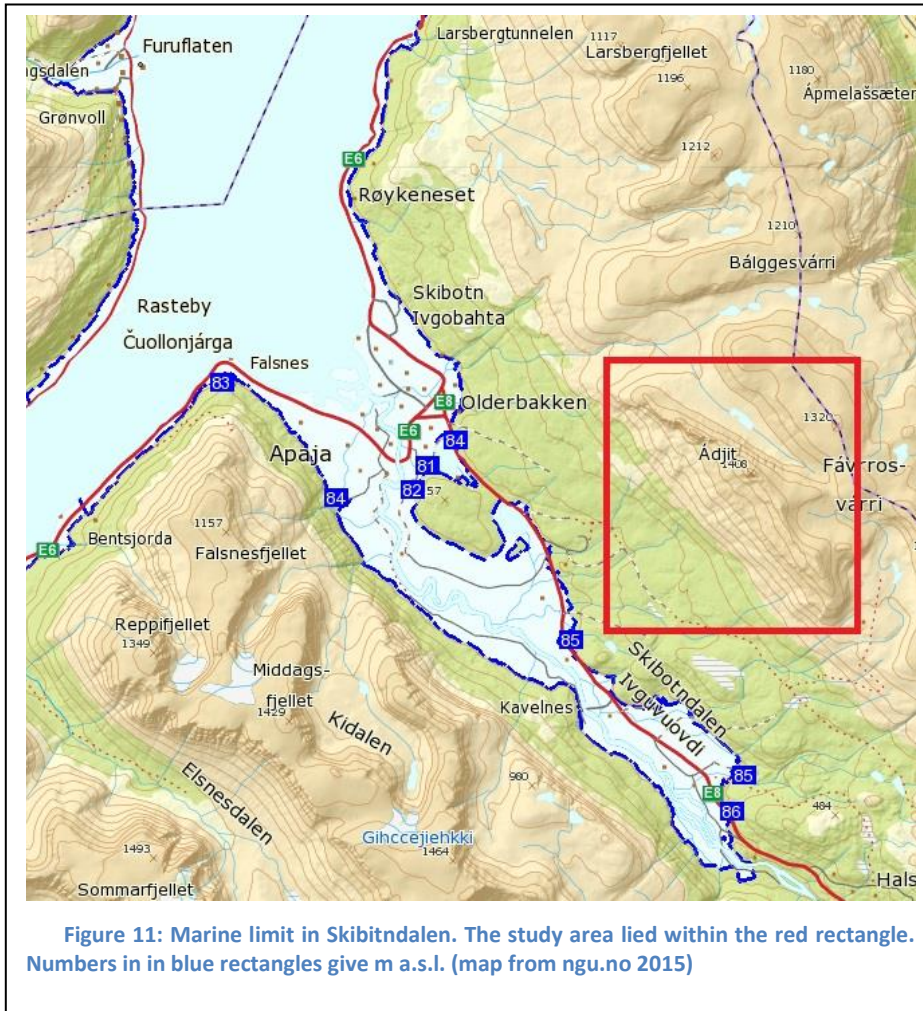
Surficial deposits

Surficial deposits are characterized by glacial, marine, fluvial, and failure materials. They have been both been influenced and deposited by Quaternary events such as deglaciation, sea-level rise, isostasy and depositional and failure events linked to those. Surficial deposits in the study area include mainly avalanche and weathered material (Fig. 12).

Figure 12: Surficial deposits in the study area (black rectangle). Map from ngu.no (2015).
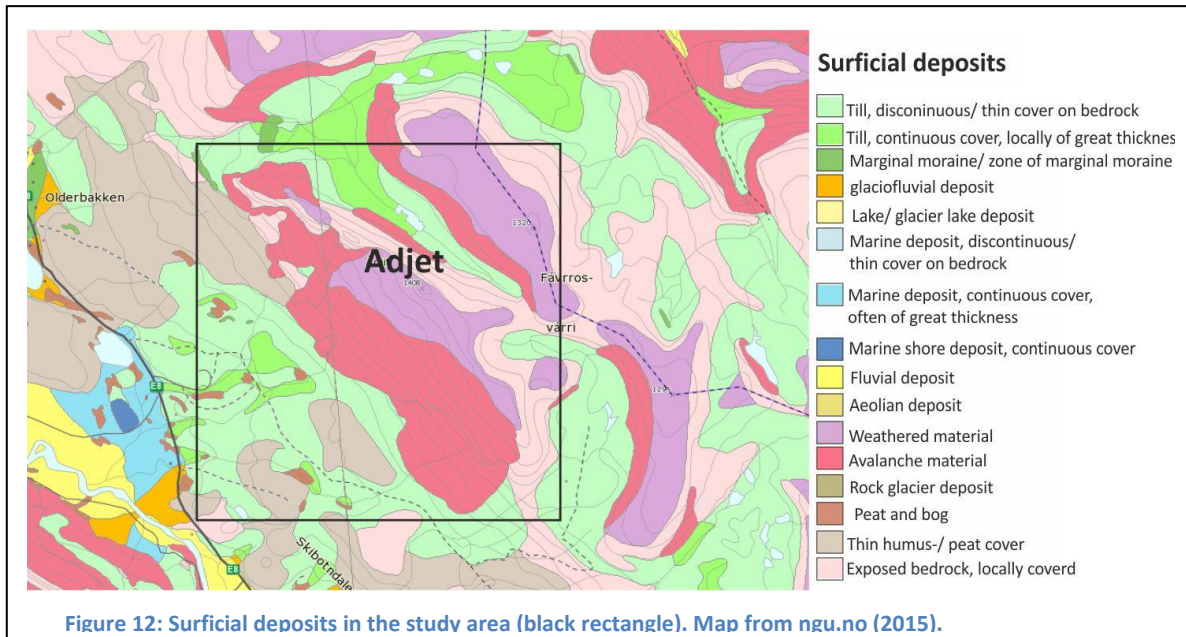
1.4 Climate and permafrost in Skibotn(dalen)

The study area lies within the subarctic climate zone. Subarctic climate is characterized by long cold winters, and short cool to mild summers. Climate information is available for Northern Norway, the Counties of Troms and Finnmark[1], and the weather station[2] near Skibotn. . Skibotn is one of the driest locations in Northern Norway (Johnson, 2014; yr, 2015).

Either January or February are the coldest months and July the warmest (Dannevig, 2009, yr.no 2015). In Finnmark and Troms ranges the annual precipitation ranges 300 mm and 600 mm in shielded valleys(Dannevig, 2009)[3]. The average annual temperature, estimated for Northern Norway over a period of 30 years (1961-1990), is just below zero (Fig. 13; yr.no). For Adjet was no mean annual

---

[1] There is no clarification of which weather stations were used for the provided data of both Northern Norway (yr.no 2015) and the Counties of Troms and Finnmark (Dannevig 2009).

[2] The station is 0.7 km away from Skibotn, Storfjod, Troms.It is 20 m a.s.l. and was established in 2004; there may be missing data (yr.no).

[3] A general climate description of Finnmark and Troms is provided.

temperatures found but information about a period of one year (Fig. In the last year (June 2014 – May 2015) were temperatures, in Skibotn, ranging between 32.7°C (July 2014) and -19.5°C (January 2015) (Fig. 14). Months of lowest precipitation were January (7.0 mm; 2015) and October (13.9 mm; 2014), and those of highest August (66.6 mm; 2014) and February (74.1 mm; 2015) (yr.no).

It is assumed that temperatures were milder respectively cooler at Adjet, due to differences in altitude. Throughout field work it has been observed that snow melts almost everywhere in the study side in sommer. Scattered snow patches are found in from the sun shielded areas, e.g. behind slide block scarps.

Figure 13: Long term statistic for yearly temperature (upper half) and precipitation (lower half) of Northern Norway. Temperature is represented by: Dots (red > 0°C, blue < 0°C) for average yearly temperature, line (red > 0°C, blue < 0°C) indicates a 10 year Gaussian distribution, and a thick horizontal line showing the average weather during a time period of 30 years (1961 – 1990). Precipitation is presented by: bars indicating average yearly precipitation compared to the normal (grey horizontal line), which is again an average distributed over a 30 years period (1961 – 1990). Blue line shows a 10 years Gaussian distribution (yr.no).

Figure 14: Weather statistic of one year, measured at a weather station 0.7 km away from Skibotn, Storfjord municipality, at an elevation of 20 m a.s.l. (yr.no 2015)

Permafrost in mountains in the Nordic area is in large parts at temperatures close to 0°C, and only in the highest mountain parts a few degrees below the freezing point (Christiansen et al., 2010). Thus, the areas are sensitive to climate changes. In general is postulated that active-layer depths increase and permafrost temperatures rise. In the outermost coastal areas, in Troms County, permafrost limits are found at 800 – 900 m a.s.l., whereas it is located between 600 to 700 m a.s.l. in more continental areas (cf.Christiansen et al., 2010). Several unstable rock slope sides are associated with warm and presumably degrading permafrost (Christiansen et al., 2010). Figure 15 shows areas and coverage of permafrost in the Nordic area postulated by Christiansen et al. (2010). Hence, Adjet is located within a discontinuous permafrost area. The study site is suggested to be located in the regional mountain permafrost zone, with a lower limit of 550-990 m.a.s.l. (Rouyet et al., 2015).
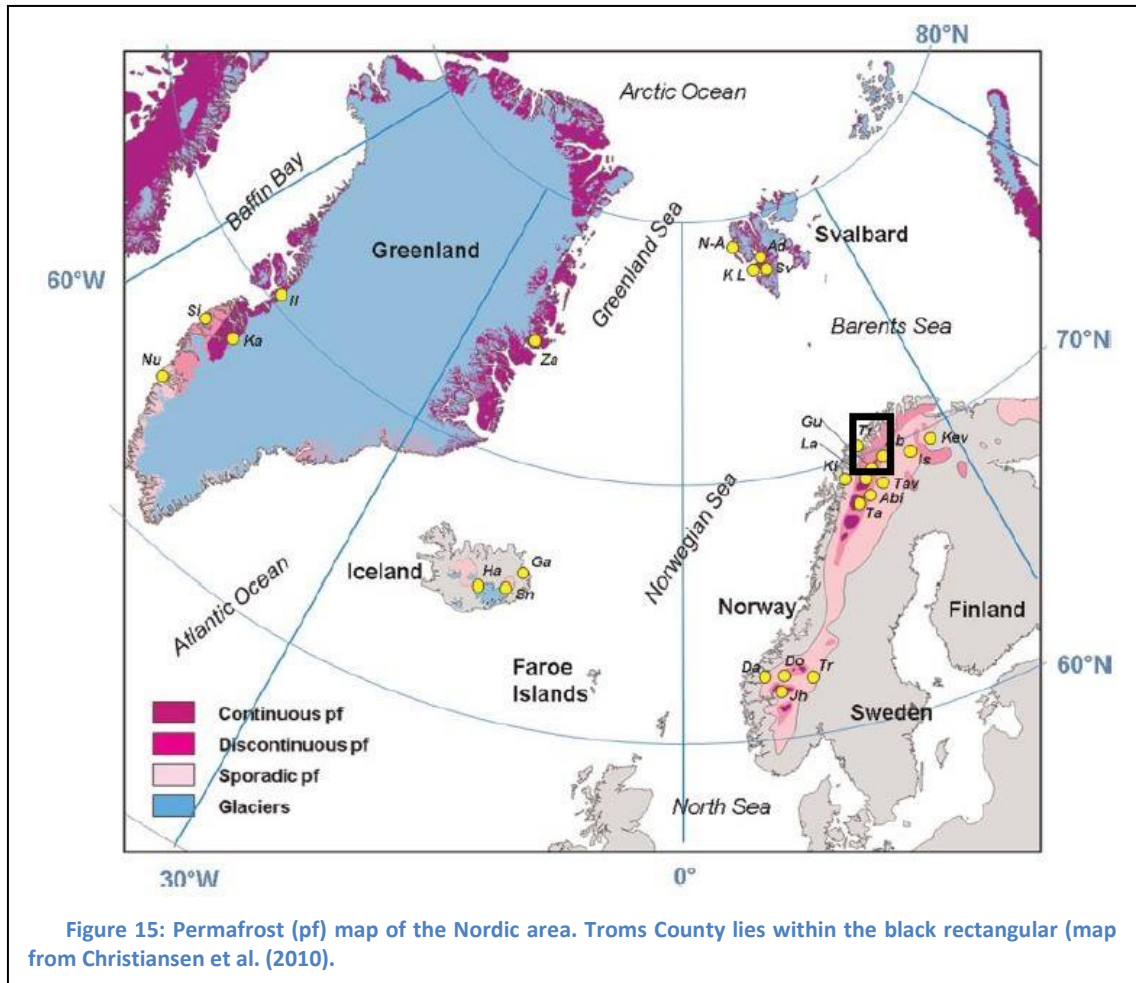
Figure 15: Permafrost (pf) map of the Nordic area. Troms County lies within the black rectangular (map from Christiansen et al. (2010).

1.5   Rock-slope failure definition and classification

In this study the term rock-slope failure (RSF) is used for rockfall and toppling processes, as well as for rockslide and landslide processes as for example creep (see below).

Different classification of rock-slope failures exist. In this study we will mainly rely on the classification by Braathen, Blikra, Berg, & Karlsen (2004). The classification is based on extensive studies of rock-slop failure (RSF) areas in Norway. The result is a division into (1) rockfall areas, (2) rockslide areas, and (3) complex fields (Fig. 16).

(1) Rockfall areas are found at steep slope gradients. Steep fractures delimit the failure block by steep fractures on one or both sides. The loosened block falls eventually by free fall. The upper part of the block may rotate outwards (toppling). Large rockfalls may evolve into rock avalanches.

(2) Rockslide areas are slope parallel and found in moderate dipping terrains. They are further influenced by zones of weakness (foliation, exfoliation). The sliding occurs on reactivated, underlying planes. Creep can mobilize rockslides.

(3) Complex fields disintegrate from deep-seated, low angle planes. They are characterized by a complex deformation, which can include a combination of rockslide, rockfall and toppling. They may be either controlled by listric or planar fault geometry. The former is characterized by horsts and grabens, whereas the latter shows domino-style block configuration.

Figure 16: Rock-slope failure geometric models, distinguishing between joints, extension fractures, shear fractures and faults (Braathen et al., 2004).
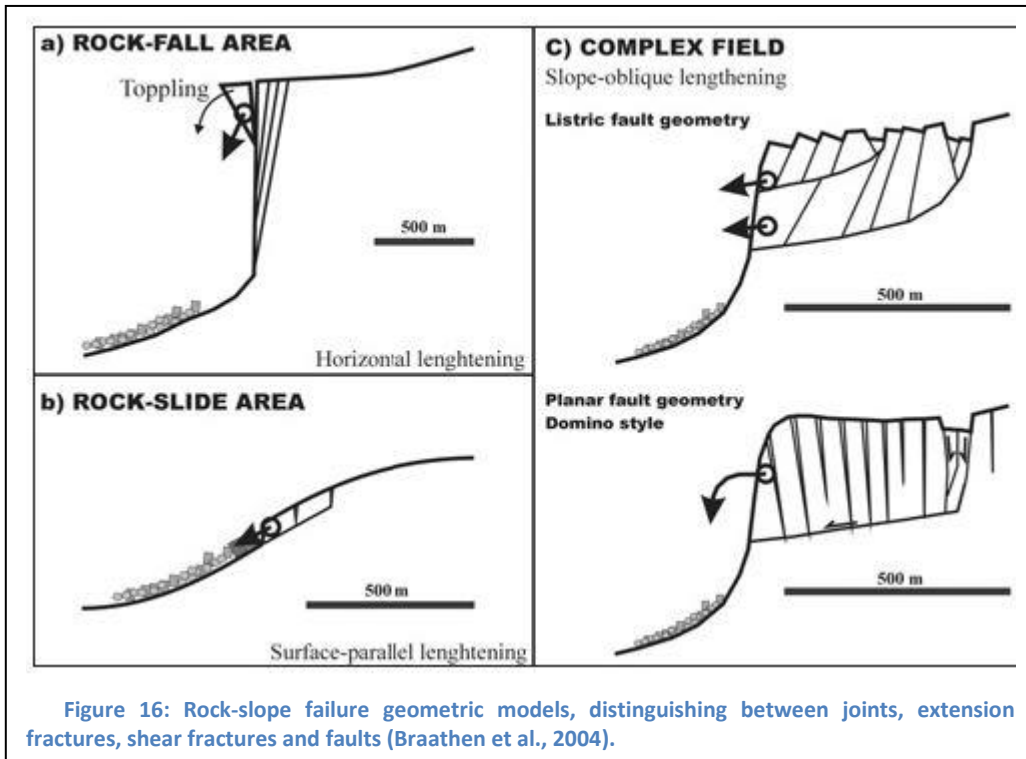
The study side includes many different geomorphological features comprising a landslide. Landslide is a general term for various mass movement landforms and processes which are driven by gravity downslope and outward transport of material forming the slope (USGS, 2004). Failure occurs along a planar or curved surface. In this study, it includes rock and soil material that moved by falling, toppling, sliding, flowing and/ or creep.

1.6 Rock Slope Failures in Troms

Rock-slope failures are stated to be common within certain regions in Norway. They can be slides of relatively intact rock masses, fully disintegrated rock avalanches, or anything in between (L H Blikra et al., 2006). In northern Troms are rock-slope failures found on glacially oversteepend valley and fjord sides (Corner, 1972 unpub.). Figure 17 shows that they are found, in large frequency, East and West of the Lyngen peninsula. They form large morphological features and provide source material for rock glaciers. A relation between bedrock and the distribution of rock-slope failures is suggested by Corner (1972, unpub.). Bedrocks are typically composed of Cambro-Silurian metasediments, especially hornblende schists or hornblende and mica schists. Seismic events, creep processes, and destabilization caused by glacial unloading during deglaciation are postulated triggers of rock-slope failures (L H Blikra et al., 2006). They are universially assumed to be evolved in a period shortly after deglaciations (Corner 1972, unpub., Blikra et al., 2006), but younger events are also taken into consideration (Blikra et al. 2006). Blikra et al. (2006) suggest that rock-slope failures occurred mainly in an early postglacial period (15000 – 14000 cal years BP), but also during the last 5000 years, with a peak activity around 3000 cal years BP. Rock-slope failures have been radiocarbon dated, or indirectly dated by use of seismic stratigraphy or sea level curves.
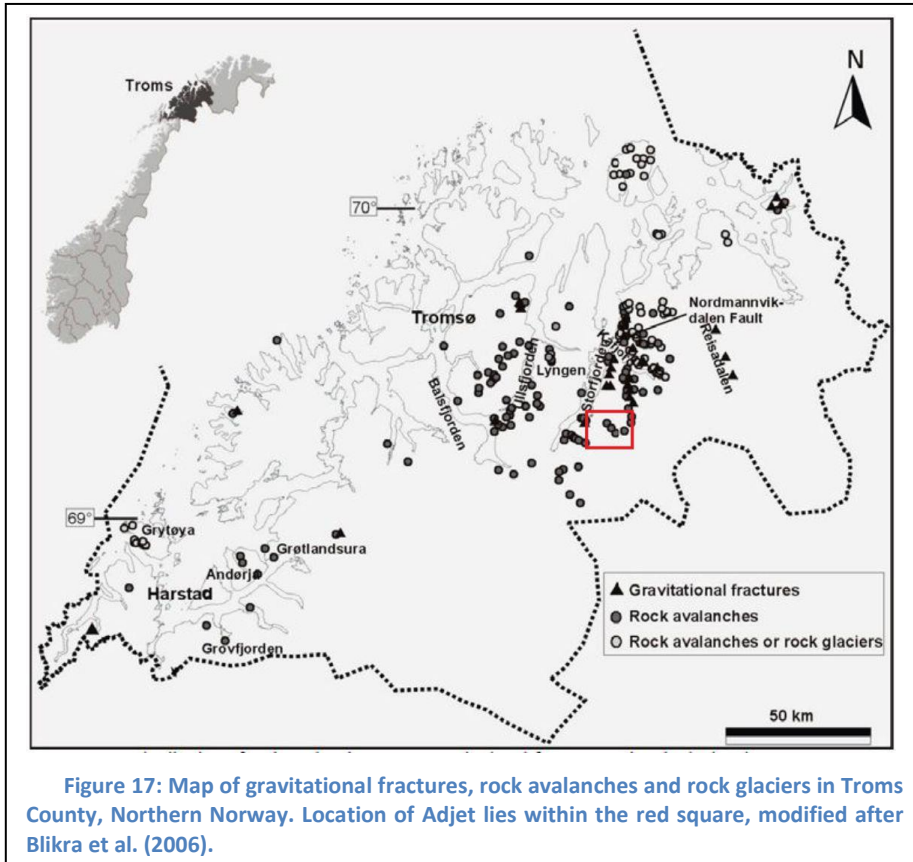
Figure 17: Map of gravitational fractures, rock avalanches and rock glaciers in Troms County, Northern Norway. Location of Adjet lies within the red square, modified after Blikra et al. (2006).

1.7   Terminology

Terminology based on the 'Glossary of Geology' (Neuendarf, Mehl Jr, & Jackson, 2011) and/ or the 'Dictionary of Geology' (Keary, 2001) are abbreviated with (GoG), respectively (DoG) in the following.

Avalanche – The sudden, rapid downslope movement of disintegrated snow, soil, rock, or their mixture. Material slides, falls, or flows under the force of gravity. (GoG)

Colluvium – A general term which is often alternately used to talus (see below) in geomorphological literature (Lars H. Blikra & Nemec, 1998). Here, it will be referred to as detached and slightly moved surface material on bedrock. .

Conjugate fault set – A set of two faults of opposing dips, that formed under shear and which are approximately 60° apart from each other (Twiss & Moores, 2007).

Creep – The gravity controlled downhill migration of grains and particles within a rock mass (Holmes, 1965)(Holmes, 1965).

Debris – A surficial accumulation consisting of rock fragments, soil/ earth material, and sometimes organic matter. These are detached from rock masses by chemical and mechanical processes, decay and/ or disintegration. (GoG) In this study debris are (a) accumulations of already disintegrated/ detachted/ decayed material forming body of landslide features such as debris field, talus fan deposit and rock glacier; (b) rock fragments (> gravel) supplying debris.

Debrisflow – A type of sediment gravity flow consisting of a mixtue of debris and water, snow or slush. It is defined as gravitational shear movement. (Blikra & Nemec, 1998)

Esker – An elongated, narrow, sinuous, and steep sided ridge composed of (irregular) stratified sand and gravel. It is probably the remnant of glacial streams, flowing between ice walls or in ice tunnels of stagnant or retreating glaciers. (GoG)

Fault – A discontinuity surface separating two rock masses across which there has been shear displacement. (GoG, DoG)

Fracture – A discontinuity between two surfaces across which there has been separation, e.g. joint, fault, crack. (DoG)

Mass movement – The movement of a mass, driven by slide (e.g. rockfall, rock slide), flow (e.g. debris avalanche, creep), or mass wasting processes (e.g. landslide). (DoG)

Normal fault – A fault with a hanging wall that has displaced, in a downward movement, relative to the footwall. (GoG, DoG)

Paraglacial/ periglacial – (a) An environment of cold, non-glacial climatic and geomorphic conditions in which frost action is an important factor, irrespective if the environment is beyond the periphery of ice. (b) A term for processes, conditions, areas, climates, and topographic features influenced by the cold temperatures of ice from adjacent, former existing glaciers and ice sheets. (GoG, DoG)

Rock avalanche – The downslope flow of rock fragments at very high velocities. The fragments my break further or pulverize during the rapid downslope movement. Typical product of rockfalls and rock slides. Characteristic features are, e.g. high porosity, angularity of fragments, lobate forms, and relative thinness of deposits compared to the large lateral extent; also referred to as sturzstrom. (GoG)
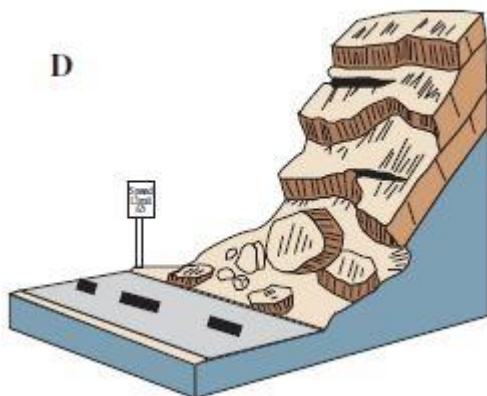
Figure 18: Sketch of rockfall as landslide movement (USGS, 2004).

Rockfall (Fig. 18) – A rapid process of mass movement, of rock, by falling under gravity from a cliff or other steep slope. It is the fastest mass movement process and is most common in mountainous areas during spring, iniciated by freeze-thaw activity. (GoG, DoG)

Rock glacier – (a) A combination of poorly sorted angular boulders, fine material, and interstitial ice or ice-cored. They are found in permafrost regions, and appear and move similar to small valley glaciers. (b) A combination of ice, water, air, and rock (Hauck, Böttcher, & Maurer, 2011).

Rock slide – (a) The process of a downslope sliding of a mass of rock on a surface of weakness, e.g. bedding, jointing, faulting, or other pre-existing structural features. It typically occurs in high mountain ranges. (b) A term for a mass of rock which moves or is moved by a rock slide. (GoG)

Sturzstrom – (a) A great and rapid mass movement of rock debris and dust as result from the collapse of a rock cliff or mountainside. They move downslope and may further include water, mud or compressed air between the rock fragments. It is a large scale landslide and the most catastrophic. (GoG)
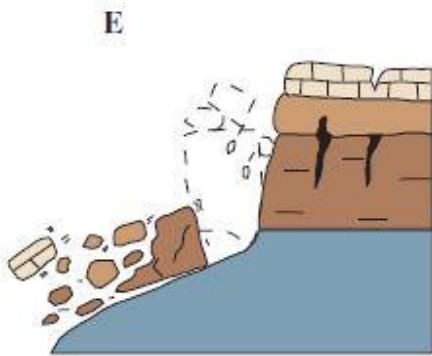
Figure 19: Sketch of toppling as landslide movement (USGS 2004).

Talus (scree) – Rock fragments of any size or shape, typically > gravel and angular, that derive as a result of weathering and erosion. Also, a sloping accumulation of loose fragmented rock at the base of a cliff or very steep, rocky slope. The derivation is possible by falling, rolling, or sliding.(GoG, DoG)

Topple/ Toppling (Fig. 19) – A term for gravity derived mass movement distinguished by the forward rotation of a unit or units about a critical point, below or low in the unit. Failure is influenced by adjacent units or fluids in cracks (USGS 2004).

2 Materials and Methodology

2.1 Field work and data collection

Field work was carried out during a period of 19 days in August and September 2014. Figure 20 shows the GPS locations where field work data was collected and where we overnighted. Field work provided the study with photographs and mapping data such as bedrock lithology, geomorphological and structural data.

. A large area, in the northern part of the study site, was covered. In the south, the southernmost cliff and loose block were covered. Most of the ridge was accessed. The great extent of the RSF site at Adjet, its steep terrains, and the generally abundant loose materials, delimited the coverage of the named during field work and made the access to possibly good outcrops difficult. Thus, the middle part and the mountain slope in the south were not mapped in field but analyzed by aerial photographs later throughout this thesis (Fig. 20).

The ridge could only be investigated by good visibility by reason of the mountain height (ridge: 1000 - 1408 m a.s.l.) respectively the low cloud cover. Thus, the ridge was investigated on the following days: 22.08., 26.08.August, 31.08., 08.09., and 13.09. − 16.09. Throughout field work we overnighted at a minimum of 453 m a.s.l. Every day an altitude between ca. 300 m (19.08.: 453 − 761 m a.s.l. and 16.09.: 1350 − 1049 m a.s.l.) and ca. 880 m (15.09.: 470 − 1347 m a.s.l) was covered.

Field work was carried out jointly with Iselin Bakkhaug for 17 days as part of a cooperative effort to collect data for both theses. In addition, two days of data collection was done by Iselin Bakkhaug (IB) and Solveig Tørstad (ST) in the northern part of Adjet (Fig. 20).

The nights were mostly spent in a tent considering the area and the difference in altitude to cover. In the southern part of the mountain we were able to spend two nights in a shepherd's hut (Fig. 20). Moreover, two nights were spent in the open while walking the ridge (Fig. 20). Low cloud cover and rain hampered visibility making field work impossible or limiting it to lower heights. Such conditions disrupted field work for one and a half day in August (19.08., 20.08.). In September field work continued. The days for field work in September were chosen according to good weather forecast conditions (07.09. − 08.09. and 13.09. − 17.09.). In total we spent 12 days in the northern part and seven days in the southern part of Adjet.

Figure 20: Orhtophotograph and DEM of Adjet showing GPS localities of the study area where observations were made. The outline of the RSF and the mountain ridge are drawn with white lines. The black dotted zig-zag line within the black dotted area represents the major area which was not covered. Orthophotograph (resolution 0.4 x 0.4 m) is provided by NMA (kartverket.no/ norgedigitalt.no).

2.1.1 Field equipment

The GPS (see Garmin BaseCamp below) was used for recording positions in the field, e.g. location of data measurements and some features (e.g. boulders, bedrock lithology). The positioning format was set to UTM UPS WGS 84.

Photographs were taken to illustrate the RSF and its features. They were either taken by Iselin Bakkhaug or Hannah Nopper and are shared (cameras: Panasonic Lumix DMC-TZ40 and Lumix DMC-LF1).

A geological compass was used to measure the orientation of structural features with regard to plunge, dip and strike using the right hand rule.

2.2 DEM & Photographs

Digital elevation models (DEMs) and photographs were mainly used to enhance visualization and thus understanding of the study area. DEMs were imported into ArcGIS (see below).

2.2.1 DEM

Digital Elevation Model (DEM) is a file showing heights above sea level for each pixel of a land area. DEM and contour lines are provided by the Norwegian Mapping Authority (NMA) and were obtained from www.kartverket.no. The resolution of the DEM used is 10 x 10 m. Throughout the study they were used to visualize and illustrate the study area better.

2.2.2 Aerial photographs

Oblique aerial photographs taken from a helicopter were provided by NGU (date: August 2011)[4], Harald Øverli Eriksen (date: 07.08.2014) and Iselin Bakkhaug (date: 07.08.2014). Black and white vertical stereographic aerial photographs (series 5526, number N9 - 11 5276 - 5278, scale: 1:30 000, taken 06. Aug. 1977 by Fjellanger-Widerøe) were viewed stereoscopically. Aerial photographs, along with field photographs and terrain models (Norge i 3D), were used to define and illustrate geomorphological elements in the study area, including those parts of the mountain which were not included in field work or were inaccessible (Fig.20).

2.2.3 Field photographs

The photographs were taken to describe and visualize both interesting features in the study area and parts which could not be accesed because they were too dangerous to approach or inaccessible. The photograph, thus, provide the possibility the latter from a distance and compare those with e.g. aerial photographs.

Objects and person were used in the photographs to provide scale. Their measurements are as follows: Iselin Bakkhaug (ca. 169 cm), Hannah Nopper (ca. 173 cm), field book (17.2 x 11.7 cm), pencil (ca. 14 cm), compass (10.5 x 6.4 cm), and a glove (ca. 20 cm in length).

---

[4] 12.08., 14.08., 16.08. and 17.08. 2011; camera: Panasonic DMC-TZ10

Software & programs

Software and programs are used to digitalize, visualize, and illustrate data. The software and programs applied in the study are listed below.

2.2.4   ArcGIS 10

ArcGIS is a geographic information system by ESRI. For this study version 10 was used, mainly ArcMap and Arc Catalog. The latter is a storage component of files and features used or created in ArcMap. The reference coordinate system was set to UTM WGS 84 zone 34. It was used to illustrate / visualize e.g. InSAR data provided by NORUT, the study site (GPS, geomorphological, and structural data). Profiles were created with help of DEMs / InSAR data.

2.2.5   Stereonet 9

Stereonet 9 is a stereoplotting program. It was used to create stereoplots of structural data collected during field work. Data is plotted on the lower hemisphere. Means were estimated with the program but drawn in by hand. Information about the algorithms behind the program can be found in Allmendinger, Cardozo, & Fischer (2012) and Cardozo & Allmendinger (2013).

2.2.6   Corel DRAW X5

Corel DRAW is a vector graphic program by Corel Corporation, Ottawa. It was used to create, change or enhance figures and pictures.

2.2.7   Garmin BaseCamp

The GPS operates with Garmin GPSmap 64st, software version 3.10. Garmin BaseCamp version 4.3.5 was used to upload data from the GPS onto the computer. The data was exported, to be able to be used in ArcMap. imported to ArcMap.

2.2.8   Norge i 3D

Norge i 3D is a globe viewer program including satellite and aerial images, elevations, maps and 3D-features. Norge i 3D was used to have a first impression of the study area before fieldwork and make first suggestions regarding geomorphological and structural features.

2.3 InSAR: satellite-based radar

In this study, remote sensing data showing recent rates of movement in the RSF was supplied by Eriksen et al. (in prep.) and are based on satellite -based radar measurements in an ongoing parallel doctoral project.Interferometric synthetic aperture radar (InSAR) was used to distinguish stable mountain terrains from those in motion as well as to determine moving rates (velocity) of the latter. The collected satellite-based InSAR data was computed by NORUT[5] and the ground-based InSAR data was computed by NORUT and GAMMA[6] (Eriksen, in prep; Rouyet et al., 2015). Of special interest associated with the InSAR data are two rock glaciers (Ch. 5 and 6).

2.3.1 What is InSAR?

Interferometric synthetic aperture radar (InSAR) is a remote sensing measuring method. SAR (synthetic aperture radar) as an observation-instrument that has gained popularity in the last 10 to 20 years (e.g. Gabriel, Goldstein, & Zebker, 1989; Rosen et al., 2000). SAR is used in several different fields to observe and measure for instance anthropogenic and natural deformation, glaciers and ice sheets as well as natural hazards e.g. landslides (e.g. Massonnet & Feigl, 1998; Rosen et al., 2000). Remote sensing techniques are increasingly used to observe unstable mountainsides to evaluate their risk (e.g. (Bozzano, Cipriani, Mazzanti, & Prestininzi, 2011; Lauknes et al., 2010) e.g. the unstable mountainside at Nordnes, Norway (e.g. L. H. Blikra & Sæther Bunkholt, 2012). InSAR can be applied by satellite, aerial or earthbound instruments. At Adjet satellite- and ground-based InSAR were put into use (see below), though only the former one is used in this study.

Data is obtained by transmitting electromagnetic microwaves and receiving their echoes from the ground in an area which lies within the line-of-sight (LOS) of the radar (e.g. GMassonnet & Feigl, 1998; Werner, Strozzi, Wiesmann, & Wegmüller, 2008)(Fig. 21). The observed area is called swath. An interferogram – an image we can see displacement on – is obtained by the comparison of at least two radar images gained by the same SAR at two different times (e.g. Pritchard, 2006; Rosen et al., 2000). Images could also be measured at the same time but with two different receivers. In this study, however, the latter method is paid no further attention. More information about different SAR methods can be found in e.g. Rosen et al. (2000). The differences between the images respectively the changes of phases of the electromagnetic microwaves provide the relative movement of the observed object in the swath (e.g. Gabriel et al., 1989; Massonnet & Feigl 1998). The data gives information about the relative

---

[5] NORUT, Forskningsparken, Sykehusveien 21, 9019 Tromsø, Norway
[6] GAMMA, Gamma Remote Sensing AG, Worbstrasse 225, 3073 Gümlingen, Switzerland

movement in the line-of-sight (LOS) from the ground to the satellite (Fig. 21), regarding to a stable reference point.
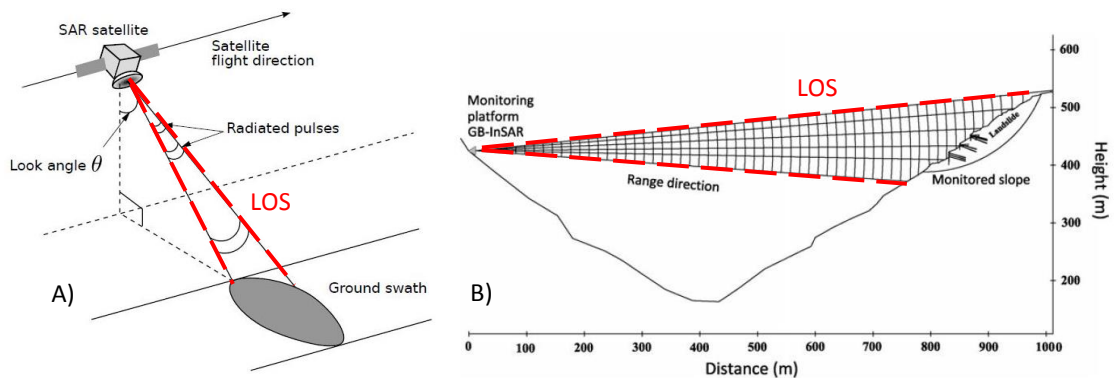
InSAR can therefore be used to study remote areas (e.g. RSF sites) without being present. It is a useful method to avoid jeopardizing humans in an unstable mountainside and to receive information about inaccessible, isolated and/ or remote areas. In addition it is an instrument independent of weather and light conditions. The swath should cover actively moving features in the RSF as well as stable features ((Werner et al., 2008; Eriksen, pers. comm.).

InSAR data is used as additional information to field work and analyses of aerial photographs linking field observations to detailed movement data (Henderson et al., 2011; Lauknes et al., 2010). InSAR gives information about surface velocities and thus changes of surface deformation in the LOS. The velocity data can range from a few cm per year (cm yr^{-1}) to m per year (m yr^{-1}) (e.g. (Kenyi & Kaufmann, 2003; Lambiel, Lugon, & Raetzo, 2000). In this study InSAR data is used to describe and analyze active mountain parts in more detail.

In the following are mentioned some of the errors of InSAR application. Velocities are only measured in the LOS thus there is no information of surface deformation which is near perpendicular to the LOS (e.g. Lauknes et al., 2010). Errors occur, further at steep mountain terrains where layover and shadows develop (e.g. H Ø Eriksen, 2013; Lauknes et al., 2010). Also, may movement be too fast to be able to be captured in two pictures (Eriksen,2015, pers. comm.). Further limitations are set by the 11-day orbital cycle of the satellite and the set wavelength. Errors may be resolved by application of different InSAR methods in combination such as ground-based and satellite-based radars (e.g. Rouyet et al., 2015).

Satellite-based InSAR data

The satellite-based radar collects data over years making it possible to compare data of several years. It is, moreover, possible to see a development of velocity rates over years. Velocity rates range from mm per year (mm yr⁻¹) to m per year (m yr⁻¹) (e.g. (Kenyi & Kaufmann, 2003; Lambiel et al., 2000). The target area is set by the flight path of the satellite and its swath width (Fig. 21). At Adjet the flight path is from ca. south to ca. north (Eriksen 2014, pers. comm.).

The data used in this study was collected by the german TerraSAR-X satellite launched in 2007 with an 11-day orbital cycle. The swath width (Fig. 21**)** is 5- 30 km (Lauknes, 2010). For more detailed information about the TerraSAR-X satellite see Lauknes (2010). The study was supplied with data collected in the summer season of a 4 years' time span (2009-2013) (Eriksen, 2014 pers. comm.). The data was computed by NORUT. Winter seasons are not included. The snow influences the echoes of the radar so strong that no movements can be measured (Eriksen, 2014 pers. comm.). In winter measurements focus on snow avalanches which are not in cluded in this study.

A ground-based radar system was installed at the Skibotn field observatory in August 2014. In this study the results of ground-based radar are not discussed, but some results, gained by Rouyet et al. (2015), have been used as additional information. The GPRI (Gamma Portable Radar Interferometer) used in this study was installed by NORUT at the Skibotn field observatory (Eriksen 2015, pers. comm.). Data was collected every five minutes within a period of 24 days in August 2014. The data was then computed by NORUT and GAMMA. The advantage of ground-based radar (GB radar) is that a specific target area can be chosen and that it offers a different looking angle to the satellite-based radar (Papke, Strozzi, Wiesmann, Wegmueller, & Tate, 2012). The radar is stationary, installed by the user who is interested in data of a specific area at a chosen time period. In addition, is the sampling rate also set by the user. The resolution is thus higher than of satellite-based InSAR providing us with velocity rates of cm per day (cm d⁻¹) instead of mm per year to m per year (see above) (Eriksen, 2015 pers. comm.).

3 Bedrock geology in the study area

3.1 Introduction

Analysing bedrock geology is not a major part of this study but is included to document lithology in the RSF and its source area, and to show how it relates the RSF as source area. Thus, bedrock lithology, folds, faults and fractures found in the study area are introduced. Field observations are used, both (1) to add lithology information to the pre-existing bedrock map by NGU, and (2) to illustrate the derivation terrain of the RSF area by structural elements. More information about structural elements can be found in Bakkhaug (2015).

Figure 22 shows the bedrock terrains, *in-situ* and slide blocks, of the study side. The subdivision into different bedrock regions is described in Chapter 4.3.2.
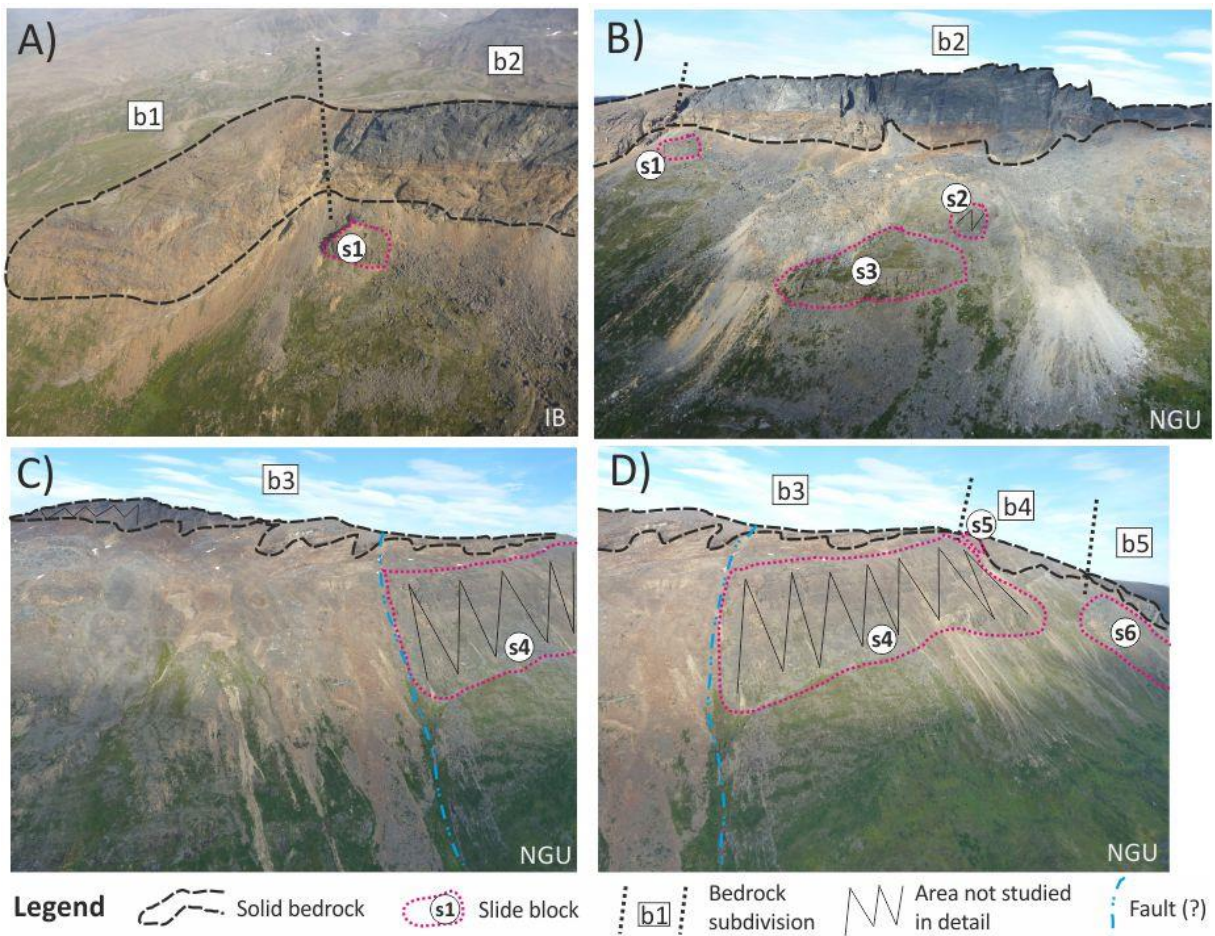

Figure 22: Photographs showing Adjet from the north to the south. Outlined are the bedrock (dashed line) and the slide blocks (pink dotted line). Aerial photographs: A) by Bakkhaug (2014), B) – D) by H. Bunkholt (2011, NGU).

3.2 Lithology

The bedrock in the study area consists mainly of garnet-mica-schists (Fig. 26). Additionally mica-schist, garnet-mica-schists with bands of hornblende and meta-arkose are found. The study area covers two different map sheets which do not exactly correspond where they meet. This may be led back to uncertainities in mapping and/ or variability in the subdivision of rock types.

In field the metamorphosed rocks, grey or rusty colored, are observed. Figure 26 includes observations during field work. The overall lithology consists of variations of mica-schists. The general mineral content of the mica-schists in the study area is composed of quartz, dark mica and white mica (Fig. 23). The variations are characterized by additional mineral compositions (e.g. garnet) and/ or variations of percentage of typical mineral content, e.g. higher quartz content. Hence, the subdivisions are concluded as quartz-rich mica-schists, garnet-mica-schist (Fig.24), and quartz-rich garnet-mica-schist.

Clearly visible in the field is a rusty layer, in the mountain wall, bedrock region b2 (Fig. 26 and 27). This layer is identified as garnet-mica-schist. Thin quartz veins (mm – cm thick) occur among the mica-schist and garnet-mica-schist successions. In the southern part of the area, in bedrock region b4 and on slide block s6, are quartz-rich mica-schists interbedded with mica-schist layers observed (Fig. 25 and 26). These individual layers are a few centimeters thick. The interbedded quartz-rich mica-schist and mica-schist succession ranges from 1202 m a.s.l. to about 1206 m a.s.l, at the ridge, region b4. The succession contains thin white quartz veins, some thin mica layers, and massive dark grey quartz layers.

Figure 23: Mica-schist, grey colored.

Figure 24: Garnet-mica-schist; brownish grey colored.
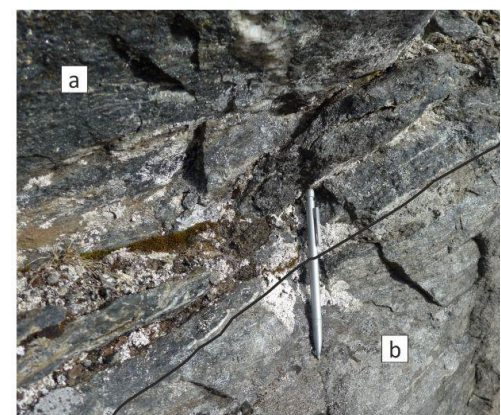
Figure 25: Interbedded mica-schist and quartz-rich mica schist layers (a), and (b) adjacent mica-schist.
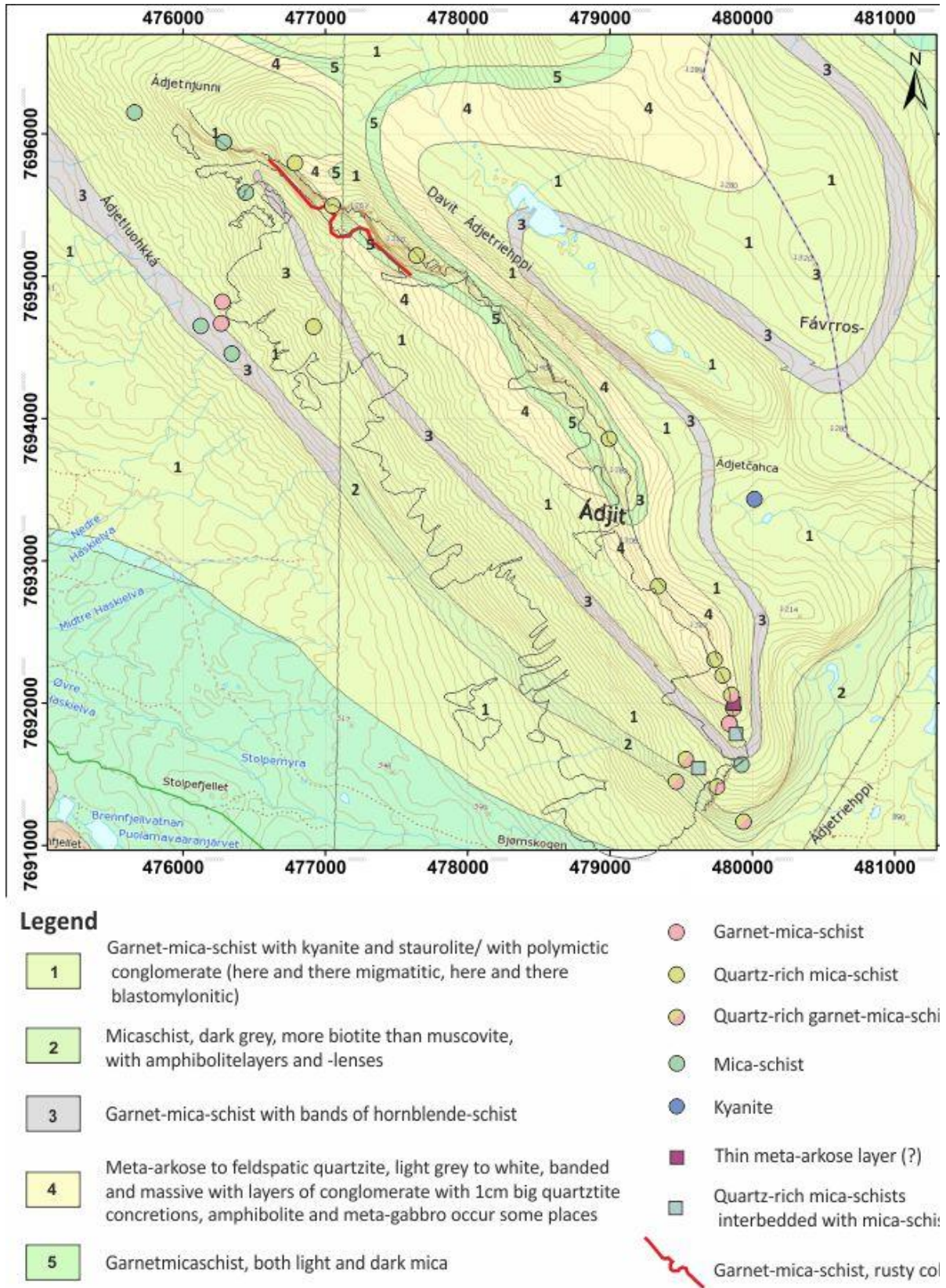
Figure 26: Bedrock map of Adjet (modified after ngu.no 2015). The map has been overlain with contours at 5 m intervals (kartverket.no) together with the outline of the RSF and the main mountain ridge (grey).

Figure 27: Garnet-mica-schist, rusty-layer.

Meta-arkose is found only as a thin layer (1257 m a.s.l. – 1293 m a.s.l.) in the south of Adjet, region b4 (Fig. 26 and 28). It is mostly white to light grey colored with big white mica crystals. Meta-arkose is also found as veins, of about 5 – 10 cm thickness, in loose boulders on the mountain slope in the north. Their source in the mountain wall, e.g. region b2, could not be found. East of the study area, at the back side of the mountain, rock fragments with kyanite are found (Fig. 29). Therefore it might be existent in the garnet-mica-schist, as NGU suggests (Fig. 26), given the assumption that it has not been displaced.

Quartz-rich mica schist is mostly found on the ridge (Fig. 26). Mica-schist and garnet-mica-schist seems to be abundant below an elevation of approximately 600 m a.s.l. The existence of conglomerate is not supported by field work results. Further, the abundance of meta-arkose is not validated by *in-situ* bedrock, only one location is marked.
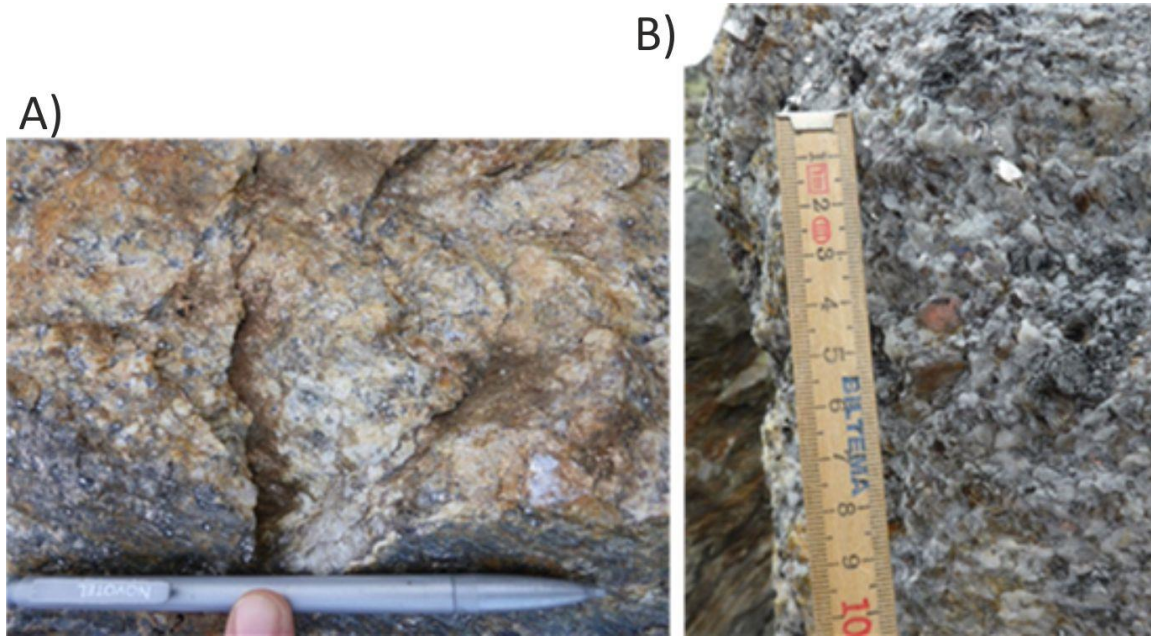
Figure 28: Meta-arkose layer: A) in-situ, in southern Adjet; B) boulder on the mountain slope, in the northern Adjet.

The general lithology at Adjet, identified during field work, conforms more or less to the lithology suggested by NGU (Fig. 26). The location of different units, however, needs to be revised on the basis of more detailed bedrock mapping.

Figure 29: Rock fragment with kyanite, found east of the study area.

3.3 Foliation

The foliation is horizontal to moderately dipping (Fig. 30). The mean dip of foliation is about 14°. The strike in the solid bedrock (Fig. 31) varies from NW-SE over NE-SW to E-W. Besides two spots (Fig.31, area 6 and 7), is found mostly relatively horizontally dipping foliation, in the north of Adjet, whereas the foliation in the south is moderately dipping. The strike and dip of the slide block s6 (Fig. bedrock overview) in the south coincide well with the foliation above at the ridge (Fig. 31, area 2, 3 and 13). Slide block s1 in the north, however, shows a different strike and dip fitting rather to the far northern parts (Fig. 31) than to the backwall. The latter (s1) is found at the foot of a steep and high mountain face (Fig. 22, A), whereas the former (s6) is rather integrated in the sloping character typical in the south (Fig. 22, D). Hypotheses to slide blocks will be given below.

Foliation orientation at the northern tip of Adjet (Fig. 31, area 10) gives the assumption of folds to be present. Folds were, however, not recognized in that particular region but at the location of stereoplot no. 8 (Ch. 3.4).

Figure 30: Horizontal to moderately dipping foliation (red dashed line). Photograph: Steffen Bergh, 2014 (pers. comm. 2014). Northern Adjet region b1 (Fig. 22).
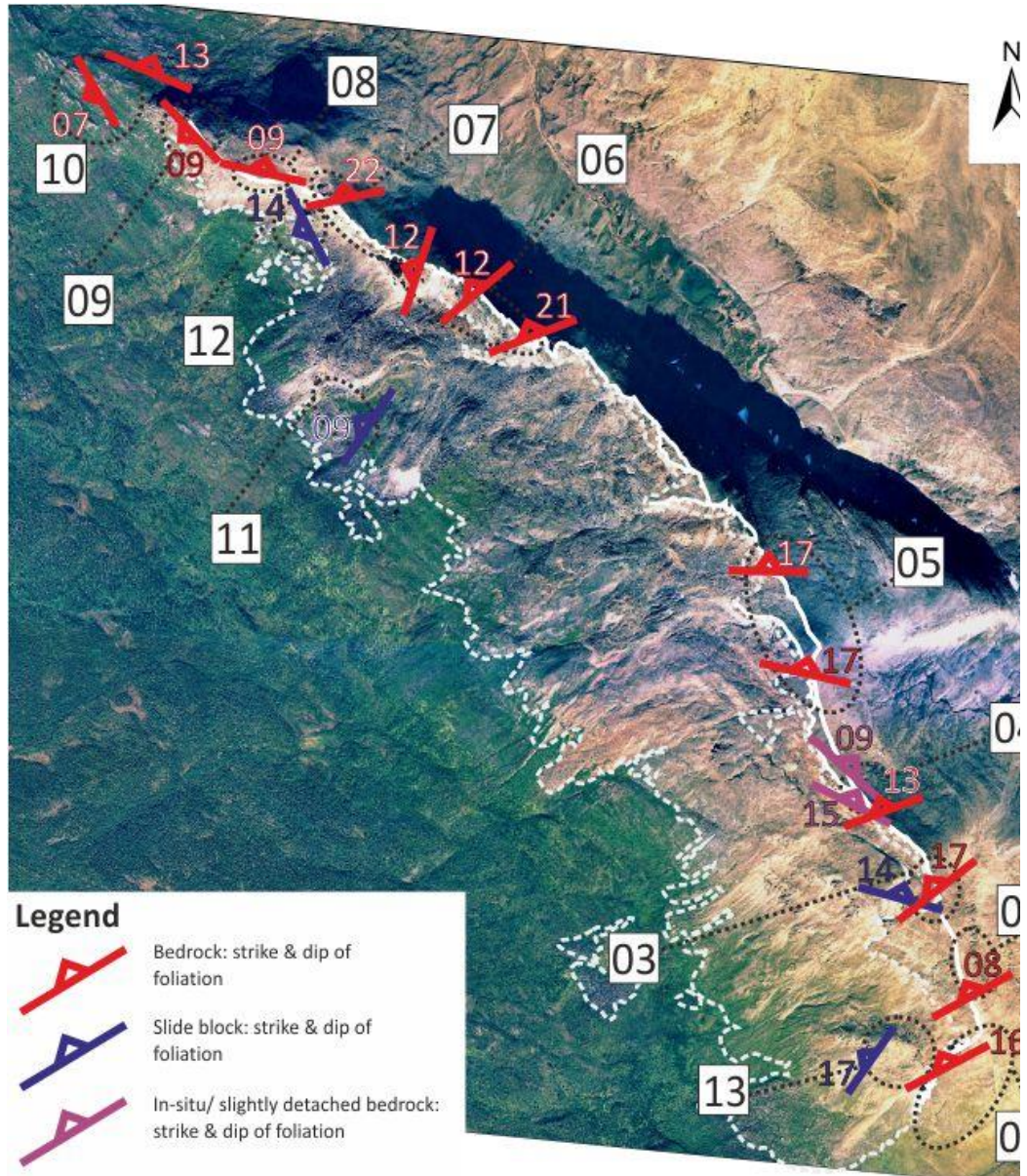
Figure 31: Bedrock foliation as strike and dip. Numbers (colored) give dip angle. Data was collected within black dotted ellipses. Numbers (within square) follow the numbering of stereoplots in Figure fractures and are used as reference in the text. Outline of the RSF (white dashed line) and mountain ridge (white line) are shown.

3.4 Folds

In region b1 (Fig. 22, A), in northern Adjet, folded foliation was observed at *in-situ* bedrock (Fig. 31, area 8). Fold limbs and, if possible, fold axis were measured and are presented in Figure 32. They are closed, upright asymmetric folds plunging southwest. Fold limbs are parallel to the mountain slope. Three different scales of folds are present: small (Fig. 33), intermediate (Fig. 33 and 34), and large (Fig. 35).

Large scale folds were observed in region b2 from distance (Fig. 35). Small scale folds could be observed sporadically. Those were mainly recognized by virtue of thin folded quartz veins within the (garnet-) mica-schists. In region b3, b4 and b5 (Fig. 22) evidence of folds was difficult to find. The only evidence for occurrence of folds in the south was the observation of one single fold in region b3, shown in

Figure 32: Stereoplot visualizing fold measurements taken in the field. Fold axis (points, n = 10) and fold limbs (contours, n = 16) are plotted.

Figure 34. It was, however, only possible to measure the approximate fold axis of 320/15, during field work, which coincides quite well with the measured fold axes in the north (b1) with a mean of 321/10.

The folds plunge southwestward towards the valley and RSF side. Fold orientations suggest that there was a NE-SW compression. The folds are supposed to have formed as a cause of Caledonian orogeny. It seems further, that the folds in b1 serve as sliding surface (Fig. 36 and 82).

Figure 33: Different scaled folds in region b1 plunging towards SW. Center photo: middle scaled fold, plunging SW. Photo in upper right hand corner: small scaled fold plunging SW.

Figure 34: Only fold (middle scaled) found at the southern ridge. Fold limbs in dashed pink line and fold axis in dotted pink line. Fold was difficult to measure; an approximate fold axis of 320/15 was measured.

Figure 35: Photograph of the mountain wall, region b2, taken from the southern ridge. It shows large scaled folds (dashed red line) and steeply dipping NE-SW (orange), NW-SE (green), and moderately dipping NW-SE (blue) fractures. In the foreground we see the upper part of the RSF area.

NNE   SSW

Sliding surface

Figure 36: Potential sliding surface along fold limbs (red dashed line). Horizontal red dashed line represents fold axis. Location in bedrock region b1 (Fig.22).

3.5 Faults and fractures

Bedrock region b1 and b2 provide good conditions for measurements. In regions b3 and b4, however, the bedrock is weathered, highly fractured, unstable, and few outcrops are found. These conditions make it difficult to decide which of the few outcrops are *in-situ* bedrock. Figure 37 shows structural measurement of in-situ bedrock and slide blocks. In this study, however, structural data from slide blocks are not included. The main orientation of faults and fractures in the bedrock are NW-SE and NE-SW (Fig. 37). Steeply and moderately dipping faults/ fractures are found.

The resulting three different main mean fracture sets are as follows (Fig. 37):

1) NE-SW steeply dipping (215/83)
2) NW-SE steeply dipping (115/84)
3) NW-SE moderately dipping (138/41)
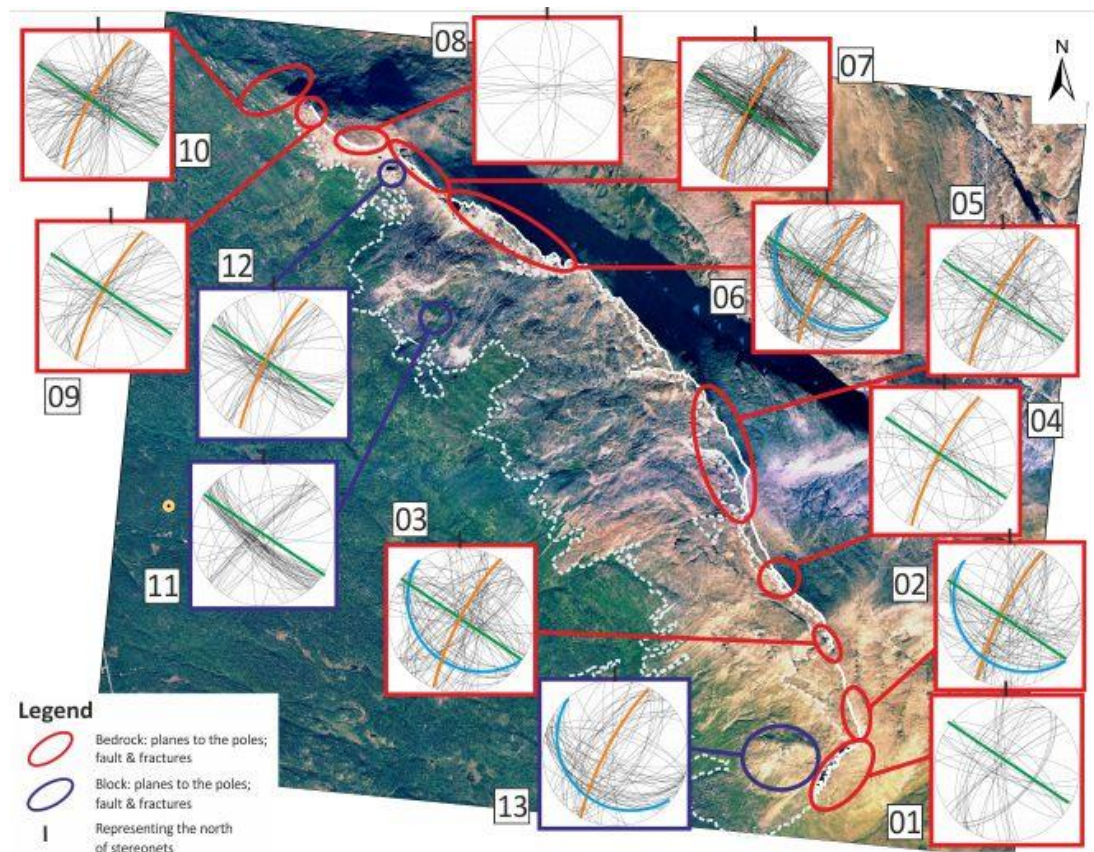
Figure 37: Faults and fractures shown in stereoplots. Colored planes show the mean fault/ fracture sets: steeply dipping NE-SW (orange), steeply dipping NW-SE (green), and moderately dipping NW-SE (blue). Yellow dot shows the location of Skibotn field observatory. Numbers are put as reference to single stereoplots in the text. Outline of the RSF (white dashed line) and mountain tidge (white line) are shown.

Steeply and moderately dipping fracture sets form conjugate fracture sets. On the steep mountain slopes and faces in the north (region b1 and b2) large fractures are abundant and clearly visible (Fig. 35 and 38).
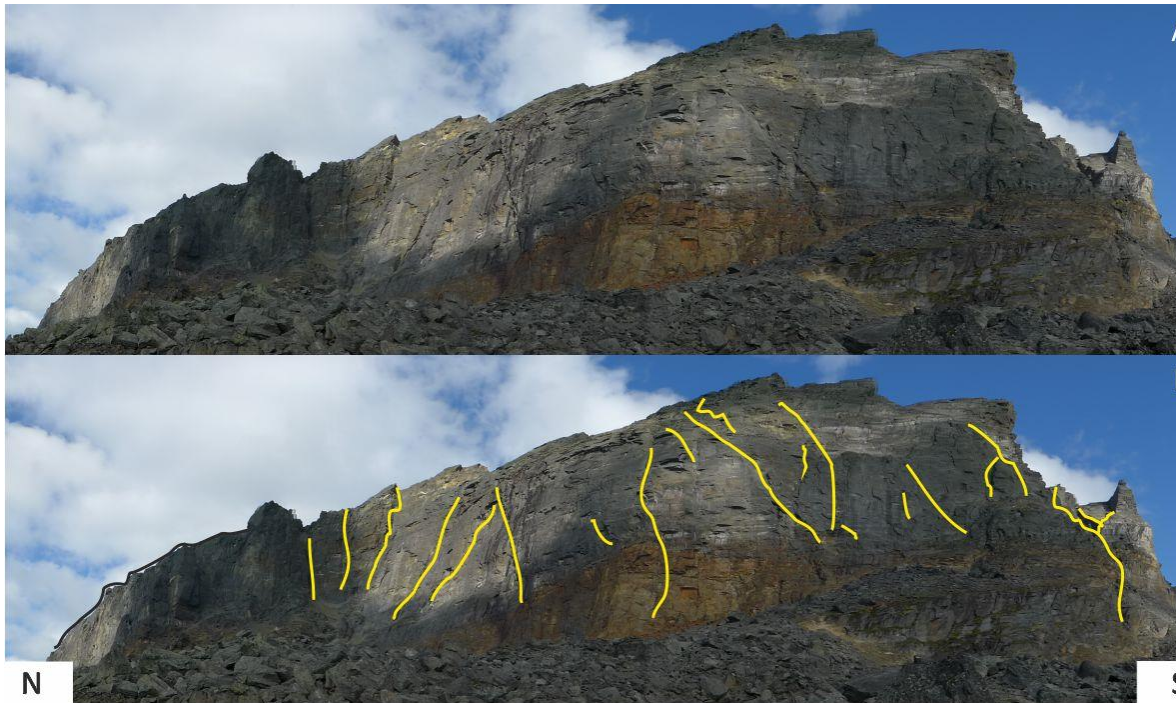
Figure 38: Bedrock region b2. Steep mountain face A) without and B) with fractures (yellow line).

Though fractures are not so distinct on more moderate slopes in the south (b3 and b4), a relation between steeply and moderately dipping fracture sets is evident (Fig. 39 and 40).

Moderately dipping faults are suggested to be the sliding surface for slide blocks s4 to s6 (Fig. 22), whereas steeply dipping fractures delimit the outline. Conjugate fracture sets delimited by steeply dipping fractures and sliding on moderately dipping fractures, can also be observed in region b2 (Fig. 83). Conjugate fracture sets are abundant in the bedrock from north to south.

In addition to sliding as a failure process, disintegration by toppling in case of slide block s1 (Fig. 22) is sugessted. Foliation of s1 (Fig. 31, area 12) shows a different strike and dip from that in the backwall (Fig. 31, area 7). Slide blocks s2 and s3 are integrated in debris fields (Ch. 4.2.4). They are therefore assumed to be part of a bigger failure event. Foliation data of s3 (Fig. 31l, area 11) coincide well with foliation data from the ridge (Fig. 31, area 6) behind the feature, suggesting mainly sliding during the failure process. There are no data for slide block s2, although it appears to form an integral part of the surrounding debris field (Ch. 4.2.4), suggesting that it may have been rearranged during the failure process.

Figure 41 shows steeply dipping fracture sets at the mountain face in region b2. They detach the rock eventually causing toppling and/ or gravity driven rockfall. Toppling and rockfall are suggested to have

occured at the steep mountain faces in regions b1 and b2. The abundance of these fractures suggests that they are likely to cause rockfall / toppling elsewhere in the mountain wall as well, e.g. region b5.
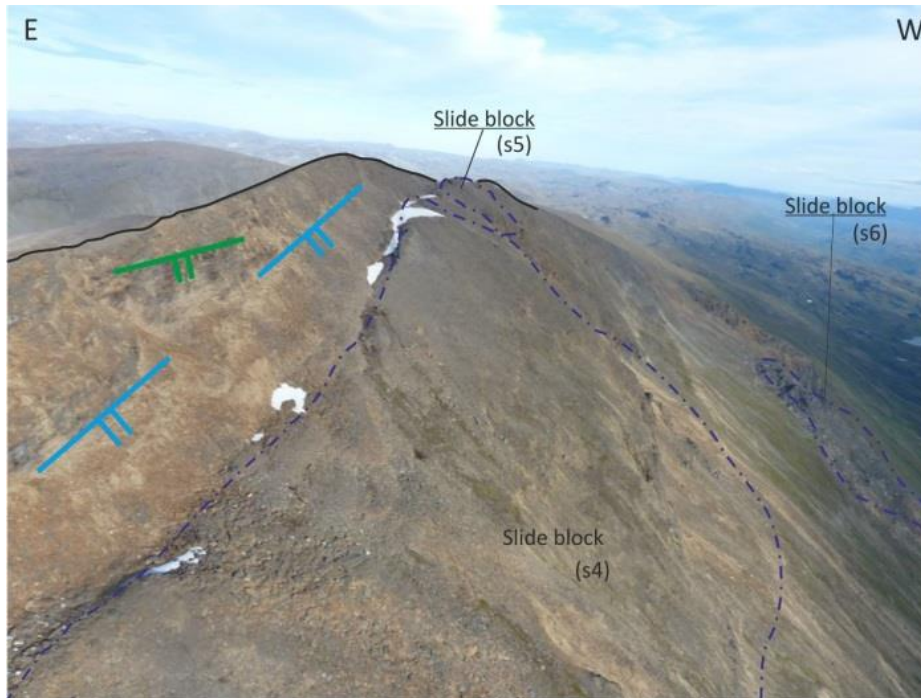
Figure 39: Southern Adjet, region b3 (Fig. 22), showing steeply (green) and moderately (blue) dipping NW-SE fractures. Data was measured at *in-situ* bedrock. Black thick line: Mountain ridge. Photo: H. Bunkholt (NGU, 2011)

Fractures have been observed to cut through Caledonian folds (see above). They coincide with the regional NE-SW and SW-NE trending lineaments in Troms, being part of the Mesozoic West Troms Basement Complex (Ch. 1.3.1 Fig. 5). Therefore it is assumed that Adjet's main fracture sets belong to the Mesozoic passive margin in Troms.
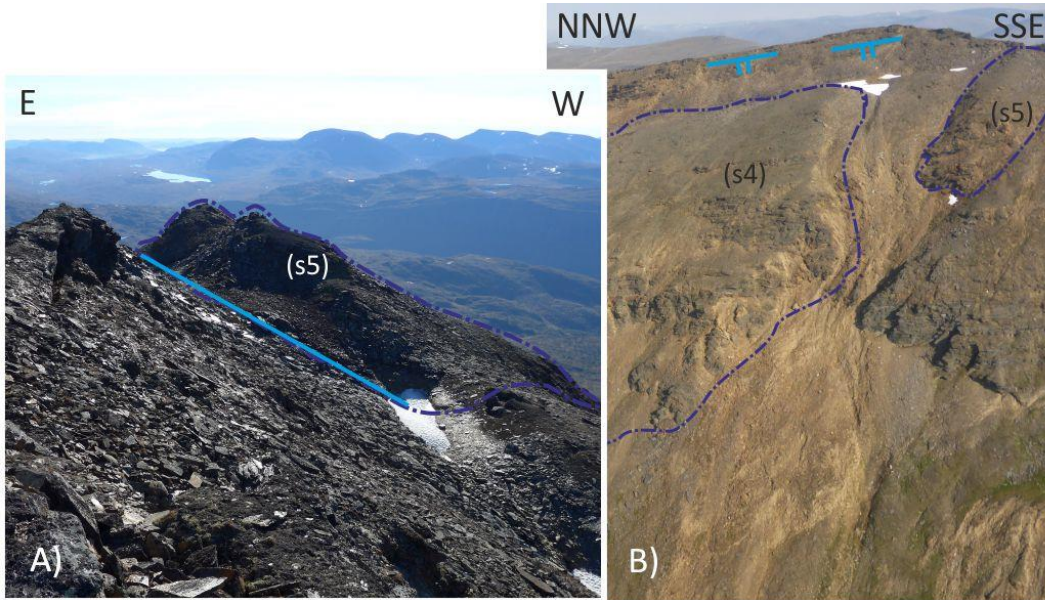
Figure 40: Bedrock region b3 and b4 (A)). Moderately dipping NW-SE trending A) fault and B) fracture (blue) are observed. Purple dashed lines outline slide blocks s4 and s5 (Ch. 4.2.4). Aerial photograph: Bakkhaug 2014.
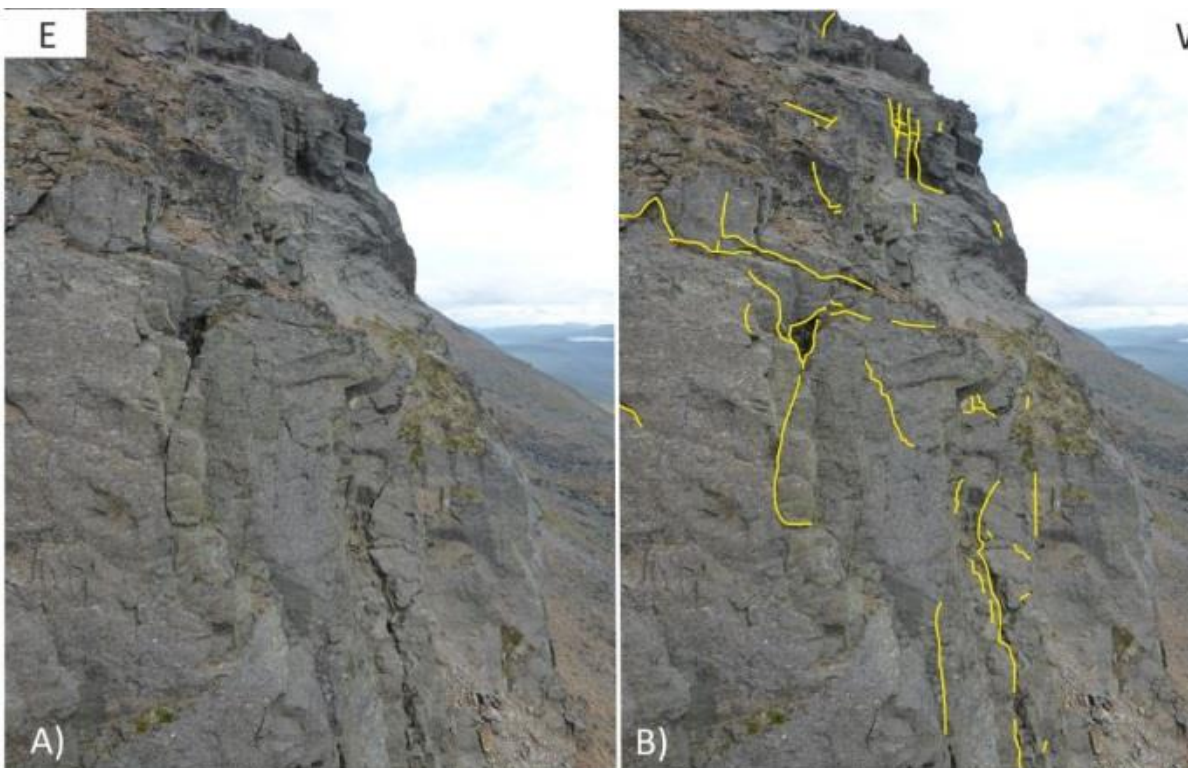
Figure 41: Highly fractured mountain wall in in region b2 (Fig. 22). Fractures (yellow lines) are marked in still intact bedrock delimiting potential rock failures through toppling or rockfall. Photo: Harald Eriksen, 2014 .

3.6   Summary

Mainly grey colored mica-schists of different mineral content are present in the study site.

Folds, faults and fractures could be distinguished as structural elements. Folds are mainly distinguished in region b1. Fold limbs are parallel to the hillside, plunge towards SW, and seem to provide a sliding surface, in the northern part of Adjet, region b1. Steeply dipping NW-SE and SE-NW dipping fractures and NW-SE moderately dipping fractures are abundant, and form conjugate fracture sets. They detache the rock so that failure such as rockfall, toppling, or sliding may occur. Conjugate fracture sets are abundant on the whole length of the ridge. Slide blocks are suggested to be influenced by different failure processes such as toppling (s1), and sliding (s4 – s6). Rockfall and toppling are mainly found in bedrock regions b1 and b3, due to its steep mountain face. Thus, fracture sets and folds influence the bedrock as source area, detaching rock and eventually causing rock failure.

4 Geomorphological elements in the rock slope failure area

4.1 Introduction

The RSF area extends laterally for about 5 km (width) and about 2 km (length) downslope below the Adjet mountain ridge (ca. 1400 m a.s.l.). The outline of the RSF ranges from about 500 m a.s.l. to ca. 1340 m a.sl. The RSF area is divided into province A, the northern part, and province B, the southern part, to better describe the area (Fig. 42). The general gradient varies between 25° and 40°. Vegetation changes with elevation. Lichens and other alpine vegetation can be found over approximately 700 m a.s.l. Below 700 m a.s.l. vegetation is lusher, with bog, ferns and small trees, mostly birch. Below about 400 m a.s.l. conifer and other ever green trees are found. Between elevation 400 m a.s.l and 500 m a.s.l. a gently dipping (W/NW) slope, in the north, with an uneven staircase-like morphology is apparent, and probably due to glacial erosion . Outcropping bedrock found at this elevation is glacially smoothed. Above 500 m a.s.l. the mountain slope becomes steeper.

Figure 42 shows the geomorphological elements distinguished in the RSF area. According to those investigations the area was subdivided into the following geomorphological elements: Talus fan deposits (Ch. 4.2.1), debris fields (Ch. 4.2.2 and 4.3.1), rock glaciers (Ch. 4.2.3), slide blocks (Ch. 4.2.4), moraine (Ch. 4.3.2) and solid bedrock (4.2.4 and 4.3.3). Further, is found a great amount of boulders, scattered across the mountain slope. The different elements and how they were distinguished is described in more detail below.

Viewing Figure 42 a difference between province A and province B attracts the eye. Province A is dominated by debris field deposits and rock glaciers, whereas province B is dominated by talus fan deposits as well as slide blocks. The two provinces are divided by an east northeast - west southwest striking fracture lineament thought to be a fault.
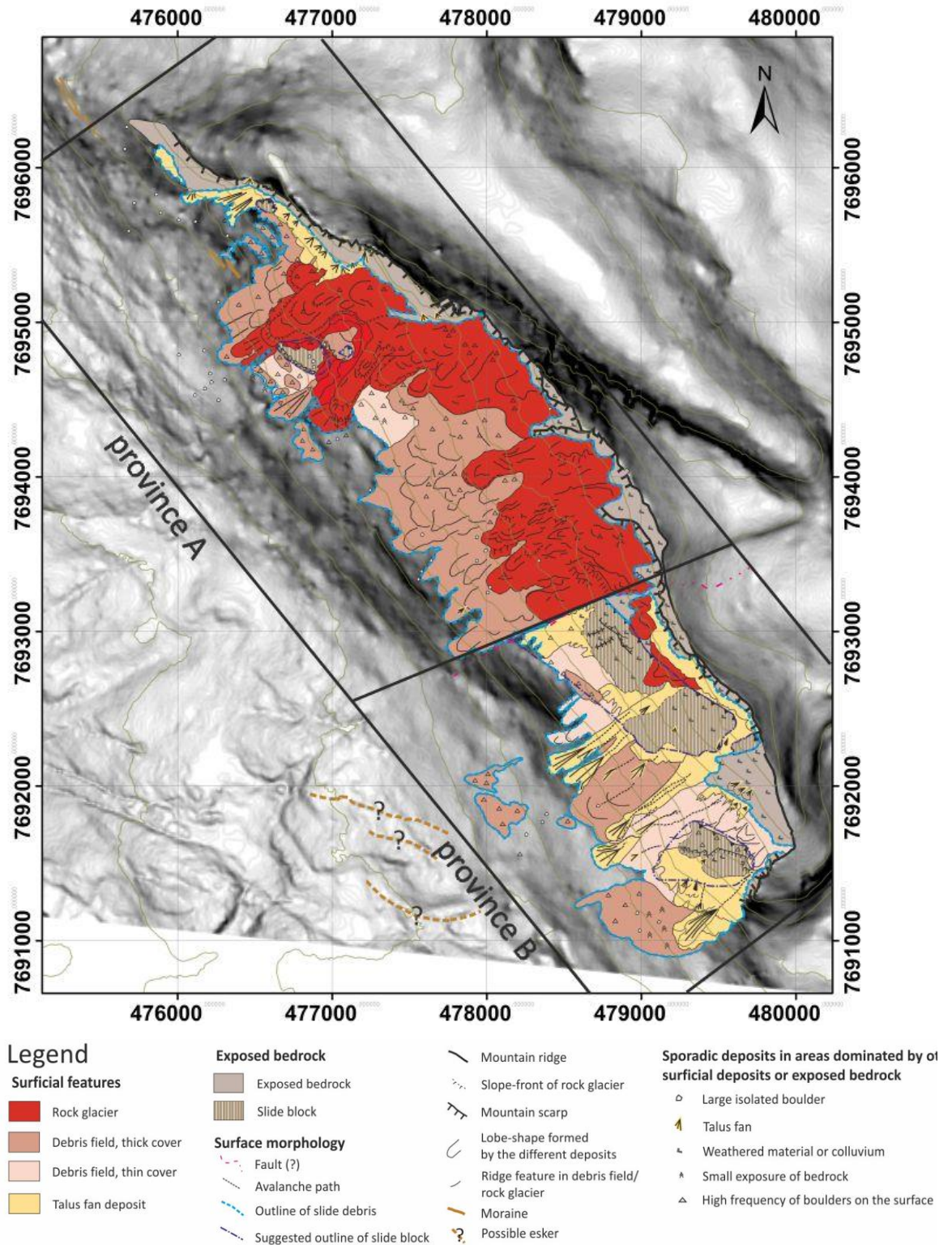
Figure 42: Map showing geomorphological elements. DEM (resolution 10 x 10m) and contour lines (100 m) are provided by NMA (kartverket.no/ norgedigitalt.no). Shading is set from 0 (white) to 80 (black).

In the north and south of Adjet towards the valley Skibotndalen, moraines and eskers can be observed (Figure 43). Eskers in province B were determined by picture analyses whereas the moraines in northern Adjet were observed throughout field work (Fig. 42). The moraines are vegetated and show few scattered boulders. Moraines are found at a maximum elevation of about 600 m a.s.l. The elevation suggests that the moraines coincide with the elevation for moraines in the Lyngen peninsula around the Younger Dryas (Ch. 1.3.3, (cf. Greig, 2011)).

The probable eskers are as such defined by their angle towards the valley and their curved to slightly curved character (Fig. 42).

Figure 43: Photographs showing the moraine in the very north of Adjet. The upper photograph showing a close-up in the moraine ridge.

Some of the geomorphological elements are numbered in the individual subchapters. This way it is easier to refer to them in the text. Abbreviations are as follows: 't' for talus fan deposits, 'dT' for debris fields thick cover and 'dt' for debris fields thin cover, 'r' for rock glaciers, 's' for slide blocks, and 'b' for bedrock.

4.2 Geomorphologic elements in the RSF area

4.2.1 Talus fan deposit

Features emplaced cumulative over time by surface mechanisms of different slope processes (Leeder, 2011) and not by the more deep-seated or large-scale RSF, are defined as talus fan deposits (Fig. 44).

The material ranges from fine grains (sand, maybe silt) to large boulders. Fine material consists of mica and probably other smashed fragments of the bedrock schist, evolved by blocks crushing into each other or due to weathering.

Talus fan deposits are derived by different surface mechanisms depending on the location where they are found. Locations are in the vicinity of the mountain scarp, debris fields or slide blocks. Generally speaking they are

Figure 44: Geomorphological elements of the RSF. Talus fan deposits discussed in chapter 4.2.1 are numbered t1 – t6. Aerial photograph provided by NMA (kartverket.no).

derived either from the backscarp of the RSF or though post-slide processes on the RSF itself. Where talus fan deposits play a minor role within another geomorphological feature, only the larger fans have been marked. Such are within debris fields (dT7, dT9, dt4, Fig. 50), adjacent to bedrock scarps, and on top of bedrock (province B, b4 Fig. 70).

Lars H. Blikra & Nemec (1998) summarized depositional processes and facies of colluvial fans, here referred to as talus fan deposits (Fig. 45). Following their example rockfall, meltwater / slush (waterflow), snow avalanche (snowflow), and debrisflow derived fans are distinguished. In this study the facies of the fan deposits was not thoroughly treated.

Rockfall derived talus fans are found where the deposits are below steep mountain scarps as deposit t1 in Figure 47 exemplifies (see also Fig. 44). These deposits are often fan shaped with the largest boulders having moved farthest down slope while boulder size decreases uphill (Fig. 46). Also snow avalanche derived talus fans (Fig. 46) show this characteristic. This is in contrast to the unsorted snowflow deposits Lars H. Blikra & Nemec (1998) describe. The linear avalanche

path, however, suggests a snow avalanche. Further, the possibility of a rockfall derived talus for t6 is eliminated, because no steep mountain scarp is found at the beginning of the path. The source area seems to be rather the debris field dt4 (Fig. 42 and 44).

Meltwater / slush avalanche path form small channels with several side arms (Fig. 49). Meltwater / slush and snow avalanche talus fan deposits are found in province B below slide blocks and in the vicinity respectively covering debris fields.

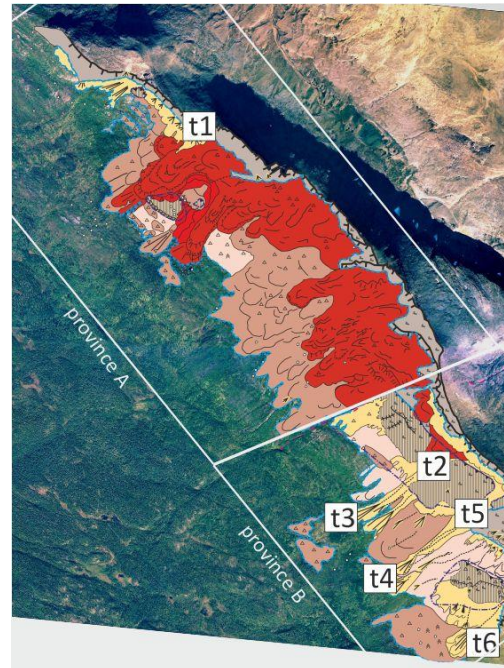| SEDIMENTARY FEATURES	DEPOSITIONAL PROCESSES			
	rockfall/debrisfall	debrisflow	snowflow	waterflow
		AVALANCHES		
TYPE/GEOMETRY OF DEPOSITS — three-dimensional view	Fresh rock debris; Resedimented gravel; Upslope fining; Varied runout; Scattered clasts; Lobate or "patchy" accumulations of debris; scattered large "outrunners"	Relatively broad lobes; Highly elongate, tongue-shaped lobes (upslope fining); Levées; Spill-over lobes; High-viscosity debrisflow; Low-viscosity/watery debrisflow	Toolmark grooves; "Debris horn"; Longitudinal grooves, debris ridges & clast-thick levées; One clast-thick levées; "Debris shadow"; "Patchy" lobes; Scattered clasts; Drier snowflows; Slushflow; Lens with sandy downslope "tail"	Levées of bypassing debrisflows; Small "digitated" lobe with frontal wash-out sand; Overbank sand; Narrow, gully-type channels; or shallow channels with braid-bars
vertical cross-section	Upward fining; Openwork; Infilled by "tail"; Upward fining; Openwork	"Imbricate" beds; Tabular beds; Large "floating" clasts	Lenticular beds with "imbricate" or more complex stacking; Indistinct boundaries; Melt-out clasts in precarious positions; Stratified waterlain infill of larger interstices; Redeposited humic soil; Waterlain infill	Remnant debrisflow deposits; Tractional infill; Isolated channel-fills (up to 1.5 m thick)
TEXTURE AND STRUCTURE	Highly immature debris; mainly angular clasts. Mature debris; subrounded to rounded clasts. Boulder to sand size grade. Clast-supported and commonly openwork, with pebbly to sandy infill at the top. Deposits often infilled with waterlain sand and/or redeposited soil material.	Matrix-rich to clast-supported. Sandy/muddy matrix. Common "coarse-tail" inverse grading and outsized cobbles or boulders.	Clast-supported, bouldery to cobbly "heads" and clast- to matrix-supported, pebbly upslope "tails". Common normal grading.	Unsorted, scattered clasts and gravel "patches" infilled with waterlain sand or pebbly sand. The sand in large interstices shows stratification, but is massive, very fine/silty and possibly shell-bearing in submarine deposits.	Clast-supported, pebbly to cobbly gravel interlayered with poorly sorted/stratified sand. Matrix-supported gravel occurs as debrisflow remnants.
CLAST FABRIC	Boulders and large cobbles often show "rolling" fabric, a(t) or a(t)b(i), when emplaced frontally in isolation. Many large clasts upslope show "sliding" fabric a(p), but a disorderly "adjustment" fabric predominates; "shear" fabric a(p) often typifies the avalanche's overriding tail, when evolved into a grainflow.	Large clasts mainly aligned downflow, a(p) or a(p)a(i), but showing a(t) orientation along the lobe front.	Common "rolling" fabric a(t) in the frontal and top part of the debrisflow head; common "shear" fabric a(p) or a(p)a(i) in the flow's tail.	Mainly disorderly (chaotic "melt-out" fabric). Boulders and cobbles deposited from turbulent snowflows may have "rolling" fabric a(t), but the scattered debris is vulnerable to rotation by subsequent avalanches. Dense snowflows and slushflows may create "shear" fabric a(p), but this loses order during the melt-out.	Common tractional fabric, poorly developed in gullies due to clast pivoting and adjustment to banks. Many large clasts are rotated in situ to a(p) position by less competent waterflow.
DEBRIS SOURCE	Weathered bedrock.	Glacial till and valley-side kame terraces.	Glacial till, kame terraces and upper-slope colluvium.	Glacial till and upper-slope colluvium, including fresh bedrock. Common slope-soil erosion.	Upper slope colluvium and glacial till.

Figure 45: Depositional processes and facies of colluvial fans, here referred to as talus fan deposits (Lars H. Blikra & Nemec, 1998).

Debrisflow derived fans at Adjet do not show specific sorting of grain size (Fig. 48). The fans are immature. Boulders are scattered all over the fan. At the fan front, however, they are absent and finer material dominates, similar to fans observed elsewhere in the region (cf. Dyrvik, 2014). Figure 49 shows examples of talus fans with both, debris derived fans at the upper part of the mountain slope, and meltwater / slush and snow avalanche derived fans at the bottom. These deposits are in the vicinity or covering slide blocks present. In the case of t2 could the rock glacier r10 (Fig. 53) be the source area. Fan t5, however, might originate from talus fan deposits below the Adjet mountain ridge.

Figure 46: Talus fan deposit t6 (Fig. 44) derived by snow avalanche. Increase of grain size is shown by enlargement of polygons. Photograph was taken downslope from the mountain top. Snow avalanche path (black dashed line) and fan (thin black lines) are illustrated. In the right hand side corner is an illustrative sketch of grain size distribution in the fan.

Figure 47: Rockfall derived talus fan deposit t1, province A (Fig. 44). Fan is illustrated by black lines. Aerial photograph: Iselin Bakkhaug 2014 and modified according to geomorphological elements.

Figure 48: Debris flow derived talus fan deposit t5 (Fig. 44). Fan is illustrated by black lines. Part of an aerial photograph (Bakkhaug 2014) and modified according to geomorphological elements.
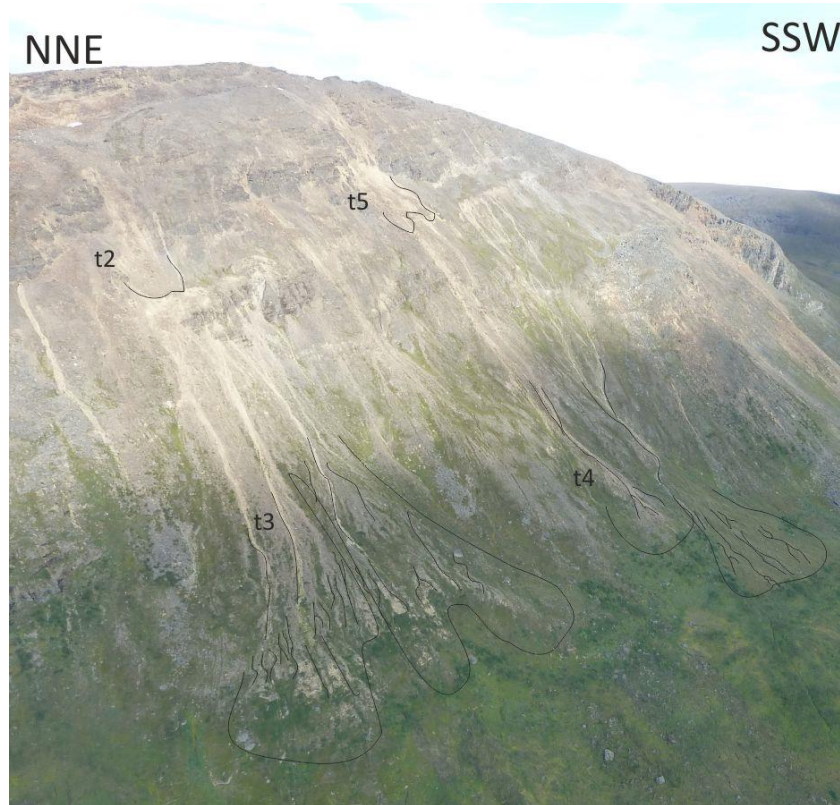
Figure 49: Meltwater / slush and debris flow derived talus fan deposits t2 - t5 (Fig.44). Fan outlines and debris flow/ meltwater / slush channels are illustrated by black lines. Fans t2 and t5 are debris flow derived, whereas t3 and t4 are meltwater / slush derived talus fan deposits. Aerial photograph: H. Bunkholt 2011 (NGU) taken from helicopter; modified according to geomorphological elements.

4.2.2   Debris fields

The term debris field is used to describe areas of the RSF which are comprised of or covered by large boulders emplaced by large-scale slope failure. Debris fields are observed as undulating terrains with lobate features both within and outlining the debris field, and scattered boulders on surface. The lobes are vegetated by moss, lichens and other alpine vegetation, even here and there with small birches.. Talus fan deposits are surficial, relatively fresh derived and are, therefore, mapped as a separate category. Rock glaciers are, also, distinguished in a separate category, for further explanation see chapter 4.2.3. Debris fields are found as thinner or thicker debris cover over the whole RSF site (Fig. 42 and 50). As thicker debris cover are defined those areas, which are assumed to cover the bedrock underneath by at least one to two meter and/ or show a great amount of large boulders on surface (Fig. 51). On the contrary, show thin debris fields lesser boulders and an estimated thickness of around one meter (Fig. 52).

Thick debris fields are mainly identified in province A and thin covered debris fields in province B (Fig. 50). An association of thick debris field and rock glacier indicated by their location and their boulder nature is presented in chapter 4.2.3 and 6.

Lobes suggest a downslope transport of debris material. The material for debris field is assumed to have been generated by collapse of large parts of the Adjet mountain ridge, perhaps even throughout several collapse phases (Ch. 6). Energy set thus free would lead to disintegration of rock material and downslope movement. Lobes then can be formed either (1) slowly by creep or (2) rapidly by sturzstrom from initial collapse.

Figure 50: Geomorphological elements of the RSF. Debris fields, thin (dt) and thick (dT) covered, are numbered. Aerial photograph provided by NMA (kartverket.no).

Sturzstrom landslides in alpine regions or regions influenced by glaciation have been described by several authors (among others Dawson et al. 2010, Ballantyne 2003, Mercier et al. 2012, Pollet & Schneider 2003). It is a scenario that might have happened at Adjet, being an alpine and glacially influenced region. The rock waste, apparent today, would thus have been deposited in one, or possibly several, big events. These are indicated by the many lobate features found in the RSF area, which seem to superimpose or spread in succession as seen in Figure 52. These might be interpreted as transverse ridges generated by creep. Such features are also present at other debris fields: dt3, dT3, dT7, and dT9 (Fig. 50).

Considering the above, the RSF at Adjet might initially have been affected by a rapid sturzstrom, after which others followed and eventually slow creep occurred which developed transverse ridges (lobes) (Fig. 52). This is, if several RSF events have occurred. The evolution of the RSF at Adjet is discussed in more detail in chapter 6.4.

Figure 51: Thick debris field dT7 (Fig.50). Aerial photograph: H. Bunkholt 2011 (NGU), taken from helicopter and modified according to geomorphological elements.
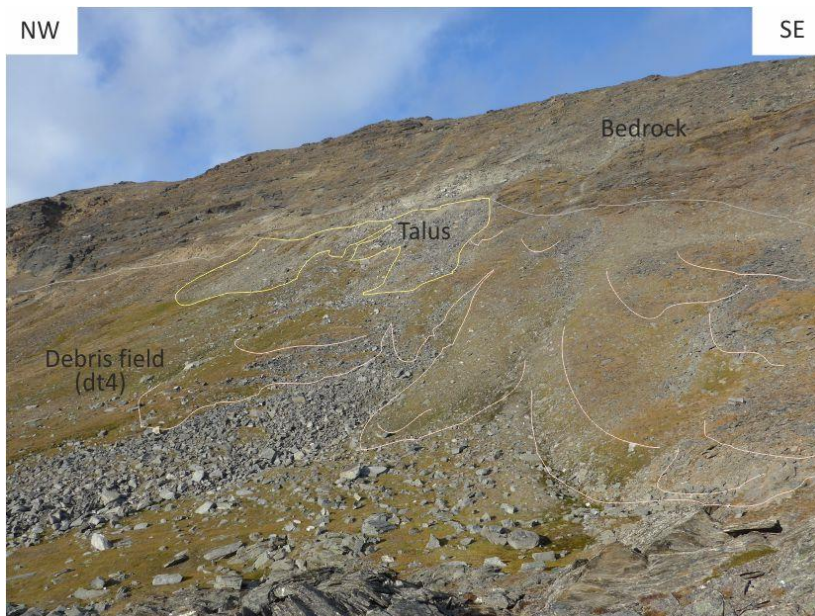
Figure 52: Showing thin debris field dt4 (Fig. 50). Lobes are marked by pink lines. Talus fan deposit is outlined with a yellow line and the bedrock is seperated by a grey line.

4.2.3 Rock glaciers

Rock glaciers were identified on the basis of their geomorphological features, e.g. transverse ridges and furrows, and lobes, compared with rock glacier descriptions in the literature (e.g. Ikeda, Matsuoka, & Kääb, 2008; Wahrhaftig & Cox, 1959). Most literature describes rock glaciers to be adjacent to or evolved from present glaciers e.g. (Griffey & Whalley, 1979; Wahrhaftig & Cox, 1959; Whalley, a, Geography, & Wallis, 1979). There are, however, no glaciers found at Adjet. Humlum (1998) and Rignot (2002), on the other hand, describes that rock glaciers may exist without the presence of a glacier, e.g. derived from thick talus

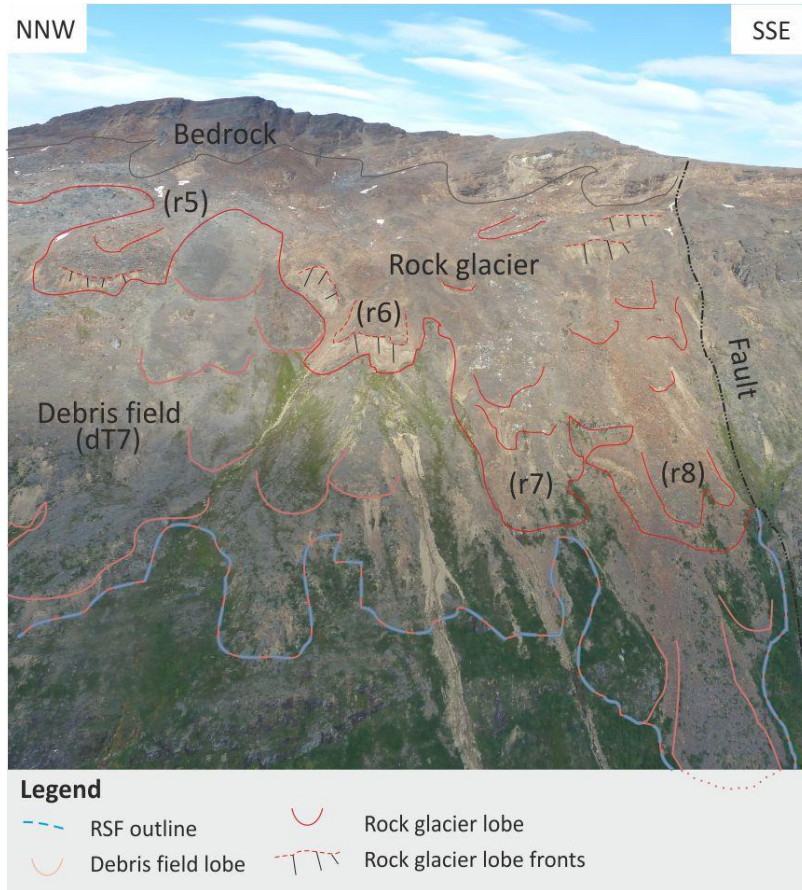**Figure 53: Geomorphological elements of the RSF. Rock glaciers are numbered. Aerial photograph provided by NMA (kartverket.no).**

(Greig, 2011). Regarding the many similarities of geomorphological features described in this subchapter and rock glaciers described by others, it is concluded that mentioned features are rock glaciers (Fig. 53). Rock glaciers occur in alpine terrain and permafrost regions (e.g. Holmes, 1965; Ikeda et al., 2008; Springman et al., 2012). Where rock glaciers occur slope angles of valley sides are between 30° and 40° (P. G. Johnson, 1984), which agrees with the overall mountain slope at Adjet .

Rock glaciers are a mixture of debris and interstitial ice or have an ice core (e.g. Humlum, 1996; Ikeda et al., 2008; Wahrhaftig & Cox, 1959). At Adjet ice cannot be observed but the many similarities of relief morphology at rock glaciers at Adjet and those described in literature, e.g. transverse ridges and furrows and steep frontal/ lobe slopes, ice is assumed to be present. Interstitial ice is presumably below a certain layer of debris and may be discovered by digging into the rock glaciers. This has not been done at Adjet. The blocky nature of rock glaciers and debris fields are similar, which could be grounds for mapping them as a single category. However, the steep active slopes,   presence of transverse ridges and furrows, and the movement indicated by InSAR velocity data (Ch. 5), in areas interpreted as rock glaciers, provides
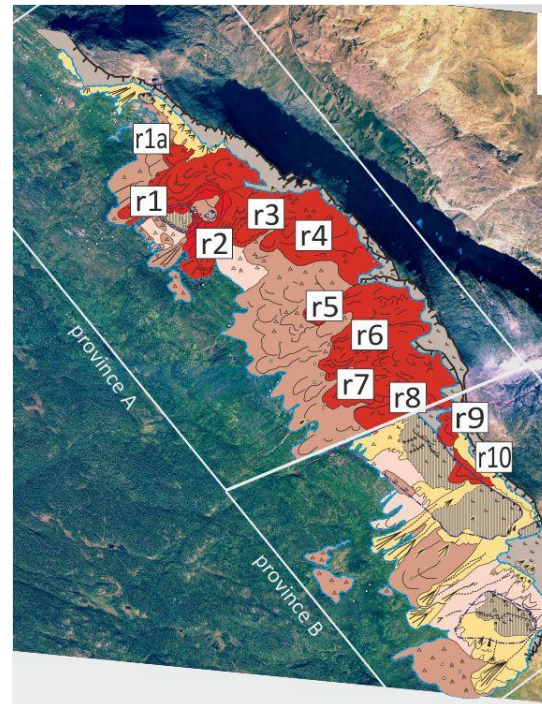
a basis for distinguishing rock glaciers as seperate category. Also, the areas mapped as rock glaciers, foremost those observed in field, contain scattered vegetation (moss, lichens) patches, whereas most debris fields show a more established vegetation cover (Ch. 4.2.2). No or little indication of movement was discovered on debris fields, concluded from InSAR velocity data, whereas the rock glaciers showed not only indication of movement in the field, e.g. rockfall activity, but also in the InSAR data (Ch. 5). Movement indicators/ velocity will be described further in chapter 5 and 6.3. The rock glacier fronts and steep sides trigger boulder fall similar to that occurring on talus fans. However, these parts are classified as rock glaciers for mapping purposes, because they are thought to still be a part of the rock glaciers, e.g. fronts of r1 and r2 (Fig. 59). Active and inactive rock glaciers are described in the following in sections.

Active rock glaciers

This chapter is divided into separate sections describing general features: General description, source, structure, texture, interstitial ice and weather.

General Description

Rock glaciers at Adjet are found mostly in province A (r1 – r8). They are prominent lobate or tongue-shaped geomorphological features, consisting of heterogeneous bedrock debris. They are orientated downslope indicating flow towards the west to southwest (Ch. 6.3).Tongue-shaped rock glaciers are longer than they are wide and lobate rock glaciers are wider than long (Wahrhaftig & Cox, 1959). Regarding this classification rock glaciers r1 – r3, and r5 are tongue-shaped, whereas rock glaciers r4, r9, and r10 are lobate rock glaciers (Fig. 42). The remaining rock glaciers and r6 – 8 are, however, not easily categorized. They are suggested to be rather tongue-shaped than lobate-shaped rock glaciers. Wahrhaftig & Cox, (1959)suggest that tongue-shaped rock glaciers are a mature stage of rock glaciers, evolving by flow. Therefore, it may be suggested, that r6 – r8 have been lobate rock glaciers that evolve into tongue-shaped rock glaciers. Also rock glaciers r4 and r10 show signs of evolving into tongue-shaped rock glaciers. R10 establishes a tongue downslope in the middle and r4 at its northern end (Fig. 42).

The part of the rock glacier adjacent to the backwall is referred to as head and the frontal part as front. Rock glaciers occur below steep but not necessarily high wall faces. The highest wall faces are found in province A at the head of r1 and r2. The lowest headwall is also found in province A, headwall of r4, and is approximately 3 m high. Wahrhaftig & Cox (1959) described vegetation on top of rock glaciers as a continuous cover which differs from the observations at Adjet. Rock glaciers are, as mentioned above, only here and there vegetated. Rock glaciers r9

68

and r10 show no vegetation at all. The latter are relatively small compared to the other rock glaciers at Adjet. They may, therefore, be relatively younger. Characteristical morphological features of rock glaciers are transverse ridges and furrows, lobes, and shallow depressions at the head of a rock glacier (Wahrhaftig & Cox, 1959; Humlum 1996). Those have been recognized at Adjet. Figure 54 shows similar morphology as rock glaciers at Adjet (e.g. Fig. 59). Lobes are tongue-like features with steep, barren fronts and sides. They look like new small rock glaciers on top of another older one, suggesting reactivation (Wahrhaftig & Cox, 1959). This feature can be observed at rock glaciers r1, r2, r6, and r7 (Fig. 42). Steep frontal slopes and cracks within the lichen cover (Fig. 55 and 56), also referred to as lines of tearing by Wahrhaftig & Cox, (1959), are indicators for rock glaciers to be active (Ch. 5).
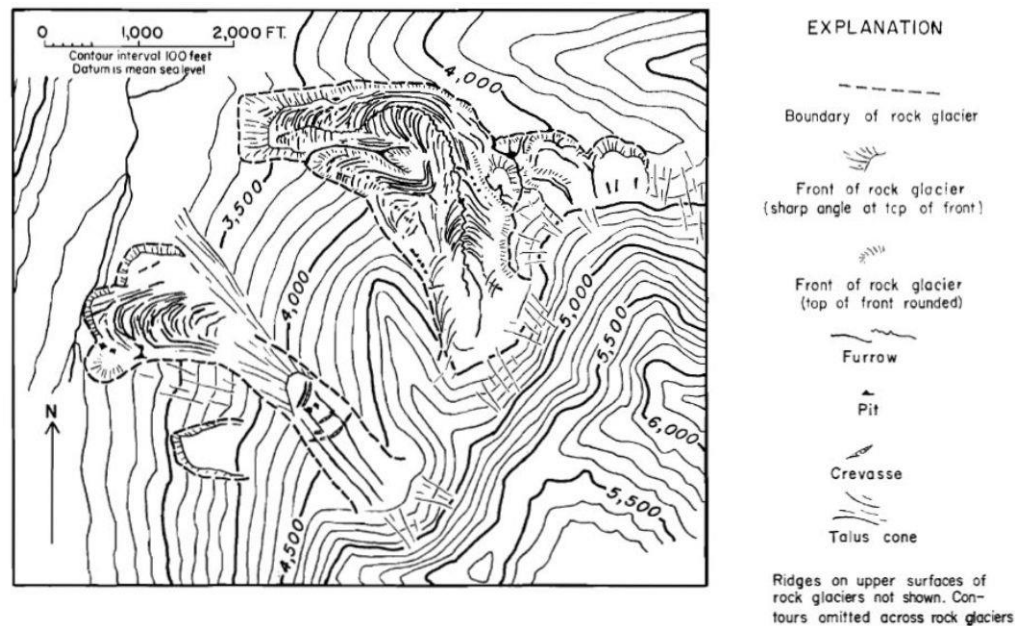
Figure 54: Map showing transverse ridges and furrows at the Alaska Range (Wahrhaftig & Cox (1959).

Source

Debris material present in the rock glaciers is derived from the backwall and thus of the same lithology. Debris material of the rock glaciers can derive from different processes, such as (1) debris-laden snow avalanches, (2) episodic rock avalanches and (3) long-lasting rockfall activity (Haeberli et al., 2006) It is suggested that rock glaciers at Adjet derive their debris material mainly from (2) episodic rock avalanches (Ch.6). This is, however, not included in this study.
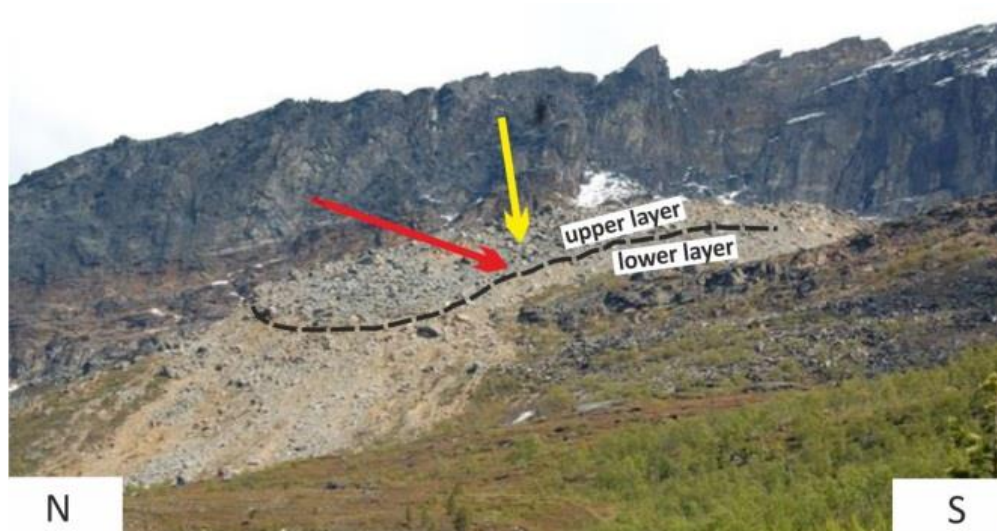
Figure 55: Location of height estimations (red arrow) and location of a line of tearing (yellow arrow) displayed in Figure 56 and 57. Black dashed line devides the upper and the lower layer of the rock glacier. Picture taken by Eriksen (2014).

Structure

The rock glaciers at Adjet appear to be fairly thin (about 10 m thick; Fig. 57) compared to rock glaciers studied elsewhere e.g. on Disko Island (20 – 100 m thick; Humlum, 1996), or Alsaska range (15 – 120 m; Wahrhaftig & Cox 1959). Rock glaciers are described in literature as being structured into two layers, (1) the upper or surface layer consisting dominantly of boulders, and (2) the lower layer consisting of a mixture of boulders and finer material (Wahrhaftig & Cox, 1959; Johnson, 1984). Whereas, Wahrhaftig & Cox (1959) suggest the upper layer to be one quarter of the lower layer, describes Johnson (1984) a 1 m

Figure 56: Crack / line of tearing in the vegetation layer of r1 (Fig. 53). Location is marked with a yellow arrow in Figure 55. Scale is a glove (left of crack) with a length of about 20 cm.

thick upper layer. The surface layer at Adjet is suggested to be about 2 m thick and the lower layer ca. 8 m thick, giving a total thickness of the rock glacier of about 10 m. The upper layer is, hence, one-quarter of the thickness of the rock glacier and therewith in accordance with the general assumption of Wahrhaftig & Cox (1959). The approximation of 2 m for the surface layer

70

was estimated by comparison of a scale, the height of the glacier and the presence of fines (gravel, sand, silt) at the steep slope (Fig. 57).
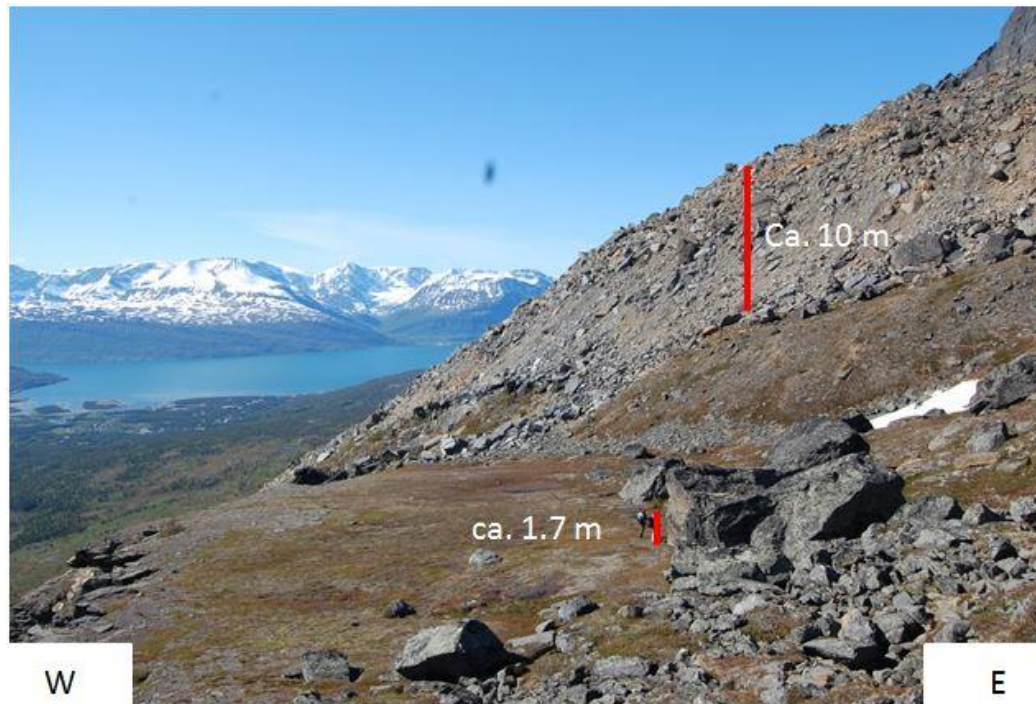
Figure 57: Rock glacier r1 (Fig. 53) and estimation of height. I. Bakkhaug as scale on top of the slide block 3 (Fig. 62).

Texture

Grain size contribution of the rock glaciers was not thoroughly investigated. A rough estimation is given, nonetheless. On the surface are mainly found angular boulders of various sizes which can reach 4 m in diameter. Below approximately 2 meters is observed a mixture of boulders, gravel, sand and silt. In the following are gravel, sand and silt referred to as fines. A similar two layer composition is described by Wahrhaftig & Cox (1959) and Johnson (1984). Steep fronts are bare of vegetation and expose fines (e.g.(Humlum, 1996; Wahrhaftig & Cox, 1959). They are at angle of repose and merge from slope to upper surface in a sharp angle. These characteristics can especially be observed at r1 and r2 (Fig. 55 and 57). The frontal slope of r1 has been measured from distance, using a compass. The resulting angles were for the upper part of the slope 30° – 32° and for the lower part of the front 38°. These measurements, however, have to be questioned towards their liability and should be testified. This is, however, not done here. Other rock glacier fronts are. Wahrhaftig & Cox (1959) describe inactive rock glacier as rather convex rounded vegetated features, where fronts merge gently with the upper

layer and are also vegetated. This can be disagreed for , because some rock glaciers at Adjet, e.g. r3 and r4, show similar characteristic and InSAR data proves those rock glaciers with rather rounded fronts, to be active too (Ch. 5). At rock glaciers r9 and r10 fines are present in a shallow depression at their head (Fig. 58).

Rock glaciers r1, r2, (Fig. 59) and r10 (Fig. 66) were observed in the field. The other rock glaciers were determined by aerial photographs at the computer and stereoscopically by comparing them with field observations. On aerial photographs steep frontal slopes are characterized by bright tones. Also transverse ridges and furrows, and lobes could be distinguished.

Interstitial ice

As mentioned above was no ice observed throughout field work but is assumed to exist. Interstitial ice accumulates in the space between the rock glacier's debris material (Wahrhaftig & Cox, 1959). An annual average temperature below 0° C is required for interstitial ice to be present. In Skibotn, temperatures in the past year (June 2014 – May 2015) range from ca. 30°C in summer to ca. -20°C in winter, at 20 m a.s.l.(yr.no).Annual average temperature for Skibotn are not provided but for northern Norway the annual average temperature is -0.5°C (Ch. 1.4). The study area is located in a discontinuous permafrost covered region (Christiansen et al., 2010), thus it may be, assumed that requirements, for interstitial ice to occur, are provided. Rouyet et al. (2015) suppose, as well, that Adjet lies within a regional mountain permafrost zone (Ch. 1.4). Humlum (1988) mentions that ice within rock glaciers is established and preserved due to a complex interplay of temperature, insolation, wind, and season dependent precipitation over time. Thus permafrost is not a necessity, but the most likely ice preserving factor. It is, however, suggested here, as has been by Rouyet et al. (2015), that areas, above a certain elevation, e.g. 550 (Rouyet et al., 2015), are located in a regional permafrost zone. Thus, it is supposed that the rock glaciers at Adjet are located in a regional permafrost zone.

Wahrhaftig & Cox (1959) give three possible formations of interstitial ice in a rock glacier: (1) compacted snow, (2) frozen meltwater or rain, and (3) frozen groundwater ascending beneath the talus. Regarding that almost all snow melts in the summer season, the first option (1) is assumed rather unlikely. The only snow, presumably from the winter before, observed in August and September, was at rock glacier r9 and in a depression formed by and behind the southern part of slide block s4. Also hypothesis (3) can be excluded, except ground water rises underneath

the rock glacier debris, and therefore out of sight. It then freezes in contact with the circulating air within the rock glacier. A stream below r2 could be traced back towards r2, walking over debris field dT5 (Fig. 50). Water could be heard streaming underneath the boulders of dT5 but could not actually see the river, but at lower an elevation where the debris field ends. No apparent water supply – snow, ice or lake – is seen on surface in the vicinity of r2, leaving only the rock glacier to be the source of the stream. Therefore, it is suggested that interstitial ice in r2 is the source of the stream and not vice versa. No further streams, which could be traced back to a rock glacier, were discovered. They may, however, exist. The stream of rock glacier r2 was only discovered by field work and is not noticed on aerial photographs. Refreezing of meltwater and freezing of rain (2) is suggested as the most likely source of interstitial ice at Adjet. Refreezing of percolating water and freezing meltwater distributing from the headwall bedrock may be a source of interstitial ice (Humlum, 1996), as well. It may also be that snow patches have been buried by rockfall and therefore too distribute to the interstitial ice.

The fact that ice is not seen surficial may be because it is below the upper layer. Perennially frozen layers are, also by other authors described, below a layer of 1.5 – 3 m (Wahrhaftig & Cox, 1959), 1 – 2 m (Griffey & Whalley, 1979) and 3 – 6 m (Ikeda et al., 2008), respectively.
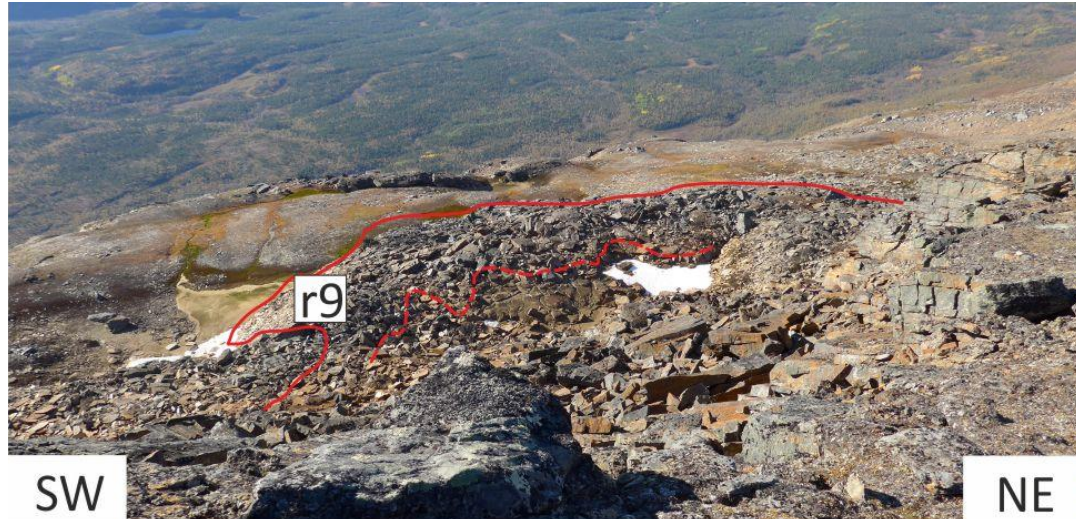
Figure 58: Rock glacier r9 (Fig. 53), looking down from the ridge. Red line delimits the rock glacier and dashed red line delimits the shallow depression with fines on the top and a small snow patch.
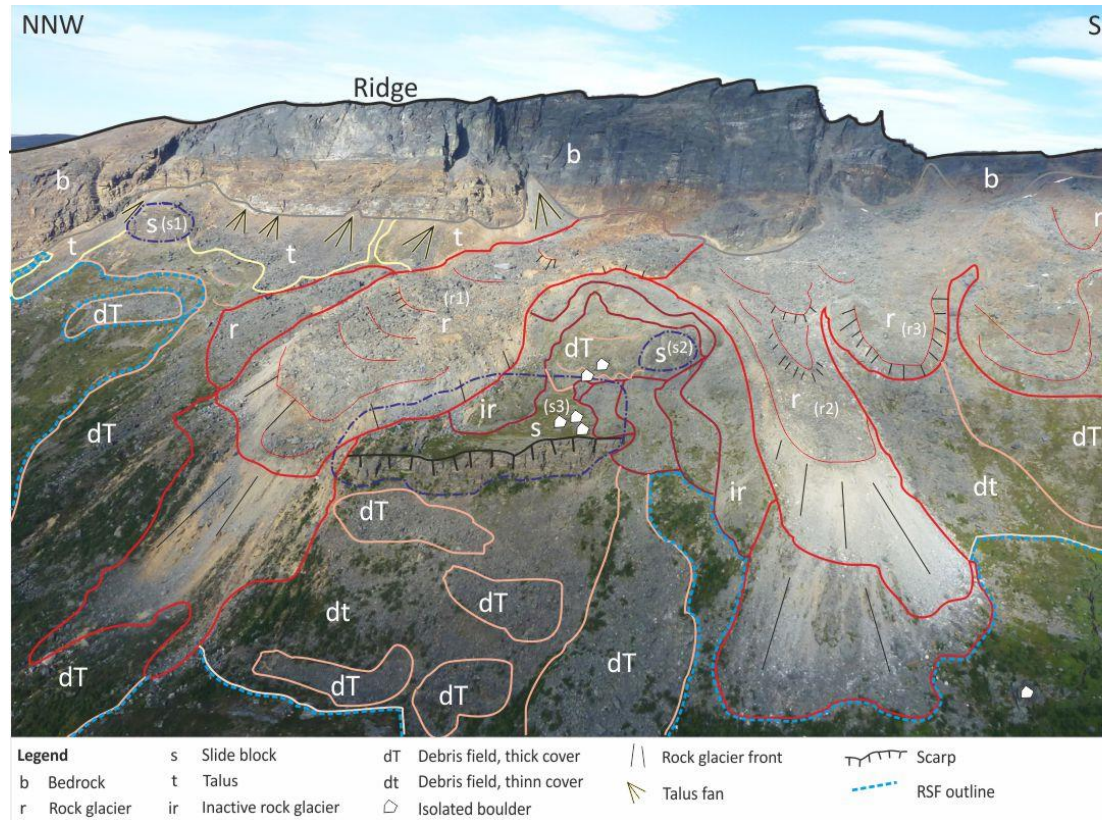
Figure 59: Aerial Photograph showing the northern part of Adjet (within province A, rock glaciers 1, 2 and 3). Photograph: H. Bunkholt 2011 (NGU), taken from helicopter; is modified according to geomorphological elements.

Weather

Throughout field work up to 15 heard rockfalls were counted within 2 hours on a rainy and foggy day (20.08.2015). The rockfall is suggested to have happened at either of rock glaciers r1 or r2 fronts, cnsidering the camping site location. Corner (pers. comm. 2015) counted 7 heard rockfalls at rock glaciers r1 and r2, within approximately four hours, on 27. June 2014. It was a calm, sunny day (ca. 17°C) and snow could still be found at the vicinity of the named rock glaciers. No other counting has been done. It was, however, noticed that the overall rockfall activity at the rock glacier fronts was much lower on dry and sunny than on humid days. Rouyet et al. (2015) suggest that the velocity at the rock glaciers measured by GBR may be due to temperature and precipitation. Ikeda (2008) suggests that the rate of deformation of the active layer of a rock glacier is connected to seasonal changes in temperature. Seasonal changes are influenced by snow melt, causing acceleration, and refreezing of infiltrated water, which in turn causes deceleration. Increasing velocity at features near the permafrost limit of a mountain may be caused by response to rising temperatures of ground and atmosphere. If it is assumed that

rock glacier fronts at Adjet are near the permafrost limit and herewith influenced by temperature changes as suggested by Ikeda (2008), it is likely that the rock glaciers are not only influenced by seasonal but also by daily changes. It is, therefore, agreed with the hypothesis given by Rouyet et al. (2015), that acceleration of movement is not only influenced by temperature but also by precipitation.

Inactive rock glaciers. –

Legend — Inactive rock glacier

r1a
r1
r2
r3

N

Figure 60: Inactive rock glaciers adjacent to active rock glaciers r1 and r2. Legend for other features can be found in Figure morphoMap.

By inactive rock glaciers it is referred to rock glaciers that are assumed to be motionless. They were visited in the field and therefore only observed in province A in between the active rock glaciers r1 and r2 (Fig. 60). Inactive rock glaciers were only identified in the field based on their appearance: shape, extended vegetation, and blocky nature.

The inactive rock glaciers in the study site are vegetated with lichens, moss and other small alpine plants. Their slopes are gentler than the sharp angle which is found at some of the active rock glaciers (see above). These characteristics are also described by Wahrhatig & Cox (1959).

It is suggested that the in active rock glaciers are remnants of the active rock glaciers r1 and r2, which are suggested to have experienced several periods of activity and inactivity and have deformed laterally and in length throughout time. Further, it is suggested that they have decreased laterally and increased in length. Their appearance shifted south- and westwards. They became inactive and subsequently reactivated several time. Wahrhatig & Cox (1959) propose two possible ways of rock glaciers to become inactive: (1) a decrease in debris supply and (2) the disappearing interstitial ice through melting. In case (1) the decrease in debris supply would result in a thinning out of the rock glacier by movement. Interstitial ice melts (2) and movement would eventually stop (Ch. 6.3). Propositions (1) and (2) do not exclude each other, but may happen in accordance. Further, rock glaciers are suggested to be inactivated by climatic warming (Ikeda et al. 2007). At Adjet are two scenarios possible. Firstly it is possible that debris
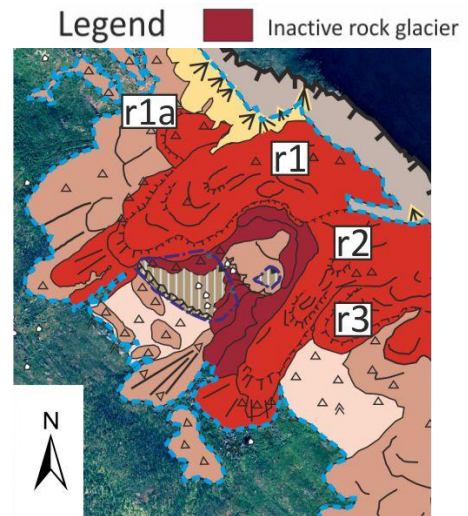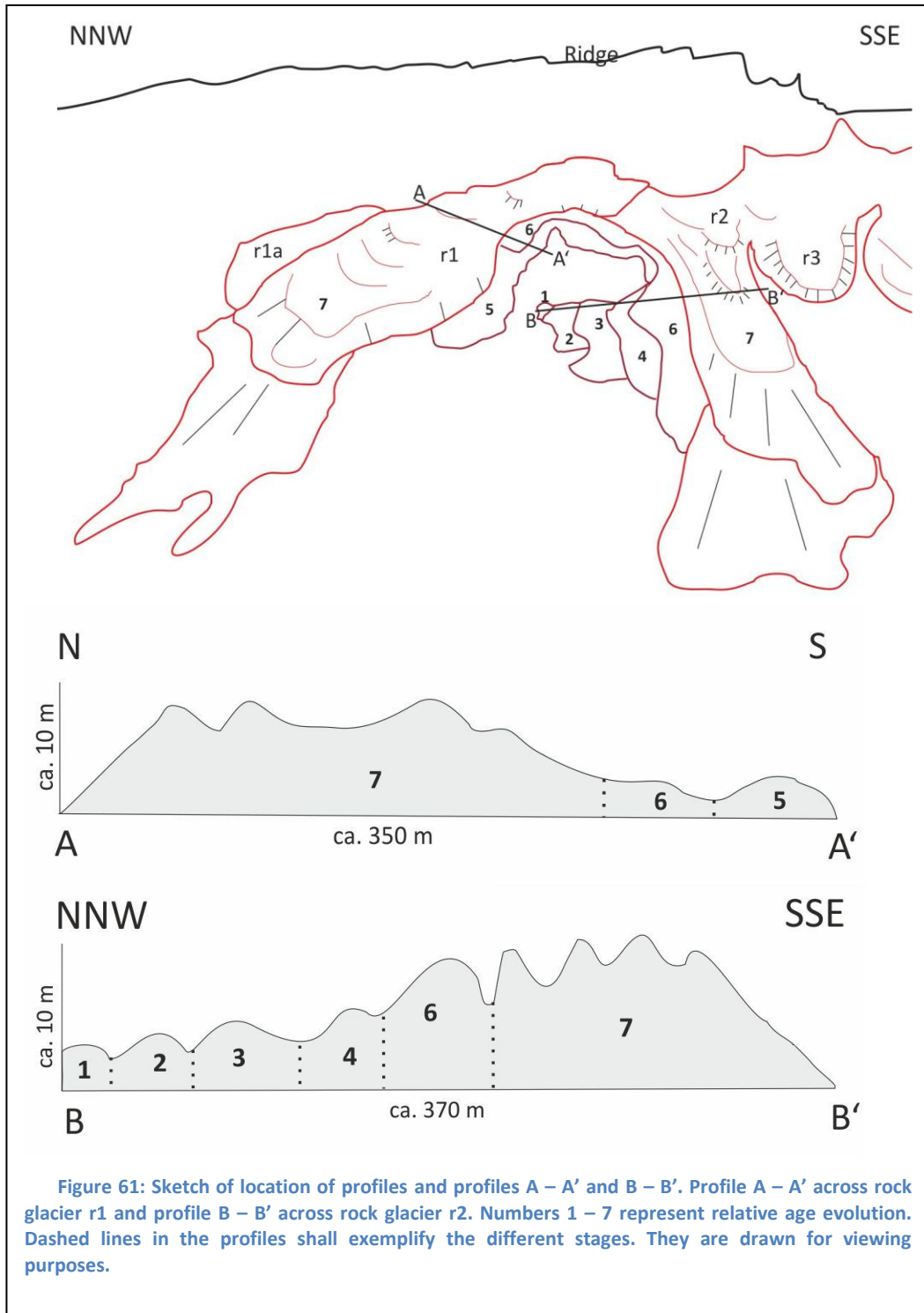
supply decreased over a certain period of time and a reactivation of supply restarted and rock glaciers were reactivated. The evolution of the RSF will be discussed in Chapter 6.4. Secondly interstitial ice may have either partly melted and rock glaciers decreased in their lateral size or interstitial ice melted nearly completely and stopped this way the movement of the rock glacier, e.g. caused by climatic warming. It then may have been reactivated and accumulated again a greater amount of interstitial ice. It is supposed that rather the partial melting out of interstitial ice caused the inactive remnants of the rock glacier than the decline of debris supply.

Figure 61 shows roughly estimated profiles of the active and inactive parts of rock glaciers r1 and r2. The numbers 1 to 7 give a relative age evolution, where 1 is the oldest and 7 the youngest (today) stage. According to this interpretation had rock glacier r2 a greater extent or may be older and was more influenced by reactivation and lying dormant than r1. This accounts also for stages 1 to 4. No similar remnants of stages 1 to 4 could be found for r1. If rock glacier r1 had a smaller extent than r2 or if it was absent or if the remnants have been overrun by r5, r6 and r7 is unknown. Stage 5 is the first inactive remnant as observed for r1. Regarding the increasing downslope extent of stages 1 to 4 at r2, it surprises that stage 5 should not show similar characteristics as the stages before. Three possibilities are suggested: (1) The stages 4 and 5 are the same and the borders were misinterpreted, (2) stage 5, adjacent to r2, is overlain by stage 6, or (3) r2 was only partly reactivated, respectively did not move as fast as r1 (due to unknown reasons). Hypotheses (1) or (2) are suggested to be the more realistic events. Stage 6, however, suggests a scenario having occurred similar to hypothesis (3), regarding r1 this time. The rock glacier remnant of stage 6, adjacent to r1, has neither advanced downslope nor laterally as much as stage 5. Stage 6 at r2 has on the contrary extended about three times as far downslope as stage 6 at r1. In stage 7 the rock glaciers r1 and r2 show a similar extent downslope. Reasons for such different behavior in time are unknown. They will also not be discussed further in this study.

It is further to be discussed whether some geomorphological features distinguished as debris field, are, in fact, inactive rock glaciers. Wahrhatig & Cox (1959) describe inactive rock glaciers as showing a continuous cover of vegetation (e.g. lichens), having a gentle slope, and less than half the thickness of an active rock glacier. All these characteristics coincide with debris field dT7. Against this hypothesis is the fact that inactive rock glaciers still retain the typical relief features of rock glaciers (Wahrhaftig & Cox, 1959). At dT7only lobes suggesting creep, are distinguished. However, the rock glaciers are described by Wahrhatig & Cox (1959) about 10 times as thick as the ones being observed at Adjet. Microrelief may, therefore, be too distinct to be distinguished

by aerial photographs alone. InSAR velocity data measurements show movement here and there in debris field dT7 (Ch. 5, Fig. 78). This may further be an indicator that the debris field is an inactive rock glacier which may have been reactivated. The evidence of an inactive or reactivated rock glacier is too weak to decide which is correct and further investigations should be done. Thus the original subdivision of dT7 as a debris field is retained.

Figure 61: Sketch of location of profiles and profiles A – A' and B – B'. Profile A – A' across rock glacier r1 and profile B – B' across rock glacier r2. Numbers 1 – 7 represent relative age evolution. Dashed lines in the profiles shall exemplify the different stages. They are drawn for viewing purposes.

4.2.4 Slide blocks

Six slide blocks are distinguished in the RSF area (Fig. 62): three in the north, province A (s1 – s3; Fig. 59) and three in the south, province B (s4 – s6; Fig. 66). The slide blocks have a slightly different appearance, which is why they are treated separately in the following.

In the very north is found an easily recognizable slide block with a distinct front similar to a scarp (Fig. 63). The block lies underneath the backwall just below talus fan deposits. Hence, it is assumed, by shape and location that slide block s1 was forced down the backwall as rockfall driven by gravity. Not all slide blocks are as recognizable, regarding outline and shape, as s1.
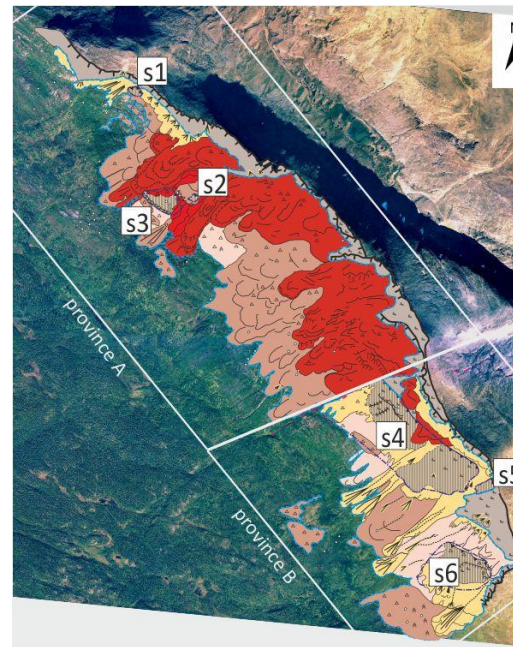
Figure 62: Geomorphological elements of the RSF. Rock glaciers are numbered. Aerial photograph provided by NMA (kartverket.no).

Figure 63: Slide block s1 (Fig. s-no) from below the slide block and from the ridge. Purple dashed line represents the outline of the slide block. Photo: from ridge downslope taken by Eriksen in 2014 (pers. comm. 2014).

The outline and shape of s2 is mostly interbedded in a thick covered debris field (Fig. 62 and 64). It is uncertain if the block is one block or if it is split into three parts, as suggested in Figure 64. The block is interbedded in the debris field around it (dT4) and only some parts of it stick out.

Slide block s3 (Fig. 62) is in between rock glaciers r1 and r2. It has a bench-like appearance with a flat top and a scarp in the front. The block is quite prominent within the RSF, because it is the only bench-like feature in the RSF area. Debris fields are present above (dT4) as well as below (dt1, dT5) s3. Due to similar strike and slip of foliation measured at the bench and the backwall (Ch.3, Fig. 31), the bench-like feature could be considered as *in-situ* bedrock exposure (Fig. 67). This, however, can be

questioned by geomorphological observations. The abundance of debris below the feature (s3) suggests partial disintegration under some movement, while the block retained its general integrity. The amount of debris seems too large to have been deposited by rockfall from the bench's scarp only. It is suggested that slide blocks s2 and s3 are part of a failure event that generated debris fields, by partial disintegration, and slide blocks.
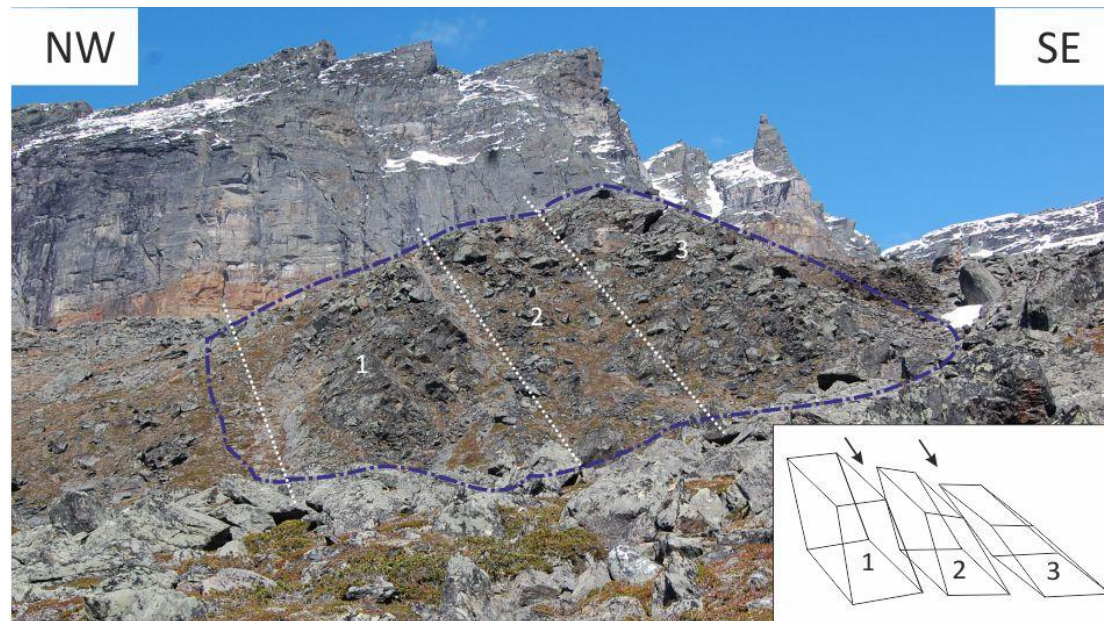
Figure 64: Slide block s2 (Fig. 62). Purple dashed line represents the outline of the block. White dashed lines and numbers suggest a possible splitting of the slide block.

In province B, the slide blocks are bigger and cover a large part of the RSF area in the province. The slide blocks show sporadic cover of weathered material or colluvium on the surface. Slide blocks s4 and s5 are only partly exposed at the surface, while the remaining parts are covered by debris fields, talus fan deposits and, in the case of s4, partly by a rock glacier (r10, Fig. 53). The slide blocks' inferred limits below the debris cover are outlined with a purple dotted-dashed line in Figure 42. They also seem to be part of a failure event as s2 and s3.

The sixth slide block s6 is adjacent to the mountain ridge. At this section of the mountain it looks as if Adjet has two ridges (Fig. 65). This appearance is given because the block s5 has just slightly slid down the slope.

Slide blocks s1, s3, s4 and s6 have in common that their northern part seems to have moved further downslope than their southern part. This is discussed below (Ch. 6.3).
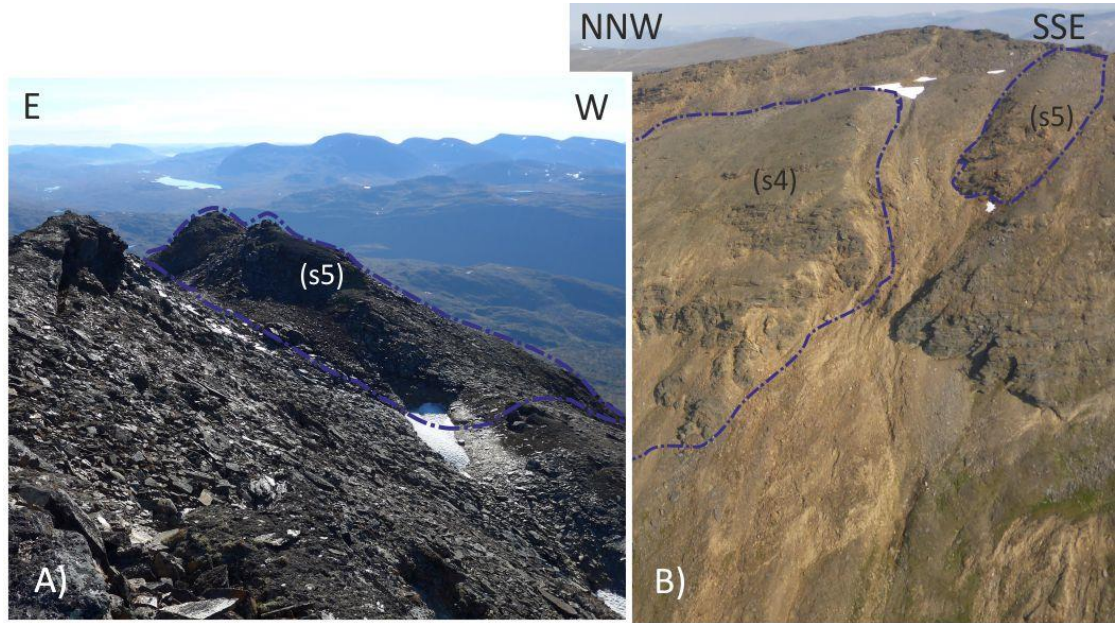
Figure 65: Slide block s5. Photo A) taken from the ridge. Photo B) is an aerial photograph taken from helicopter, Bakkhaug in 2014. Purple dashed line outlines slide block s4 and s5.

Figure 66: Aerial Photograph showing the northern part of Adjet (within province B). Photograph: H. Bunkholt 2011 (NGU); taken from helicopter and modified according to geomorphological elements.

4.2.5 4.2.5 Solid bedrock

There are no places within the area covered by the RSF area, where solid bedrock or what is interpret as *in-situ* bedrock, is found. The only place where solid bedrock could be present is between rock glaciers r1 and r2 (s3, Fig. 63 and 67). The fractures measured at the site (Ch. 3.4, Fig. 37s, stereoplot 11) coincide well with the faults and fractures on the mountain wall behind (Ch. 3.4, Fig. 37, stereoplot 6).Considering the geomorphological characteristics mentioned in Chapter 4.2.4 – debris field below and bench-like morphology - is the feature , nonetheless, suggested to be a slide block. To be certain further and more detailed investigation at the site are suggested.
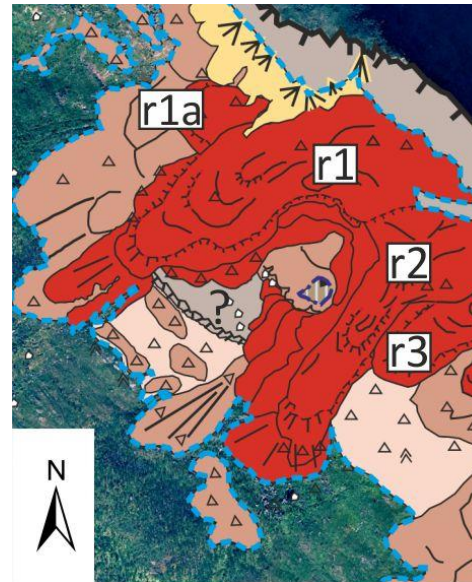
Figure 67: Bench marked with a question mark as possible bedrock.

4.4   4.3 Geomorphologic elements outside the contiguous RSF area

4.4.1   4.3.1   Debris fields and boulders

Outside the main RSF areasingle boulders and debris fields are present. Single boulders seem to have rolled further than others and travelled beyond the borders of the RSF outline that is drawn. This can be observed, all over the RSF area (Fig. 42). Boulders are of different sizes, and of fairly equant shapes and rather angular. Sizes are often around 1 to 2 m in diameter, but also larger boulders are observed. One of the largest boulders discovered on the slope is about 6 to7 m diameter in length and about 4 m diameter in width (Fig. 68). Further, are found accumulation of boulders marked as debris fields (dT1, dT2, dT6, and dT11 – dT13, Fig. 50). Debris fields dT6 and dT11 – dT13 show a southwest facing lobate form. The deposits are vegetated and seem thus older than the deposits within the main part of the RSF (Fig. 69). This suggests that they may relate to an earlier rock slope failure event at Adjet. Thus, more than one failure event may have occurred (Ch. 6).

Figure 68: Single Boulder outside the contiguous RSF area. About 4 m diameter in height and 6 – 7 m diameter in length. White line represents a dimension of 2 m length.

Figure 69: Photograph showing vegetated debris field dT2 (Fig. 50), province A, outside the RSF area.

4.4.2   4.3.2 Solid bedrock

Solid bedrock is solely found outside the slide area – with the possible exception of slide block s3 (Ch. 4.2.5) – and composes the backwall of the RSF (Fig. 70). Adjet's ridge consists of more or less stable bedrock. In the north steep scarps are present whereas the mountain develops a slope-like nature southwards (Ch. 3.1, Fig. 22). It can be mentioned that, at Adjet, both sides of the mountain ridge are influenced by rock slope failures (Fig. 71). The east side of Adjet has not been of investigative interest in the study but is included in the description of the mountain ridge, to better understand the character of the mountain top. In the following it is referred to as backside of the mountain. The fact that both sides of

Figure 70: Geomorphological elements of the RSF. Different bedrock areas are numbered. Aerial photograph provided by NMA (kartverket.no).

the mountain are influenced by RSF, makes it difficult to determine whether highly fractured outcrops on the ridge are stable or have slightly moved. Slight movement is suggested by the measurements of foliation in what may have been loose bedrock on the ridge (Ch. 3, Fig. 31). Lithology and bedrock fabrics are described in more detail in chapter 3.

Figure 71: Photograph showing the eastern side of Adjet.

Figure 72: Glacially smoothed surface on top of Adjet in region b1 (Fig. 70).

The mountain wall at Adjet is subdivided into five bedrock regions according to their appearance. Region b1 (Fig. 70) is characterized by a relatively broad top which is glacially smoothed (Fig. 72), and a, from west- to east, ascending slope (Ch. 3.1, Fig. 22). The cliff face is several meters high but even more prominent in region b2 (Ch. 3.1, Fig. 22). Region b2 ridge has a scarp facing the RSF area and a slope towards Adjet's back side which is vegetated by lichens (Fig. 73). The ridge is good to walk until above rock glacier r1. South of r1 a peak-like ridge is observed, characterized by a blocky steep slope facing east and changing, towards the west, into a steep scarp face, of approximately 30 m (Fig. 74). The peak-like ridge continues further into region b3. Scarp faces appear irregular, become smaller in height and disappear eventually, giving way to a more moderate slope-morphology below the ridge (Fig. 75).

Figure 73: Ridge of Adjet in region b2 (Fig. 70).

Vegetation (lichens) in region b2 and 3 is sparse and sporadic weathered material and/ or colluvium is abundant. The narrow and blocky nature of the ridge offers some challenge to walking the ridge. Often the backside of the Adjet is safer to walk along. Region b4 is different to the mentioned regions having no sharp ridge or scarp face (Fig. 76). It rather comprises a gradual slope. The bedrock is vegetated and widely covered by weathered material and / or colluvium. Also region b5 reveals a different nature. It is comprised of a northwest-facing steep scarp face (Fig. 77) and represents the southern end of the RSF area. The mountain wall is supposed to be the source area for the RSF (Ch. 6).

Figure 74: Peak-like ridge above rock glacier r1 (Fig. 53).
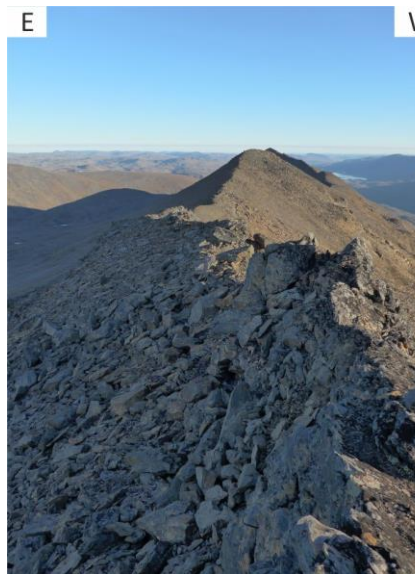
Figure 75: Peak-like ridge in region b3 (Fig. 70).

86

NW SE

Figure 76: Ridge in bedrock region b4 (Fig.70).

E
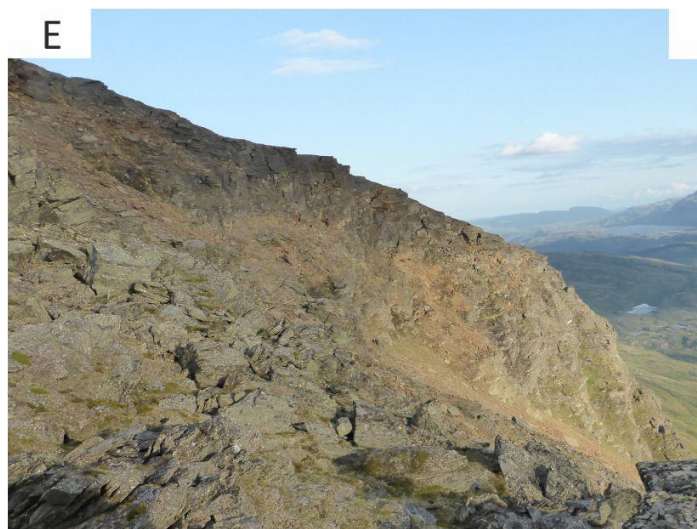
Figure 77: View towards bedrock region b5 (Fig. 70). Photograph: Eriksen in 2014 (pers. comm. 2014).

4.5   4.4 Summary

Talus fan deposits are either rockfall derived (steep scarps, province A and B), snow avalanche derived (province B), meltwater / slush avalanche derived (province B), or debris flow derived (province B).

Debris fields are divided into thin and thick covered debris fields depending on their assumed thickness and amount of surface boulders. Debris field outside and within the RSF area suggest that different RSF events have occurred. They may be derived from large-scale rock-slope failures and later influenced by creep movement (Ch. 6).

Rock glaciers are mainly found in province A. Lobate- and tongue-shaped rock glaciers are present. Rock glaciers were subdivided into active and inactive rock glaciers. Inactive rock glaciers were only identified by field work observations.

Slide blocks are found in both provinces. In province A they are of smaller size and either a single block (s1) or integrated in, respectively part of (s3) a debris field. Bigger slide blocks are found in province B and are partly covered by other geomorphological features (s4 and s5). Slide blocks were either driven by gravity rockfall (s1), a failure event generating debris field and slide blocks (s2 – s5), or a failure event generating a slide block (6).

Solid bedrock is found in the scarp and ridge above the rock slope failure area and is the source area for the material in the RSF. From north to south is found: a glacially smoothed top (province A), a ridge which slopes towards its backside and has a steep wall face towards the RSF (Province A), and a peak-like ridge with scarp faces that disappear eventually (from province A into province B) and evolve into a slope-like ridge (province B). In the south the RSF area is delimited by a steep towards northwest-facing cliff face (province B).

Province A and B show different degrees of dominance, of different geomorphological elements. In province A rock glaciers and debris fields dominate, whereas in province B slide blocks and talus and collluvial fan deposits dominate.

5   InSAR data of the study area

5.1   Introduction

InSAR data gives information about recent surface movement rates in the LOS. An InSAR velocity map of the RSF site was supplied by (Eriksen, in prep.), and is shown in Figure 78. The data was collected in the summer seasons in a period of 4 years (2009-2013). The InSAR data is additionally used to analyze geomorphological features in the RSF, respectively their topographic deformation. Negative numbers refer to movement away from and positive numbers towards to the satellite. The InSAR data provides velocities of mm per year (mm yr^{-1}), which will be presented in cm yr^{-1}. Spots lacking data within the RSF area are proven to move up to 15 cm per day (cm d^{-1}) by GBR measurements (Rouyet et al., 2015). They are found within the most pronounced geomorphological features interpreted as rock glaciers (Ch. 4.2.3). Loss of data in high velocity areas may result from the 11-day cycle of measurements by the satellite (Eriksen pers. comm. 2015), (Ch. 2.4). Six profiles (A-A' to F-F') are drawn (EsriArcGIS) across the investigated area to illustrate the surface displacement in the RSF area, using the provided velocity map (Fig.79).

5.2   Velocity data by satellite-based InSAR

The profiles illustrate recent activity in the RSF site. They cover different features such as bedrock regions, rock glaciers, debris fields, slide blocks, and talus fan deposits. They shall help to exemplify the movement data of the complete study site.

Profile A – A'

The profile is drawn across bedrock (b2) and a rock glacier (r1). The area shows a great acceleration away from the bedrock towards the rock glacier. The fastest movement, shown in the profile, is slightly higher than 5 cm yr^{-1}, but is not the real maximum. The real maximum velocity is found in the area without data (Fig. 78), marked by the dashed line (Fig. 79).It covers the front and steep frontal slope of the rock glacier (r1). In Figure 78p it represents the area without data. Due to limitations of measurement cycles and wavelength of the satellite-based InSAR data could not be provided for this area (Eriksen pers. comm. 2015), (Ch. 2.4). This area has been proven, by additional ground-based radar measurements, to be very active with a speed of several cm per day (Rouyet et al., 2015). This relates also to other rock glacier areas where spots without data can be seen (Fig. 78). The profile, further, shows several peaks where velocity increases and decreases in turns (Fig. 79; feature 3, 4). This suggests

that the rock glacier moves not as one body but in discrete parts at different velocities. These parts coincide with ridges and furrows and lobes on the rock glacier (r1).

Profile B – B'

The profile is drawn across bedrock (b3), a rock glacier (r4), and a debris field (dT7). The only feature in motion is the rock glacier, whereas the bedrock and debris field are stable to semi-stable. The rock glacier r4 deforms with a maximum velocity of ca. 10 cm yr^{-1}.

Profile C – C'

The profile is drawn across bedrock (b3), a rock glacier (r7), and a debris field (dT7). Overall, the transect is in motion (ca. 2 – 11 cm yr^{-1}) except of when it reaches the debris field, there it reaches a semi-stable state. Surface displacement is found at the bedrock b3 (max. ca. 5.5 cm yr^{-1}) and at rock glacier r7 (ca. 11 cm yr^{-1}). The movement of the former is suggested to be caused by colluvium material rather than that the mountain wall is in motion. The latter (r7) shows additionally indications for different movement of features on the rock glacier, coinciding with lobes, ridges and furrows. The bedrock b3 exhibits weathered material and/ or colluvium on surface (Fig. 42). They are implied to be moving by the profile.

Profile D – D'

The profile is drawn across bedrock (b3), a talus fan deposit (not numbered; Fig. 42), a rock glacier (r10), a slide block (s4) respectively talus fan deposit (t2) on top of the slide block, a talus fan deposit (t2), as well as a debris field (dt3). The profile crosses from a stable area (b3) over fluctuating (r10, s4 and/ or t2) velocities towards a stable area (t2, dt3) again. Across rock glacier r10 and slide block s4 surface displacement is seen. Between the bedrock b3 and the rock glacier r10 is a talus fan deposit that shows acceleration towards the rock glacier. The rock glacier r10 shows a maximum velocity of nearly 9 cm yr^{-1}. Slide block s4 shows displacement with a maximum of ca. 5.5 cm yr^{-1}. It is covered with talus fan deposit t2 which may be assumed as movement indicators, if creep is suggested. Otherwise these data indicate slide block movement.

Profile E – E'

The profile is drawn across a slide block (s5), bedrock (b4), and a debris field (dt4). Overall the area is relatively stable with low maximum velocities of 3 cm yr^{-1} (s5) and ca. 2.5 cm yr^{-1} (b4). Bedrock b4 shows different surface velocities in different parts, ranging from close to zero to ca. 2.5 cm yr^{-1}. The drastic velocity distribution of b4 going from maximum velocity to stable conditions and back again suggests

movement of possibly two separate features. It is supposed that these displacements are related to superficial creep of sporadic talus fan deposits and/ or weathered material and colluvium on the surface of b4. Slide block s5shows an increase in velocity towards b4. The debris field below b4 shows displacement as well.

Profile F – F

The profile is drawn across bedrock (b4), a debris field (dt4), a slide block (s6), and a talus fan deposit (t6). The transect is generally in motion except of the talus fan deposit (t6). The latter is stable. Surface displacement is present on bedrock b4, talus fan deposit dt4, and slide block s6. Maximum velocities range from around 2.5 cm yr^{-1}, for both b4 and dt4, to 4.5 cm yr^{-1} for s6. Again it is suggested that weathered material and colluvium or sporadic talus fan deposits on the bedrocks surface are displaced by creep, and responsible for the acceleration. Figure 78 shows that s5 and the area around it are moving (Fig. 78). It is difficult to distinguish whether the surface deposits of the slide block or the slide block itself is in motion. Considering that the slide block is covered with sporadic colluvium and weathered material, with talus fan deposits, as well as with debris field (Fig. 78), it can be suggested that those feature move by creep which then is measured by the radar. On the other hand it is likely that the slide block s6 itself is in motion. This is suggested due to the activity across the whole slide block, given by the InSAR data (Fig. 78). Debris field dt4 is characterized by lobe-like features suggesting creep (Ch. 4.2.2 Fig. 52). InSAR data confirms the suggestion by showing displacement.

Figure 78: InSAR velocity map over Adjet. Green are stable areas and red marks high velocity rates. Outline of RSF (blue dashed line) and geomorphological elements (black lined features) are put on top. Six exemplified profiles are drawn and shown in Figure 79.). Velocity map is underlain by DEM.
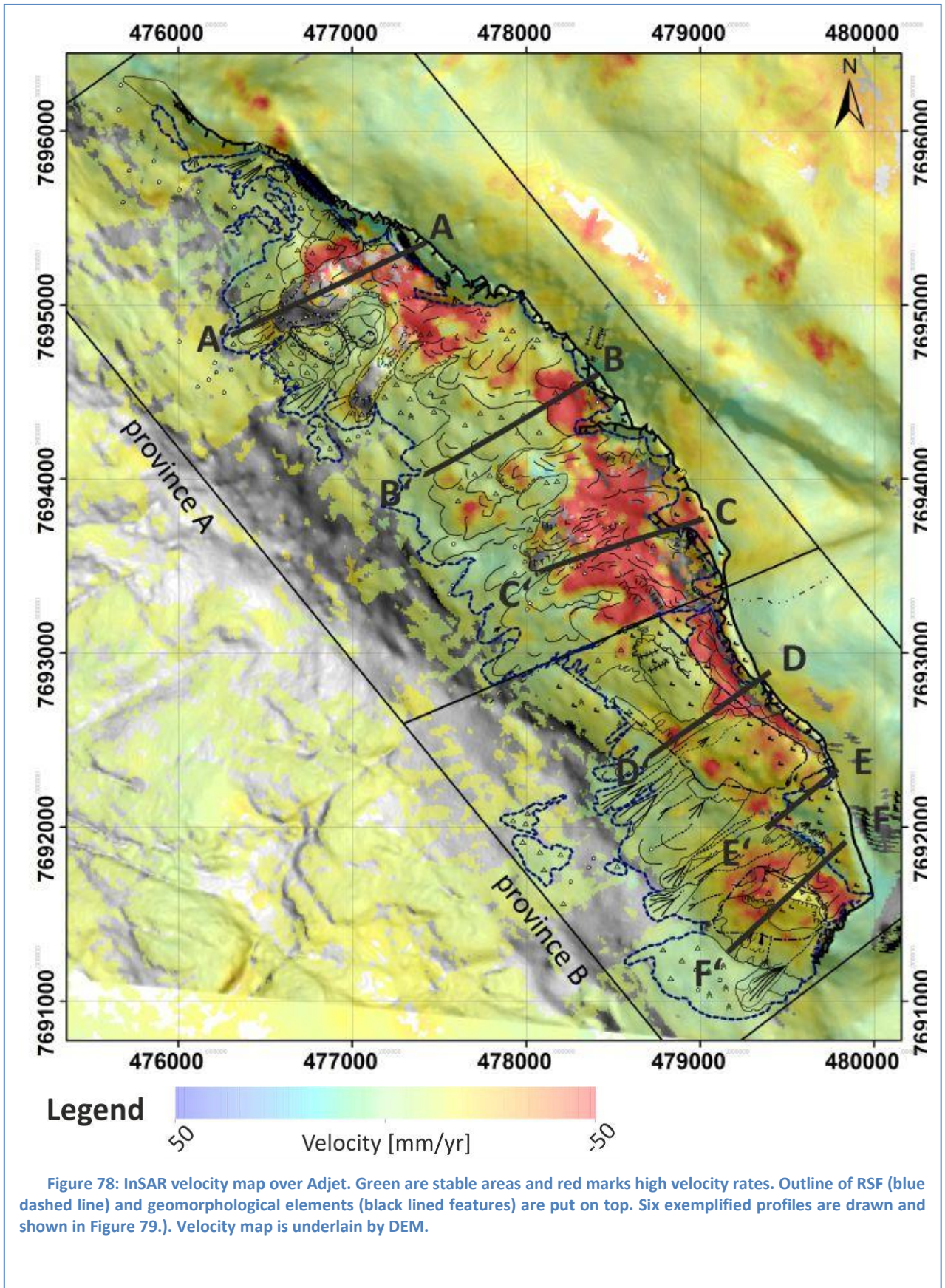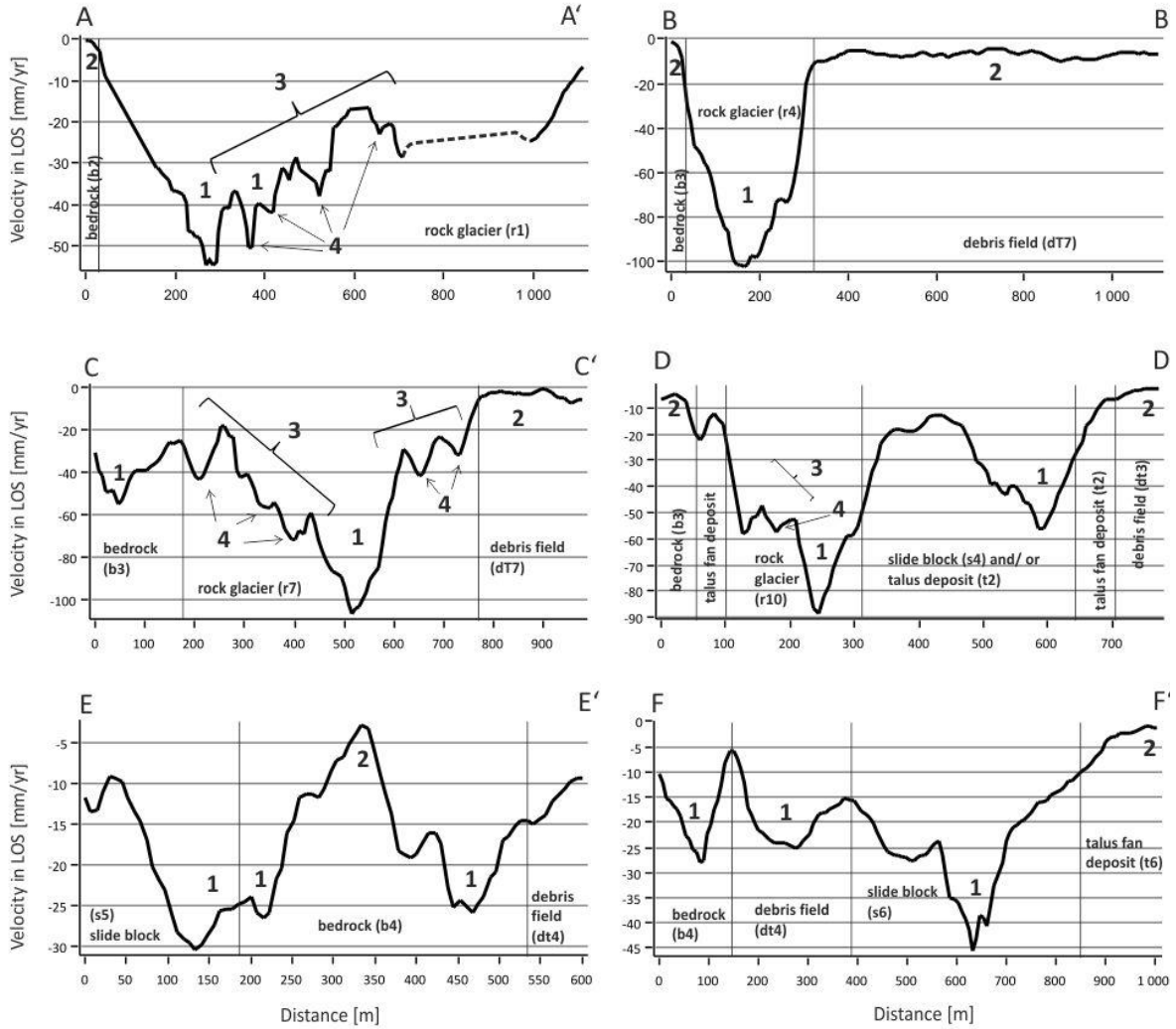
Figure 79: Representative profiles of the RSF area. Profile lines in Figure 78. Thin vertical lines represent the division into the different geomorphological elements. Numbers represent different features: (1) maximum velocity of the element, (2) stable/ semi-stable area, (3) lobes and/ or ridges and furrows, (4) suggested furrow/ lobe frontal slope. Dashed line represents area that lacks data in the velocity map (Fig. 78). Abbreviation of respective features are in parentheses and relate to numbering introduced in Chapter 4 (if present).

5.3 Summary

Talus fan deposits show maximum velocities of 2 cm yr⁻¹. Single talus fan deposits on top of slide blocks show higher movement rates (max. ca. 5.5 cm yr⁻¹). These velocities, however can be argued to be referred to talus movement by e.g. creep. Considering that they occur only in the vicinity to slide blocks.

Debris fields are mostly stable. Velocities of debris fields in the profiles range from 0 cm yr⁻¹ to 2.5 cm yr⁻¹. In the complete RSF, single areas may be of higher velocity (orange - red areas), (Fig. 78). Debris fields do not move as whole body but show single areas in motion. Those areas are often adjacent to lobes. Thus, creep is the suggested movement process.

Rock glaciers are the most distinct features in the velocity data. They move up to 15 cm per day (Rouyet et al. 2015). Thus, InSAR data supports the hypothesis that these features are active.

The southern slide blocks (s4, s5, s6) show displacement. Slide block s5 moves by a maximum velocity of 3 cm yr^{-1}. The southernmost slide block (s6) shows velocities up to ca. 4.5 cm yr^{-1}. The area of and around the slide blocks indicates movement. Thus is supposed that the slide blocks s6, as well as s5, are moving. On slide block s4 velocities range from 0 cm yr^{-1} to ca. 5.5 cm yr^{-1}. Velocities on the latter are mainly detected where talus fan deposits or sporadic weathered material and colluvium occur. This suggests that those features are moving and not the slide block. A possible movement process could be creep. Northern slide blocks are not shown in profiles but the Figure 78 displays them as non-moving features.

Bedrock in the mountain wall is generally suggested to be stable, in the study site. The profiles C-C', E-E', and F-F', however, provide evidence that some parts of the ridge are in motion. Maximum velocities displayed in the profiles are ca. 2-5 cm yr^{-1} (b4) and 5.5 cm yr^{-1} (b3). High movement rates may indicate that either the mapping of these regions or the InSAR data has errors. In the geomorphological map (, Fig. 42) this region is identified as bedrock with a sporadic cover of weathered material and colluvium. The movement of b3 (ca. 5.5 cm yr^{-1}), however, seems to be too high to generated by sporadic features. Hence, this region could be distributed by even more colluvium deposits than postulated before (Ch. 4), or this part of the ridge may be disintegrated and moving towards the RSF site below. Reasons for the acceleration of geomorphological features at Adjet are still to be explored and not included in this study. Furthermore relatively high velocities of some bedrock regions (b3 in profile C-C' and b4 in profile E-E' and F-F') will not be discussed in more detail.

Overall, InSAR data confirm the presence of active surface movement in addition to field work, analysis of aerial photographs, and DEMs. The suggested existence of rock glaciers is supported by this velocity data as well. The velocities range from 2 cm yr^{-1} to ca. 11 cm yr^{-1}. The maximum speed cannot be detected with satellite-based InSAR alone, and thus are assumed to be too fast to be measured by satellite-based InSAR (Eriksen, pers. comm. 2014).

6 Discussion

6.1 Introduction

This chapter attempts to bring the structural features of the bedrock and the movement of geomorphological feature in the study site into a broader context. Both movement and bedrock, as source area, provide a scope for a hypothetical relative evolution of the RSF at Adjet which is presented at the end of this chapter. Controlling factors of slope failure related to the bedrock, include different types of structural features related to failure, and are discussed. Those are (1) fold limbs as sliding surface (A – A'), (2) conjugate fracture sets at

Figure 80: Orthophotograph of Adjet with profile lines across three representative locations of failure. Profiles are shown in figures 3 and 4.

steep mountain faces (B – B'), and (3) conjugate fracture sets where moderately dipping faults provide sliding surface (Fig. 80). Movement pattern are presented and suggest both historical and present movement of geomorphological features.

6.2 Discussion of bedrock as source area

6.2.1 Bedrock instability

Slope evolution in alpine terrains is primary and dominantly affected by the gravitational failure of mountain slopes (McColl, 2012). The evolution of different mass movements develops through long-term ridge disintegration (Hradecký & Pánek, 2005) which is controlled by different failure mechanisms. Slope instabilities are affected by: (1) oversteepening through erosion at the base of a slope , (2) earthquake/ seismic activity caused by glacio-isostatic rebound , (3) weathering by freeze-thaw or moisture in the bedrock, (4) glacial debuttressing and stress release (e.g. Haeberli et al., 2006; McColl & Davis, 2013), (5) fracture distribution (Haeberli et al,. 2006, Hradecký & Pánek, 2005), and (6) growth and decay of permafrost (L H Blikra et al., 2006; Shakesby, Dawson, & Matthews, 1987).

Stress release of a valley side by withdrawal of glaciers resulting in failure processes, e.g. rockfall, or sturzstrom, has been stated by several authors (e.g. McColl & Davis, 2012; Johnson, 1984).

Destabilization of the slope during deglaciation initiates slope failure processes. Failure events decrease through time as stress-release, on the rock, declines after glacial unloading (Ballantyne, 2001). Stress release after glacial retreat is suggested to be a primary cause of RSF (Ballantyne, 2003; Blikra et al., 2006). Failure occurs either during or immediately after deglaciation, or is delayed due to depleting residual internal stresses. The latter may result in failure after several millennia (Blikra et al., 2006). McColl (2012), on the other hand, postulates that slope failure may be initiated prior to deglaciation. Destabilization due to glacial retreat influences, then, only the rate of landslide movement; as glaciers thin and retreat, slope destabilization accelerates and spreads in distance. Also, the melting of permafrost shortly after deglaciation may further have influenced the (in)stability of the mountain slope (Blikra et al., 2006). In northern Iceland a major RSF, the Höfðahólar rock avalanche (sturzstrom), has been dated to early-Holocene age, 10200 − 7975 ± 45 cal. Yrs BP (Mercier et al., 2012). Hence, it is associated to paraglacial stress release shortly after glacier retreat.

Isostatic uplift began during deglaciation. The uplift of land is greatest, where ice was thickest. Glacio-isostatic uplift reactivates ancient faults and thus triggers earthquakes leading to failure processes (Ballantyne, 2003). Blikra et al. (2006) suggest that seismic activity such as earthquakes may have triggered RSFs in Norway, even though there are no certain examples of the hypothesis. The regional concentration of RSFs in Troms (Ch. 1.6 Fig. 17), however, suggests that they were caused in relation to a regional earthquake (cf. Blikra et al., 2006).

The RSF at Adjet may be a product of large slope failures caused by stress release associated with deglaciation or glacio-isostatic uplift, or a combination of both. The large size of the debris field suggests large scale failure events.

Catastrophic failures of unconsolidated talus and glacial deposits at valley sides are suggested to generate rock glaciers (Johnson, 1984). Also Ballantyne (2001) postulates that paraglacial rock-slope failure and rockfall are important in the formation of some rock glaciers. Debris fields in the study site may, thus, have been deposited by large failure events e.g. as sturzstrom, and then evolved into rock glaciers and became eventually inactive.

Johnson (1984) suggests that rock glaciers were formed during either one or several catastrophic failure events after which no or little change in the form of the features follows. This is based on the suggestion that no or little movement occurred after the rapid formation. The inactive rock glaciers identified in northern Adjet (province A), may be products of catastrophic failure. They may have been reactivated, e.g. due to climate conditions (cf. Wahrhaftig & Cox, 1959).

The abundance of basal lobes suggests further that failure occurred over a larger time span. This implies further that several failure events occurred.

The failure of bedrock is, also, dependent on factors such as the steepness and height of the rock face and the orientation of fracture sets (Ballantyne, 2003). This may explain the differences between the northern (province A) and the southern part (province B) of Adjet, as a steep mountain face is found in the north and a relatively gradual slope in the south. Thus the differences in failure result from pre-failure differences in the height and steepness of the rock face and the orientation of the fracture sets.

It is likely that a combination of several failure mechanisms affected and still affects the RSF at Adjet. Those mechanisms are stress release after deglaciation and climatic conditions causing weathering. Also, seismic activity related to glacio-isostatic uplift may have triggered failure processes. The foremost precondition of failure at Adjet, however, is suggested to be the abundance of fractures.

Figure 81: Rockfall derivation from headwall conjugate fault set failure. Just below is rock glacier r2 situated (towards SW). Moderately dipping fracture as sliding surface.

6.2.2 Folds

Folds are not visibly abundant at Adjet. They are mainly linked to intermediate scale folds in bedrock region b1 in the north, where limbs of the folds are observed as sliding surfaces (Fig. 82). The mean dip of intermediate scale folds is ca. 32° towards SW. Blocks are suggested to be delimited by fractures and slide on fold limbs after disintegration, resulting in talus fan deposits at the foot of the cliff. Regarding the great extent of the RSF area, the derivation of rockfall material by disintegration from folds in region b1 seems not as fundamental.
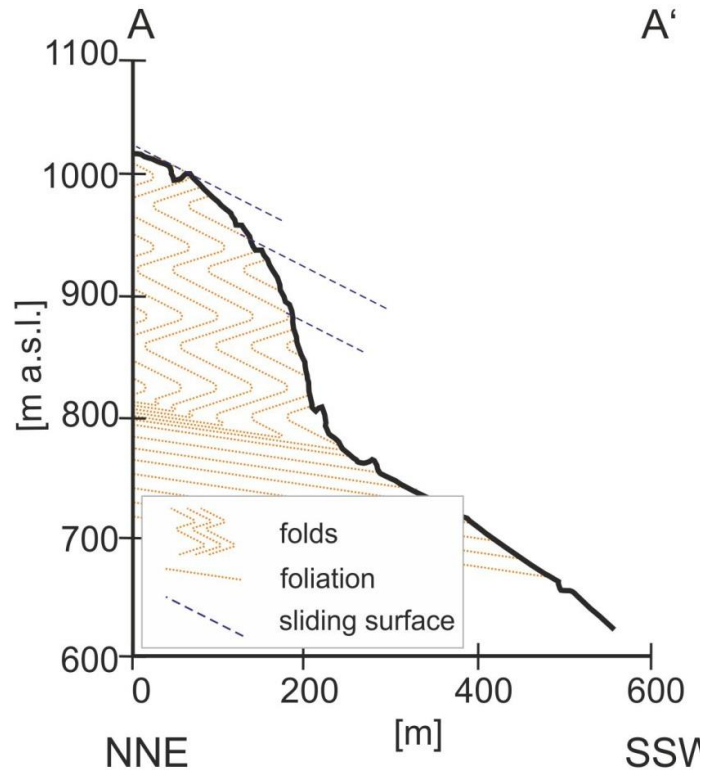
Figure 82: Showing fold limbs as sliding surfaces. For the location of profile line see figure 1.

6.2.3 Faults and fractures

Conjugate fracture sets largely found on the ridge, are, in contrast to folds, suggested to be the fundamental failure zones. Steep fractures delimit the outline and moderate dipping fault/ fractures define the sliding surface (Fig. 83 and *Ch. 3 Fig. 39*). In addition to sliding as a failure process, also toppling and rockfall are suggested to occur. Toppling and gravity driven rockfall are assumed to periodically supply talus fan deposits as well as additional debris to the rock glaciers (Fig. 83). The northernmost slide block (s1) is assumed to have disintegrated by toppling. The southern slide blocks (s4 to s6) are disintegrated by sliding on a moderately dipping fault plane and delimited by steep fractures. Slide blocks (s2 and s3) in between rock glaciers in northern Adjet (province A) are assumed to be part of a bigger failure event, in which they were transported downslope together with the surrounding debris field. Overall, the scarps of the slide blocks seem perpendicular to the NW-SE trending back scarps of the mountain. This may indicate a main disintegration by NE – SW trending fractures.

Toppling and gravity driven rockfall are suggested to occur at the steep mountain faces, especially in the north (regions b1 and b2).

Folds, faults and fracutres provide sliding surfaces where failure occurs. The failure is delimited by steeply dipping fractures. Folds are minor suppliers to the RSF site, whereas fault and fracture set are the major distributers. It is suggested that several larger failure events occurred. The difference in slope nature of the provinces A and B at Adjet, suggest further that they relate to two different RSF classifications (cf. Braathen et al., 2004; Ch. 1.5). Province A is, thus, classified as a rockfall area, whereas province B is a rockslide area.

Figure 83: Showing conjugate fault sets as potential sliding mechanism. Profile B – B' includes major fold and rock glacier r2 (not to scale). Profile C – C' includes slide block s4 above the potential sliding surface. For the location of profile lines see figure 1.
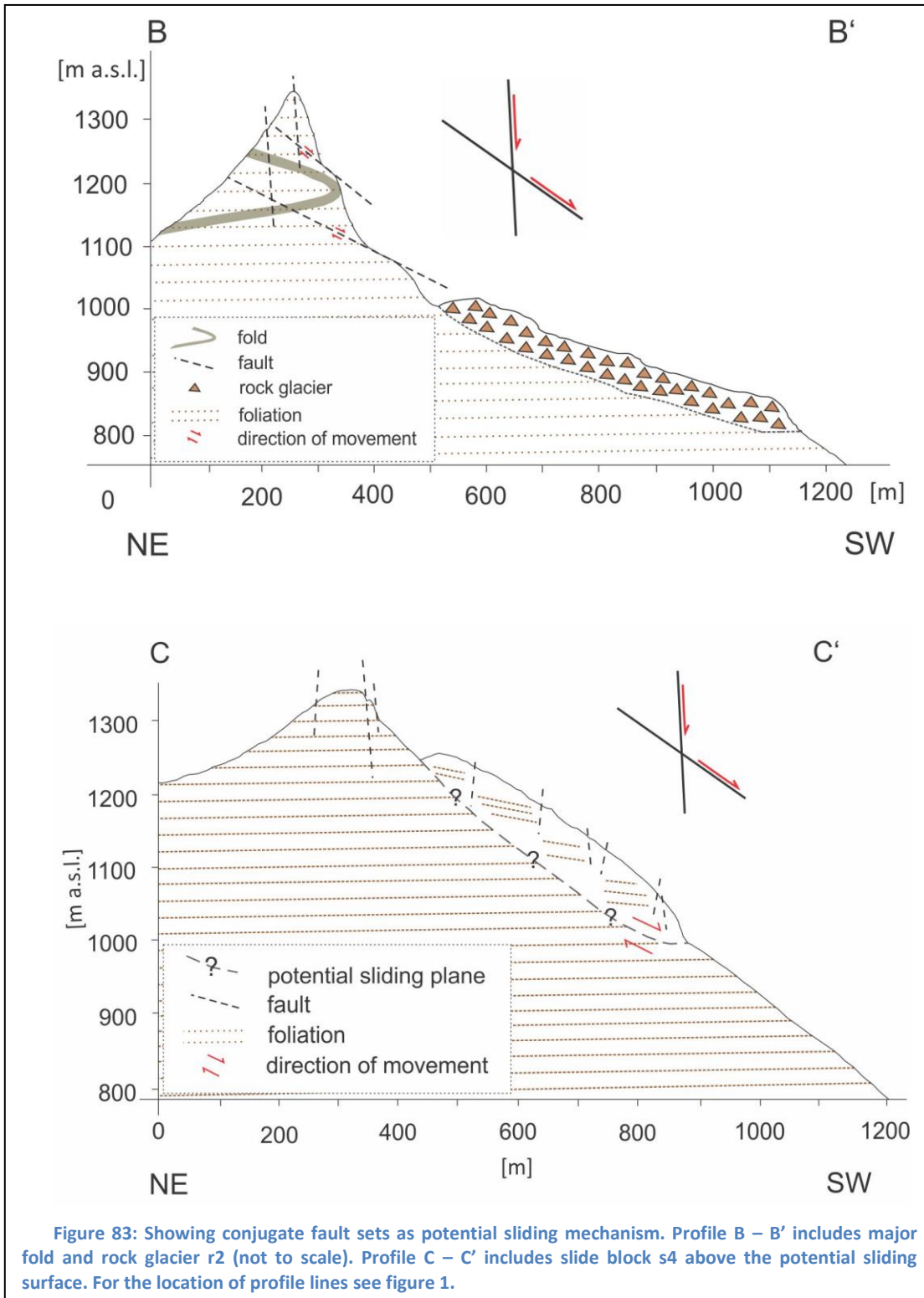
6.3 Movement pattern and direction

The RSF extends downslope towards the valley of Skibotndalen. It is supposed that large failure events, creep and sliding influence the RSF. Movement pattern of the RSF area is indicated by basal lobes of debris fields, transverse ridges and furrows, and lobes on rock glaciers, and the way slide blocks are situated within the RSF. Movement pattern is postulated regardless of the present activity of the feature. Figure 84 illustrates the downslope movement of rock glaciers, debris field and slide blocks in the study side. The general trend is towards west and southwest.

The RSF at Adjet is proven to be active (Ch. 5). Most movement is observed below the ridge and associated with geomorphological features. Some ridge regions (b2, b3; Ch. 5), however, show displacement. This may suggest that recent disintegration processes of rock occur. Also, the abundance of weathered material and colluvium on top of the ridge suggests disintegration processes to occur. Thus, smaller failure processes, e.g. rockfall or toppling, may occur (e.g. slide block s1; see above). These may be related to climatic conditions. Influences of seasonal weathering through snow melt and heavy rainfall affect well-developed fracture networks (Blikra et al., 2006). Freezing of water in fractures creates significant forces that may result in further opening and eventual failure of bedrock as rockfalls and rockslides. This presupposes two requirements: (1) increasing pore fluid/ water pressure along the shear surface, and (2) weathering/ abrasion along the shear surface. Haeberli et al. (2006) postulate that debris input is mainly supplied through physical weathering. Diurnal weathering such as freeze-thaw and thermal weakness affects the outermost cm to dm of the rocks and triggers small rockfalls, whereas seasonal weathering may affect the rocks up to a few meters depth causing ultimately larger rockfalls. Colluvial fans are often caused by active faults triggering rockfall avalanches (Leeder, 2011).

Failure by weathering is of special interest regarding the active rock glaciers in the study area. Whereas seasonal weathering is the most important factor affecting talus depositions, annual freeze-thaw activity may also add boulders to rock glaciers (Haeberli et al., 2006). Figures 2 and 3 suggest that rock glacier debris derive by rockfall from their headwall. Derivation by rockfall was also observed by (e.g. Haeberli et al., 2006; Humlum 1996).

Secondary process of debris derivation through removal of already loosened rock such as snow avalanches and debris flow are described by Haeberli et al. (2006). In addition, meltwater/ slush flows are suggested as secondary processes as well. They are observed in southern Adjet (province B). Weathered material and/ or colluvium on top of the ridge may eventually slide, forced by gravity, and derive geomorphological features below.

6.3.1 Talus fan deposit, colluvium and/or weathered material movement

Talus fan material eventually loses stability at the apical part of the fan and is reactivated as secondary rockfall or debrisflow moving farther downslope (Blikra & Nemec, 1998). This is suggested to occur at Adjet, e.g. in province B (t2 – t5; Ch. 4). Sudden acceleration triggered by excessive rain or melting snow may force a talus to creep (Holmes, 1965). Thus, debrisflow-derived talus fan deposit are caused. Failure processes as mentioned above are supposed to have affected different derivation of talus fan deposits and cause different movements. Talus fan deposits at Adjet are defined as active surface processes mobilized by gravity fall (rockfall), freeze-thaw processes (rockfall), heavy rainfall (debrisflow), snow avalanches and melt processes (meltwater/ slush flow) (cf. Blikra & Nemec, 1998). They are features created by present failure processes which are suggested to be related to seasonal and diurnal weathering.

Weathered material and/ or colluvium on top of the mountain ridge are suggested to be products of seasonal weathering e.g. freeze-thaw processes. Velocity data imply movement of these sporadic features (´78). These loose materials may displace so much, that they eventually fall of the ridge by gravity and supply the geomorphological features below with debris, e.g. talus fan deposits and rock glaciers.

InSAR data

Talus fan deposits show in general little movement of an approximate maximum of 2 cm yr^{-1} (Fig.84). In province B higher velocities are found in the vicinity of slide blocks, they reach around 5.5 cm yr^{-1} (Ch. 5). These movement rates are, however, suggested to be related to the slide blocks.

Weathered material and colluvium on top of *in-situ* bedrock moves with maximum velocities of ca. 2.7 cm yr^{-1} – 5.5 cm yr^{-1}.

Low velocities may indicate that movement is seasonally dependent. Most movement is supposed to occur during snow and ice melt in spring. This is not further discussed in this study.

Figure 84: Movement pattern of geomorphological elements at Adjet on top of InSAR velocity map.
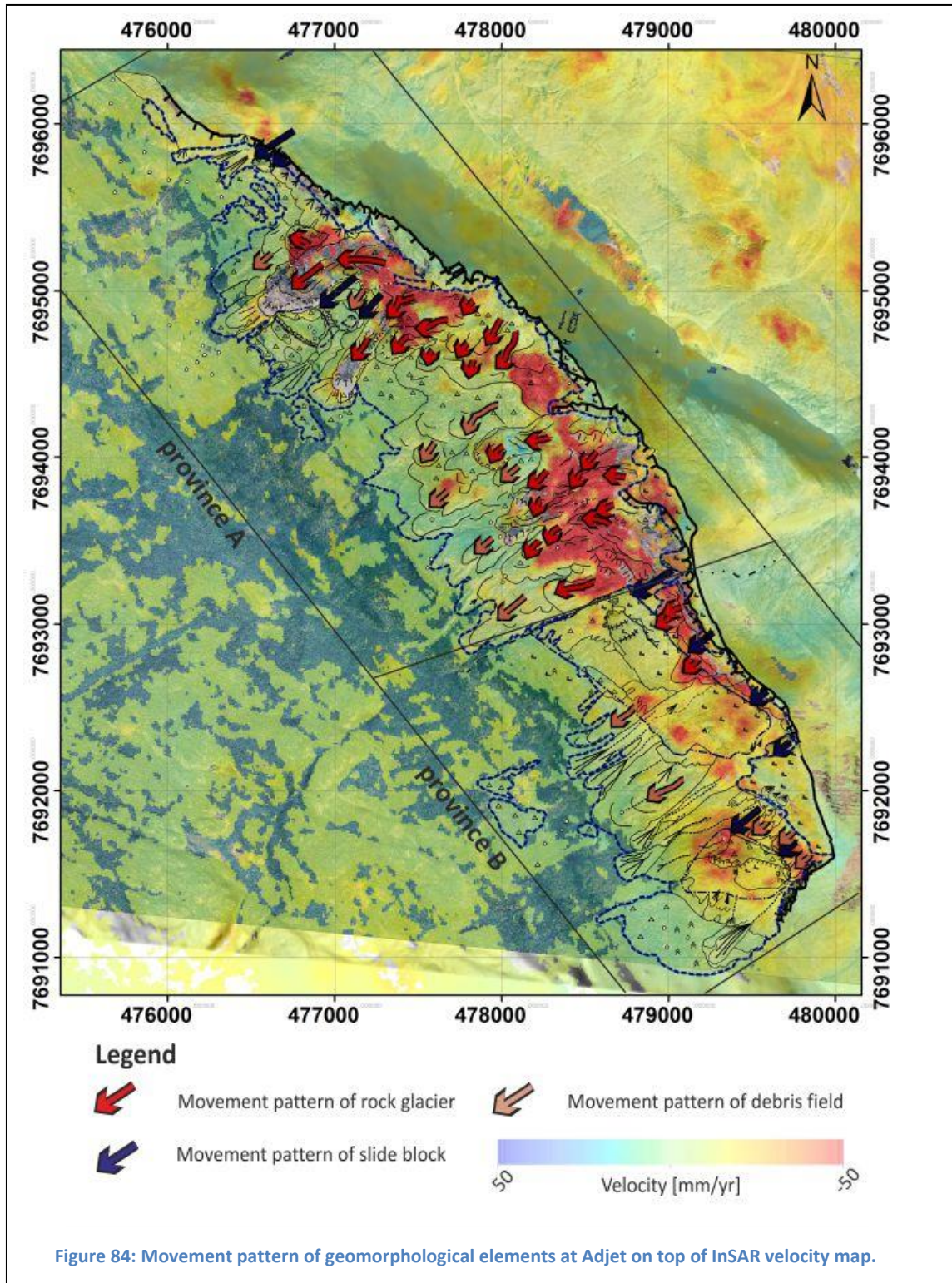
6.3.2 Debris field movement

Movement direction of debris fields is foremost inferred by lobes facing towards SW (Fig. movement). Debris movement in two steps is postulated by Dawson et al. (1986): (1) an initial phase of failure followed by (2) a phase of rapid flowage. Large failures as sturzstroms are triggered by disintegration of a large rock mass (Hsü, 1975). They are fast-moving debris streams that show similar geometry to lava flows or glaciers. Hsü (1975) suggests that sturzstrom can flow by fine debris colliding with one another and in this way offer a sliding surface; instead of water saturated mud (Hsü 1975) or compressed air being the sliding source. Subvertical fractures and consequent sliding have been identified to initiate a sturzstrom in northern Iceland (Mercier et al. 2012). Debris fields at Adjet are supposed to have been triggered by a catastrophic failure event followed by smaller failures causing further downslope movement respectively reactivation. The abundance of fracture sets at the ridge in Adjet suggests further the participation of fractures within the failure process. The downslope progress respectively reactivation of features, indicated by basal lobes lying on top of one another, indicates more failure processes. Further may debris-slide and rock-avalanches be triggered by increasing weight and decrease of friction of a mass (Holmes,m 1965). Creep movement is mainly influenced by the percolation of rain-water through the soil and frost heaving processes, but also expansion and contraction due to temperature changes e.g. soaking and drying influence downslope creep (Holmes 1965).

InSAR

Debris fields, at present, are generally stable but at individual spots they show movement (Fig. 84). The large debris field, below the band of rock glaciers in province A, is in motion in places. In province B debris fields show motion where they surround slide blocks. Velocities of debris fields range between 0 cm yr^{-1} and ca. 2.5 cm yr^{-1} (Ch. 5). Though, they are presumed to have been deposited in large failure events, present movement is presumed to be due to creep due to seasonal climate conditions.

6.3.3 Rock glacier movement

Rock glaciers' movement pattern was defined by their fronts, transverse ridges and furrows, and lobes. Changes in movement direction are observed from a west to northwestern movement to a southwest termination. Ballantyne (2003) suggests that rock waste follows the steepest slope angle throughout downslope flow. Thus may account for the rock glaciers in the study side. Rock glacier movement is liable to continue over millennia (Haeberli et al., 2006), if the ice-content is stable enough and does not melt. Melting of ice deforms the rock glacier (Humlum, 1996).

Transverse ridges and furrows give the impression of a lava-like or glacier-like flow (W and C 1959). The forward movement of rock glaciers is caused by ice, flowing under its own weight plus that of the debris (e.g. Whalley 1979, Wahrhaftig & Cox 1959, Johnson1984). Thus, the flow mechanism is related to the ice content, which is one-third the density of rock (McColl & Davis 2012). The ice flows, therefore, under low applied stress caused e.g. by additional weight. Debris derivation of the rock glaciers from rockfall/ talus has been postulated by several authors (e.g. Holmes 1965, Whalley 1979,Haeberli et al. 2006). Figure 85 implies a theoretical composition of a rock glacier in the study area. Steep fronts of the rock glaciers suggest that the upper half of the rock glacier moves faster than the lower half (e.g. Springman et al. 2012). Therefore, a two layered flow system is suggested.
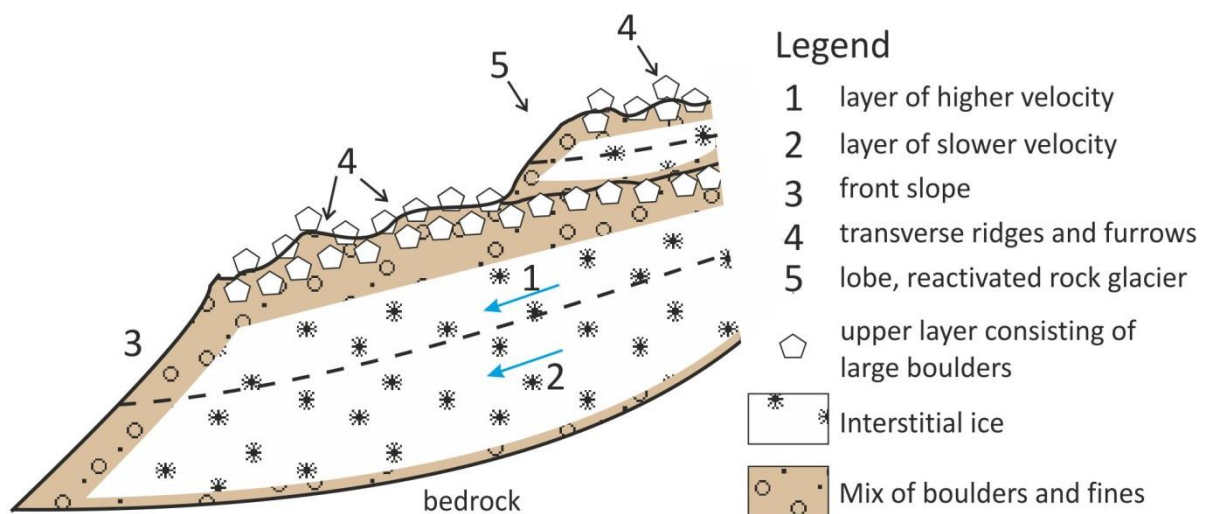
Figure 85: Potential inner structure of rock glaciers in the RSF side. Blue arrows indicate flow direction. The boarder of different velocity layers is marked by the dashed black line. Not to scale. Adapted from Springman et al. (2012).

Holmes (1965) refers to rock glaciers in permafrost regions as being stable due to interstitial ice but show increased flow during spring thaw. Movement is, thus, affected by differences in the thickness of the debris cover (Griffey and Whalley 1979), but also by seasonal climate conditions and the associated melting of ice (e.g. Humlum 1988, 1996). Seasonal changes in temperature of the active layer result in deformation of the rock glacier (Ikeda 2008). Deceleration occurs in winter and acceleration in summer seasons. It is postulated that diurnal changes associated with temperature and precipitation respectively humidity, further affect movement.

InSAR

Velocities of rock glaciers in the study area range roughly from 5 cm yr^{-1} up to 15 cm d^{-1} (Ch. 5). Velocities of rock glacier, in general, range from a few cm to a few m a year (Wahrhaftig & Cox 1959, Lambiel et al., 2008). (Lambiel et al., 2000) divides active rock glaciers into very high velocity (several cm

d^{-1} or several m yr^{-1}), high velocity (1 – 2 m yr^{-1}), medium velocity (20 cm yr^{-1} to 1 m yr^{-1}), low velocities (max. 20 cm yr^{-1}), or very low velocity (a few cm yr^{-1}). Springman et al. (2012) distinguishes between slow moving (10 cm yr^{-1}) to faster moving (> 50 cm yr^{-1}) rock glaciers. Adjet's rock glaciers are thus categorized in two of the categories. Firstly, the rock glaciers are of low velocity respectively slow moving, regarding velocities mainly displayed by the velocity map (ca. 5 cm yr^{-1} to 11 cm yr^{-1}). Secondly, the high velocity rock glaciers – data-free spots on the rock glaciers in Figure 84 – moving with speeds of several cm per day.

Low velocities refer either to low ice content, cold permafrost temperature, or low inclined slope (Lambiel et al. 2008). Considering the location of Adjet and the slope angle of 25° to 40°, the latter two suggestions are dismissed. Having the relative thinness of the rock glaciers in mind (ca. 10 m, Ch. 4.2.3) it is assumed that low interstitial ice content may be the reason for low velocity.

Ikeda (2008) suggest that higher surface velocities are found at the permafrost limit, due to the correlation of mean annual and seasonal surface displacements to permafrost temperatures. Surface displacement is, thus, connected to air temperature (Ikeda et al., 2008; Liu, Millar, Westfall, & Zebker, 2013). Recalling Chapter 4.2.3 the activity of the active layer of the rock glacier may be not only dependent on temperature changes but also precipitation. Assuming that r1 and r2 fronts (large rock glaciers in the north) are near the permafrost limit, the acceleration is linked to a warmer permafrost temperature. It explains, however, not the acceleration at r6, which is found at a higher elevation and therefore above the permafrost limit.

Inactive rock glaciers

The velocity data seems to support the hypothesis of inactive rock glaciers (Ch. 4.2.3.2). Inactive rock glaciers, here, are features adjacent to active rock glaciers but show no indices of motion and are vegetated. Overall is the area where inactive rock glaciers are identified, in between rock glaciers r1 and r2, stable. Little displacement is seen adjacent to steep slopes of associated active rock glacier. Hence, little displacement is supposed to be talus or rockfall from active slopes rather than displacement of as inactive identified rock glaciers.

6.3.4   Slide block movement

The slide blocks move to the SW. Northern parts of the blocks seem to have moved further than their southern parts, inferring a slight counterclockwise rotation.

Dilatation, slight rotation, and the disturbance of single blocks is possible in a sturzstrom failure (Hsü 1975). This is interesting regarding the slide blocks in the study side. Hence, the large slide blocks (s4, s6)

in the south (province B) are regarded to be part of large failure events, causing slight counterclockwise rotation of the blocks. The smaller slide block (s5) near the ridge may have been of a smaller failure event and has only slightly slid downslope and rotated counterclockwise.

The Elm sturzstrom mainly retained its original dimension and is not much deformed (Hsü 1975). This is interesting regarding the bench-like slide block (s3) observed in between two rock glaciers (r1, r2) in northern Adjet (province A). It is hence suggested, that the slide block was part of a catastrophic failure where the slide block was moved down, but not rotated or disturbed. The smaller slide block (s2) above the bench-like slide block (s3), on the contrary, may have been affected by dynamic disintegration processes within the debris field (dT4). Internal shearing within the moving mass produces dynamic disintegration (Pollet and Schneider 2004).

The northernmost slide block (s1) is supposed to have been disintegrated by toppling. It shows a slight counterclockwise rotation which may have been caused due to the mountains topography.

InSAR

Slide blocks show no to little movement (Fig. 84). Slide blocks in province A, are stable and show no indication for motion. Low velocities are, in contrast, detected on slide blocks in province B. On slide block s4, the largest in province B, velocities range from 0 cm yr^{-1} to ca. 5.5 cm yr^{-1}. Slide block s5, just below the ridge, shows a maximum velocity of ca. 3 cm yr^{-1} (Ch. 5 79). The southernmost slide block (s6) shows velocities up to ca. 4.5 cm yr^{-1}. Its northern side displays the highest velocities. Hence, slide blocks in province B seem to be moving. It has, however, to be kept in mind, that the velocity map gives us surface displacements, and the big slide blocks (s4 and s6), in province B, are largely covered by sporadic colluvium and weathered material, as well as by talus fan deposits, and debris fields. It is, thus, to question if s4 and s6 are moving or their covering features. Further investigation should be done to bolster the hypothesis of movement. The smaller slide block s5, adjacent to the ridge, however, is supposed to be in motion.
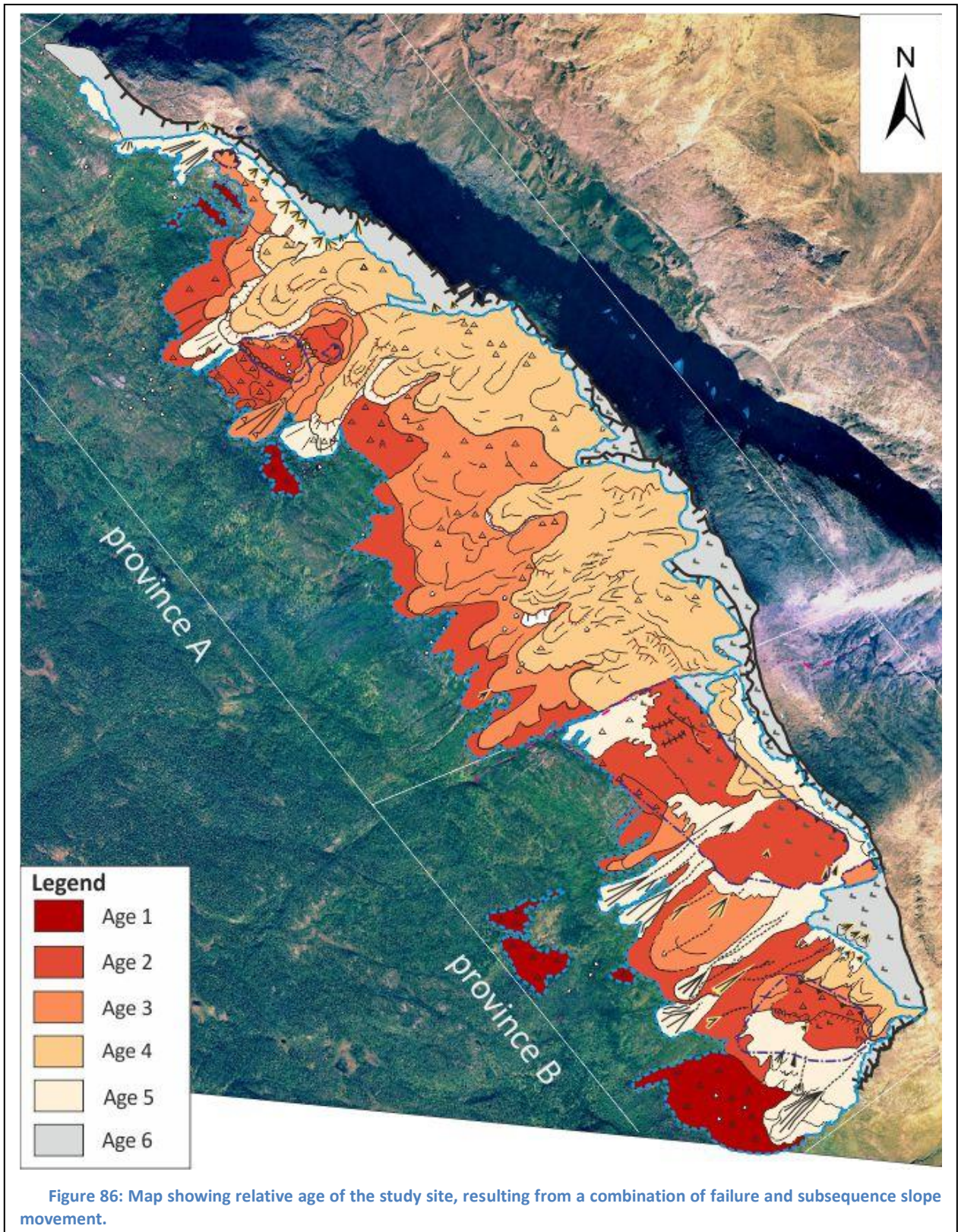
6.4 Evolution of failure activity in the study area

The complexity of the RSF at Adjet indicates that several failure events caused the present RSF side. In this chapter a rough evolution of the study site is presented. Figure 7 sums up the different relative 'ages' resulting from a combination of failure and subsequence slope movement. It has to be mentioned that relative ages are given without proof, and that features of one age may not be caused synchronously but by different/ several failure or creep events, e.g. debris field of age 3 and slide blocks of age 3. Thus, features of one relative age stage may be caused by failures that are several decades/ centuries/ millennia apart from each other. The relative ages are mainly resulting from the appearance of the geomorphological features, which are deposited on top of each other. Six stages are suggested: Age 1 represent the oldest and age 6 the youngest failure stage.

6.4.1 Age 1

As relative age 1 are mainly suggested debris fields outside the RSF. They are largely vegetated and at a considerable distance to the RSF side. The southernmost debris field is the exception regarding the distance.

McColl & Davis (2012) suggest that a slope may collapse catastrophically when a failure surface is exposed after ice retreat and before the glacier terminus retreated fully from the slope. Destabilization of the slope during deglaciation triggers slope failure processes and taluses develop along the valley slopes (Johnson 1984). Stress release after glacial retreat is further suggested to be a primary cause of RSF, and may occur either during or immediately after deglaciation (Ballantyne 2003, Blikra et al. 2006). Hence, age 1 is suggested to have been deposited shortly after glacial retreat before the terminus of the glacier has fully retreated from the area, so that the debris fields (age 1) have been deposited slightly outside the contiguous of the RSF side.

Figure 86: Map showing relative age of the study site, resulting from a combination of failure and subsequence slope movement.

6.4.2 Age 2 and 3

Relative age 2 is represented by debris fields and the majority of the slide blocks, except the northernmost (s1) and the southernmost slide block (s6). The latter slide blocks are included in relative age 3. Age 3 includes further debris fields which are assumed to be either generated by another failure or reactivated after a considerable time span and inactive rock glaciers.

Ballantyne (2003) suggests that RSF is primary induced by paraglacial stress release after the last glaciers retreated and is then triggered by isostatic uplift (Ballantyne, 2003). Debris fields and slide blocks of age 2 are suggested to be products of catastrophic failure events triggered by either relatively delayed stress release after deglaciation, earthquakes as part of isostatic uplift, a glacially overdeepend slope, or a combination of those. Large landslides caused by failure and flow of the whole mountain slope, are supposed to have a longer travel distance than smaller landslides (Johnson 1984). Thus may explain the large extent of the debris fields.

Basal lobes evolve by repeated reactivation of the feature, which may then assemble in age 3 features. The initial stage may have been a collapse followed by progression of debris by flowage and later creep. Failure and reactivation of features may be induced by climate change (Johnson 1984).

Slide blocks s1 and s5 are suggested to be part of a disintegration maybe even delayed to debris deposition/ reactivation of age 3 but are assumed to have displaced before age 4.

The inactive rock glaciers may have developed during either of the failure events causing debris fields and slide blocks of age 3. This is suggested because the inactive rock glaciers lie on top of a debris field of age 2, and are older than active rock glaciers (age 4). Wahrhaftig & Cox (1959) postulate that active and inactive rock glaciers developed throughout different periods of rigorous climate, segregated by periods of less rigorous climate. The activity and inactivity of rock glaciers in the Alaska Range is dated in the post-Wisconsin time (< 50 ka).

Overall, several failure events are suggested to have generated features of relative ages 2 and 3, which were followed by rapid flowage and/ or slow creep. It is supposed that a combination of slope destabilization through glacial retreat, glacio-isostatic uplift and climate changes triggered the disintegration of those featuers.

6.4.3 Age 4

Relative age 4 is mainly composed of rock glaciers but also a debris field in province B. It is suggested that rock glaciers were caused by a catastrophic failure event, whereas the debris field has been reactivated.

Hradecký & Pánek (2005) postulate, that more humid climate conditions and historical colonization affect the acceleration of older landslides. Adjet is not colonized but it is supposed that changing climate has an effect on the velocity of the RSF. As has been stated before are especially the rock glaciers influenced by temperature and precipitation. Lobate rock glaciers represent an initial stage, whereas tongue-shaped rock glaciers refer to a more mature stage (Wahrhaftig & Cox, 1959). Lobate- as well as tongue-shaped rock glaciers were identified in the study area. Thus, active rock glaciers suggest that they either were formed during different failure events, were inactive for a period of time and to different times reactivated, or have separately accelerated e.g. due to location near the permafrost limit. The rock glaciers (r9, r10) in province B, are suggested to be slightly younger than the bigger rock glaciers in province A. Not only the size but also the observations in field suggest a younger age, as was observed that the rock glaciers (r9, r10) show no vegetation. This, however, is very speculative.

If one or more large failure events generated the rock glaciers at Adjet, as is suggested to have happened in southwest Yukon (Johnson 1984), or if climate changes are responsible would be part of further investigations in the study are. The abundance of lobes on the rock glaciers suggests further that they were more or less constantly supplied by rockfall material. Blikra et al. (2006) suggest that rock glaciers were formed during the Younger Dryas period, or older phases, when climate conditions were cold enough and permafrost abound.

The formation of rock glaciers is supposed to be caused by larger failure events triggered by eventual stress retreat after deglaciation, glacio-isostatic uplift, and not the least climate change.

Reactivation of the debris field was probably caused by climate changes. Both features are supposed to be influenced by seasonal weathering.

6.4.4 Age 5

Relative age 5 includes mainly talus fan deposits and the fronts of rock glaciers. The latter are fresh taluses which are still assumed to be rock glacier features but are younger of age due to failure by downslope movement of the rock glaciers. Triggering is most likely indicated by seasonal weathering mechanisms.

6.4.5 Age 6

Relative age 6 represents in-situ bedrock and thus feature that are not or only slightly disintegrated. Features representing age 6 are thus the mountain ridge and including sporadic deposits overlying the bedrock. Sporadic deposits are suggested to be caused by seasonal weathering mechanisms.

6.4.6 Summary

The evolution of the RSF is subdivided into 6 relative age stages. Beginning with the oldest age 1 to the youngest age 6 the triggers of failure change slightly. Mechanisms of failure begin to combine and change throughout the evolution of the RSF stages.

- Age 1: Formed during glacier retreat, caused by destabilization of the slope
- Age 2: Formed immediately after glacial retreat, and
- Age 3 relatively delayed to glacial retreat, both caused by destabilization of the slope, probable seismic activity through glacio-isostatic uplift and probable changing climate; several failure events are supposed to have occurred
- Age 4: Formed after delayed glacial retreat and caused by above named triggers plus possible influence of seasonal weathering
- Age 5: Formed by relatively recent disintegrations caused by seasonal weathering
- Age 6: Relatively stable area, influenced by seasonal weathering

The likeliness of the RSF evolution hypothesis should be confirmed or disproved by further investigations in the area.

7 Conclusions

7.1 Features

Several geomorphological features are identified on the rock-slope failure. They originate from different mass movement processes, such as rockfall, toppling, rock slide, and sturzstrom. We find different rock fragment accumulations as well as detached large blocks. Geomorphological features are identified as debris fields, rock glaciers (active and inactive), talus fan deposits, and slide blocks. All features but the slide blocks, show basal lobes. Bedrock is foremost found in the contiguous of the RSF side. It consists mainly of variations of mica-schist: mica-schist, quartz-rich mica-schist, garnet-mica schist, and quartz-rich garnet-mica-schist. The ridge constitutes the derivation terrain of the failure material. Its character changes southward. Beginning in the north it shows high, steep mountain faces which decrease southward until they diminish completely and a slope-like character from ridge to the mountain base is developed. The study area is subsivided into two provinces which are separated by a ENE-WSW trending fault: province A, northern part of Adjet, is dominated by rock glaciers and debris fields, and province B, southern part of Adjet, is dominated by slide blocks as well as talus fan deposits.

7.2 Cause of rock-slope failure

Folds, faults and fractures at the mountain wall of Adjet are considered to cause rock-slope failures and thus supplied and supply the rock-slope failure area below. Steeply (NE-SW, NW-SE) and moderately (NW-SE) dipping fracture sets are identified. Fold limbs and moderately dipping faults/ fractures are considered as sliding surface of detached rocks, which are delimited by steeply dipping fractures. Rockfall and toppling are considered as main failure processes in province A, whereas failure in form of sliding is the main-process in province B. Climatic and non-climatic influenced processes are suggested to play and have played a part in failure processes. Non-climatic failure processes are triggered by fault/ fractures and their reactivation through both glacial debuttressing, and seismic activity linked to glacio-isostatic uplift. Climatic failure processes are linked to deglaciation and milder climatic conditions, as well as seasonal and diurnal weathering processes.

7.3 Present slope movement at Adjet

The RSF area is characterized by stable parts as well as very high velocities of several cm per year. The latter is proven by GBR measurements (Rouyet et al.. 2015). Movement of the geomorphological features is indicated by different observation during field work and supported by InSAR velocity measurements.

(1) Talus fan deposits are rockfall derived, snow avalanche derived, meltwater / slush derived, or debris flow derived. Their movement, thus, differs depending on derivation process. Talus fan deposits as well as weathered material and colluvium on the mountain move with low velocities of maximums of 2 – 6 cm yr⁻¹.

(2) Debris fields are generally stable. Here and there is low displacement observed. Velocities range from 0 – 5 cm yr⁻¹. Creep is the suggested movement process.

(3) Present activity of rock glaciers is indicated by steep baren slopes, heard and seen rockfalls, and cracks in the upper surface layer. These observations are supported by InSAR velocity data. The maximum velocities range from ca. 5 – 15 cm yr⁻¹. Rock glaciers move due to their interstitial ice content. The steep fronts led to the conclusion that the upper part of the interstitial ice body moves faster than the lower. Their activity is considered to be influenced by temperature and precipitation, thus diurnal and seasonal weathering processes.

(4) Slide blocks in province A show no movement, whereas slide block in province B show some low velocities; s4: 0 – 5.7 cm yr⁻¹, s5: max 3 cm yr⁻¹, s6: max ca. 5 cm yr⁻¹. If the slide blocks themselves or just their surficial deposits are moving, has to be proven by more detailed investigations.

Recent activity is generally suggested to be influenced by seasonal weathering processes.

7.4   Evolution of the rock-slope failure

The RSF at Adjet has been caused by several failure events throughout time. First failure may have been during glacial retreat, followed by several events after deglaciation building up the present stage. Conclusions of different failure events are drawn by the fact that geomorphological features overlap one another. Debris fields, for example, show several basal lobes. These suggest other failure events that provided material for further accumulations. Also the inactive rock glaciers and the larger extent of active rock glacier provide the hypothesis of several failure events with periods of no action in between them. Hence, 6 relative ages of rock-slope failure are suggested. Age 1 is chosen to represent the initial failure deposits. Ages 2 – 4 are failure processes, occurring between age 1 and age 5. Age 5 represents relatively recent failure processes. The last stage, age 6, represents the relatively stable area, and potential derivation terrain of future failure processes.

The RSF is an ongoing failure side providing an interesting investigation side.

8 Future work

The great size and complexity of the RSF area at Adjet gives multiple possibilities for future work. Presently, work is being carried out on the rock slope deformation in the study area using InSAR and GBR observations (Eriksen & Rouyet, pers. comm. 2014). More detailed investigation of rock glaciers may bring further understanding of such features. For example, it would be interesting if evidence for interstitial ice can be found. The very active rock glaciers (r1 and r2), in northern Adjet, are poorly suitable for coring as has been done in other rock glaciers (e.g. Haeberli et al. 2006, Hauck et al., 2011). The upper surface layer is very unstable and hazardous for equipment and people. Possibly one of the other less active rock glaciers could provide a suitable coring side.

Also more detailed mapping of different parts promises interesting results. The following sides could be of interest:

- The bench-like feature in northern Adjet; verification or invalidation of the feature as slide block
- The ENE-WSW trending fault; how is the RSF influenced by the fault?
- The southernmost slide block (s6); is it in motion or just its surficial deposits?
- The bedrock; more precise bedrock maping.

It would also beinteresting if different geomorphological feature could be dated, so that failures events can be classified according to ages. Dating of RSF was, for example, done at the Scottish Beinn Alligin rock avalanche by Ballantyne (2003). The rock avalanche was dated back ca. 4000 yr BP by 10 Be dating, indicating thath it is not related to the last glaciation, which ended around 11.5 ka BP Dating the different geomorphological features could give us better understanding of failure events and triggering processes.

The relatively high movement rates of different parts on the ridge, provide another scope for further scientific investigation.

The long-term movement of rock glaciers could be investigated by photographs from earlier years and compared to present expansion. If it shows a continuous trend future expansion could possibly be predicted.

9 References

Allmendinger, R. W., Cardozo, N., & Fischer, D. (2012). *Structural Geology Algorithms: Vectors and Tensors*. Cambridge: Cambridge UNiversity Press.

Bakkhaug, I. (2015). *Undersøkelse av ustabilt fjellparti ved Adjet, Storfjord, Troms: betydningen av ulike kategorier av glideplan i berggrunn og mekanismer for utrasing.* University of Tromsø.

Ballantyne, C. K. (2001). Paraglacial geomorphology. *Quaternary Science Reviews*, *21*(18-19), 1935–2017. http://doi.org/10.1016/S0277-3791(02)00005-7

Ballantyne, C. K. (2003). A Scottish sturzstrom: The Beinn Alligin rock avalanche, Wester Ross. *Scottish Geographical Journal*, *119*(2), 159–167. http://doi.org/10.1080/00369220318737169

Blikra, L. H., Longva, O., Braathen, a, Anda, E., Dehls, J. F., & Stalsberg, K. (2006). Rock Slope Failures in Norwegian Fjord Areas: Examples, Spatial Distribution and Temporal Pattern. *Landslides from Massive Rock Slope Failure*, 475–496.

Blikra, L. H., & Nemec, W. (1998). Postglacial colluvium in western Norway: depositional processes, facies and palaeoclimatic record. *Sedimentology*, *45*(5), 909–959. http://doi.org/10.1046/j.1365-3091.1998.00200.x

Blikra, L. H., & Sæther Bunkholt, H. S. (2012). *Tunnel gjennom Nordnesfjellet i Kåfjord, Troms: Oversikt over nærliggende ustabile fjellparti og påvirkning på stabilitet*. Troms.

Bozzano, F., Cipriani, I., Mazzanti, P., & Prestininzi, A. (2011). Displacement patterns of a landslide affected by human activities: Insights from ground-based InSAR monitoring. *Natural Hazards*, *59*(3), 1377–1396. http://doi.org/10.1007/s11069-011-9840-6

Braathen, A., Blikra, L. H., Berg, S. S., & Karlsen, F. (2004). Rock-slope failures in Norway; type, geometry, deformation mechanisms and stability. *Norsk Geologisk Tidsskrift*, *84*(1), 67–88.

Cardozo, N., & Allmendinger, R. W. (2013). Spherical projections with OSXSteronet. *Computers & Geosciences*, *51*(0), 193–205.

Christiansen, H. H., Etzelmüller, B., Isaksen, K., Juliussen, H., Farbrot, H., Humlum, O., … Ødegård, R. S. (2010). The thermal state of permafrost in the nordic area during the international polar year 2007-2009. *Permafrost and Periglacial Processes*, *21*(2), 156–181. http://doi.org/10.1002/ppp.687

Corner, G. D. (1972). *Rockslides in NorthTroms, Norway*.

Corner, G. D. (1980). Preboreal deglaciation chronology and marine limits of the Lyngen-Storfjord area, Troms, North Norway. *Boreas*, *9*, 239–249.

Corner, G. D. (2005a). Atlantic coast and fjords. In M. Seppälä (Ed.), *The Physical Geography of Fennoscandia* (pp. 203–228). Oxford University Press.

Corner, G. D. (2005b). Scandes Mountains. In *The Physical Geography of Fennoscandia* (pp. 229–254).

Dannevig, P. (2009). Troms: klima. I Store norske leksikon. Retrieved May 20, 2005, from https://snl.no/Troms%2Fklima

Dehls, J. F., Olesen, O., Olsen, L., & Harald Blikra, L. (2000). Neotectonic faulting in northern Norway; the Stuoragurra and Nordmannvikdalen postglacial faults. *Quaternary Science Reviews*, *19*(14-15), 1447–1460. http://doi.org/10.1016/S0277-3791(00)00073-1

Dyrvik, A. (2014). *Geomorfologisk og sedimentologisk analyse av avsetjingsforløp og skredmekanikk for debris-flow- hendingar frå 14. juli 2012 i Signaldalen, Troms. —*. University of Tromsø.

Eriksen, H. Ø. (n.d.). *Analyzing Complex Rock Slope Deformation at Ádjet, Northern Norway, Relating Combined Ground- and Satellite-based Interferometric Observations with Geomorphological- and Structural Elements*.

Eriksen, H. Ø. (2013). *Slope displacement patterns observed using satellite InSAR data in the Storfjord-Kåfjord-Lyngen region, Troms, Master thesis, University of Tromsø, Tromsø, Norway*. University of Tromsø. Retrieved from http://hdl.handle.net/10037/5240

Fjeldskaar, W., Lindholm, C., Dehls, J. F., & Fjeldskaar, I. (2000). Postglacial uplift, neotectonics and seismicity in Fennoscandia. *Quaternary Science Reviews*, *19*(14-15), 1413–1422. http://doi.org/10.1016/S0277-3791(00)00070-6

Fossen, H., Pedersen, R.-B., Bergh, S., & Andresen, A. (2008). Creation of a mountain chain. In I. B. Ramberg, I. Bryhni, A. Nøttvedt, & K. Rangnes (Eds.), *The Making of a land - Geology of Norway* (pp. 178–231). Trondheim.

Gabriel, A. K., Goldstein, R. M., & Zebker, H. a. (1989). Mapping small elevation changes over large areas - Differential radar interferometry, *94*(1), 9183–9191. http://doi.org/10.1029/JB094iB07p09183

Gabrielsen, R. H., Braathen, A., Dehis, J., & Roberts, D. (2002). Tectonic lineaments of Norway. *Norsk Geologisk Tidsskrift*, *82*(3), 153–174.

Greig, D. (2011). *Moraine chronology and deglaciation of the northern Lyngen Peninsula, Troms, Norway*. University of Tromsø.

Griffey, N. J., & Whalley, W. B. (1979). A rock glacier and moraine-ridge complex, Lyngen Peninsula, north Norway. *Norsk Geografisk Tidsskrift*, *33*(3), 117–124. http://doi.org/10.1080/00291957908552049

Haeberli, W., Hallet, B., Arenson, L., Elconin, R., Humlum, O., Kääb, A., … Vonder Mühll, D. (2006). Permafrost creep and rock glacier dynamics. *Permafrost and Periglacial Processes*, *17*, 189–214. http://doi.org/10.1002/ppp.561

Hansen, J. A., Bergh, S. G., & Henningsen, T. (2012). Mesozoic rifting and basin evolution on the Lofoten and Vester??len Margin, North-Norway; time constraints and regional implications. *Norsk Geologisk Tidsskrift*, *91*(4), 203–228.

Hauck, C., Böttcher, M., & Maurer, H. (2011). A new model for estimating subsurface ice content based on combined electrical and seismic data sets. *Cryosphere*, *5*(2), 453–468. http://doi.org/10.5194/tc-5-453-2011

Henderson, I. H. C., Lauknes, T. R., Osmundsen, P. T., Dehls, J., Larsen, Y., & Redfield, T. F. (2011). A structural, geomorphological and InSAR study of an active rock slope failure development. *Geological Society, London, Special Publications*, *351*(1), 185–199. http://doi.org/10.1144/SP351.10

Holmes, A. (1965). *Principles of Physical Geology* (2nd ed.). Nelson.

Hradecký, J., & Pánek, T. (2005). Deep-seated gravitational slope deformations and their influence on consequent mass movements (case studies from the highest part of the Czech Carpathians). *Natural Hazards*, *45*(2), 235–253. http://doi.org/10.1007/s11069-007-9157-7

Hsü, K. J. (1975). Catastrophic Debris Streams (Sturzstroms) generated by rockfalls. *Geological Society of American Bulletin*, *86*(129-140).

Humlum, O. (1996). Origin of rock glaciers: observations from Mellemfjord, Disko Island, central West Greenland. *Permafrost and Periglacial Processes*, *7*(4), 361–380. http://doi.org/10.1002/(SICI)1099-1530(199610)7:4<361::AID-PPP227>3.0.CO;2-4

Humlum, O. (1998). The climatic significance of rock glaciers. *Permafrost and Periglacial Processes*, *9*(4), 375–395. http://doi.org/10.1002/(SICI)1099-1530(199810/12)9:4<375::AID-PPP301>3.0.CO;2-0

Ikeda, A., Matsuoka, N., & Kääb, A. (2008). Fast deformation of perennially frozen debris in a warm rock glacier in the Swiss Alps: An effect of liquid water. *Journal of Geophysical Research: Earth Surface*, *113*(1), 1–12. http://doi.org/10.1029/2007JF000859

Indrevær, K., Bergh, S. G., Koehl, J., Hansen, J., Schermer, E. R., & Ingebrigtsen, A. (2013). Post-Caledonian brittle fault zones on the hyperextended SW Barents Sea margin : New insights into onshore and offshore margin architecture, 167–188.

Johnson, M. G. (2014). No Title. Retrieved from http://site.uit.no/spaceweather/2014/07/15/skibotn-observatory/

Johnson, P. G. (1984). Rock Glacier Formation by High-Magnitude Low-Frequency Slope Processes in the Southwest Yukon. *Annals of the Association of American Geographers*, *74*(3), 408–419. http://doi.org/10.1111/j.1467-8306.1984.tb01463.x

Keary, P. (2001). *Dictionary of Geology* (2nd ed.).

Kenyi, L. W., & Kaufmann, V. (2003). Estimation of rock glacier surface deformation using SAR interferometry data. *IEEE Transactions on Geoscience and Remote Sensing*, *41*(6), 1512–1515. http://doi.org/10.1109/TGRS.2003.811996

Lambiel, C., Lugon, R., & Raetzo, H. (2000). ERS InSAR for Assessing Rock Glacier Activity Methods and Datasets InSAR-detected Velocities.

Lauknes, T. R., Piyush Shanker, a., Dehls, J. F., Zebker, H. a., Henderson, I. H. C., & Larsen, Y. (2010). Detailed rockslide mapping in northern Norway with small baseline and persistent scatterer interferometric SAR time series methods. *Remote Sensing of Environment*, *114*(9), 2097–2109. http://doi.org/10.1016/j.rse.2010.04.015

Leeder, M. R. (2011). *Sedimentology and Sedimentary Basins: from turbulence to tectonics* (2nd ed.). Wiley-Blackwell.

Liu, L., Millar, C. I., Westfall, R. D., & Zebker, H. a. (2013). Surface motion of active rock glaciers in the Sierra Nevada, California, USA: Inventory and a case study using InSAR. *Cryosphere*, *7*(4), 1109–1119. http://doi.org/10.5194/tc-7-1109-2013

Massonnet, D., & Feigl, K. L. (1998). Radar interferometry and its application to changes in the Earth's surface. *Reviews of Geophysics*, *36*(4), 441. http://doi.org/10.1029/97RG03139

McColl, S. T. (2012). Paraglacial rock-slope stability. *Geomorphology*, *153-154*, 1–16. http://doi.org/10.1016/j.geomorph.2012.02.015

McColl, S. T., & Davis, T. R. H. (2012). Large ice-contact slope mivements: glacial buttressing, deformation and erosion. *Earth Surface Processes and Landforms*, *38*, 1102–1115.

Mercier, D., Cossart, E., Decaulne, a., Feuillet, T., Jonsson, H. P., & Saemundsson, T. (2012). The Hofthaholar rock avalanche (sturzstrom): Chronological constraint of paraglacial landsliding on an Icelandic hillslope. *The Holocene*, *23*(3), 432–446. http://doi.org/10.1177/0959683612463104

Neuendarf, K. K. E., Mehl Jr, J. P., & Jackson, J. A. (Eds.). (2011). *Glossary of Geology* (5th ed.). Alexandria.

No Title. (n.d.). Retrieved from yr.no

Osmundsen, P. T., Redfield, T. F., Hendriks, B. H. W., Bergh, S., Hansen, J. -a., Henderson, I. H. C., … Davidsen, B. (2010). Fault-controlled alpine topography in Norway. *Journal of the Geological Society*, *167*(1), 83–98. http://doi.org/10.1144/0016-76492009-019

Papke, J., Strozzi, T., Wiesmann, A., Wegmueller, U., & Tate, N. J. (2012). ROCK GLACIER MONITORING WITH SPACEBORNE SAR GAMMA Remote Sensing AG , Worbstrasse 225 , 3073 Guemligen , Switzerland, 3911–3914.

Pritchard, M. E. (2006). InSAR , a tool for measuring Earth's surface deformation. *Physics Today*, (July), 68–69. http://doi.org/10.1063/1.2337843

Rignot, E. (2002). Rock glacier surface motion in Beacon Valley, Antarctica, from synthetic-aperture radar interferometry. *Geophysical Research Letters*, *29*(12), 48–51. http://doi.org/10.1029/2001GL013494

Rosen, P. a., Hensley, S., Joughin, I. R., Li, F. K., Madsen, S. N., Rodriguez, E., & Goldstein, R. M. (2000). Synthetic aperture radar interferometry. *Proceedings of the IEEE*, *88*(3), 333–382. http://doi.org/10.1109/5.838084

Rouyet, L., Hindberg, H., Eriksen, H. Ø., Lauknes, T. R., Larsen, Y., Eckerstorfer, M., & Werner, C. (2015). Ground- and Satellite-based Interferometric Observations of a Fast Moving Rock Glacier Complex (Ádjet mountain , Northern Norway). In *paper 152*. Frascati.

Shakesby, R. a, Dawson, A. G., & Matthews, J. a. (1987). Rock glaciers , protalus ramparts and related phenomena , Rondane , Norway : a continuum of large- scale talus-derived landforms. *Boreas*, *16*(1971), 305–317.

Springman, S. M., Arenson, L. U., Yamamoto, Y., Maurer, H., Kos, A., Buchli, T., & Derungs, G. (2012). Multidisciplinary investigations on three rock glaciers in the swiss alps: Legacies and future perspectives. *Geografiska Annaler, Series A: Physical Geography*, *94*(2), 215–243. http://doi.org/10.1111/j.1468-0459.2012.00464.x

Svelan, H., & Corner, G. D. (2004). *Lyngens isbreer før og nå*.

Tasrianto, R., & Escalona, A. (2015). Rift Architecture of the Lofoten-Vesterålen Margin, Offshore Norway. *Marine and Petroleum Geology*, *64*, 1–16. http://doi.org/10.1016/j.marpetgeo.2015.02.036

Twiss, R. J., & Moores, E. M. (Eds.). (2007). *Structural Geology*. Susan Finnemore Brennan.

USGS. (2004). Landslide Types and Processes. *Highway Research Board Special Report*, (July), 1–4. http://doi.org/Fact Sheet 2004-3072

Vorren, T. O., & Mangerud, J. (2008). Glaciations come and go. In I. B. Ramberg, I. Bryhni, A. Nøttvedt, & K. Rangnes (Eds.), *The Making of a land - Geology of Norway* (pp. 480–533). Trondheim.

Vorren, T. O., Mangerud, J., Blikra, L. H., Nesje, A., & Svelan, H. (2008). The emergence of modern Norway. In I. B. Ramberg, I. Bryhni, A. Nøttvedt, & K. Rangnes (Eds.), *The Making of a land - Geology of Norway* (pp. 534–559). Trondheim.

Wahrhaftig, C., & Cox, A. (1959). Rock glaciers in the Alaska Range. *Bulletin of Geological Society of America*, *70*, 383–436.

Werner, C., Strozzi, T., Wiesmann, A., & Wegmüller, U. (2008). Gamma's Portable Radar Interferometer. *Symposium on Deformation Measurement and Analysis*, 1–10. Retrieved from https://fig.net/commission6/lisbon_2008/papers/ps02/ps02_04_werner_mc016.pdf

Whalley, W. B., a, G. A. S., Geography, P., & Wallis, K. (1979). the Relationship of Glacier Ice and Rock Glacier At Grubengletscher. *Geografiska Annaler, Series A: Physical Geography*, *61*(1/2), 49–61.

Zwaan, K. B. (1988). NORDREISA, berggrunnsgeologisk kart – M 1:250 000. Norges geologiske undersøkelse.

These webpages were frequently consulted from October 2014 to June 2015:

yr.no

norgedigitalt.no , respectively kartverket.no